
**UNIVERSIDAD NACIONAL AUTÓNOMA DE MÉXICO**

POSGRADO EN CIENCIAS (FÍSICA)

MATERIA CODENSADA Y NANOCIENCIAS

**BERRY PHASE IN REAL SPACE AND MAGNETIC ITINERANT SYSTEMS**

# T E S I S

QUE PARA OPTAR POR EL GRADO DE:
**MAESTRA EN CIENCIAS**

PRESENTA:
ERÉNDIRA SANTANA SUÁREZ

TUTOR PRINCIPAL

DR. ISAAC PÉREZ CASTILLO
UNIVERSIDAD AUTÓNOMA METROPOLITANA

MIEMBROS DEL COMITÉ TUTOR

DR. PABLO BARBERIS BLOSTEIN
INSTITUTO DE INVESTIGACIONES EN MATEMÁTICAS APLICADAS Y EN SISTEMAS (UNAM)

DR. LUIS ANTONIO PÉREZ LÓPEZ
INSTITUTO DE FÍSICA (UNAM)

CIUDAD UNIVERSITARIA, CIUDAD DE MÉXICO; SEPTIEMBRE DE 2023.

# Abstract

In this work, a theoretic analysis of the Berry phase was done. In particular we studied the Berry phase in systems with finite spin-orbit coupling (SOC), in order to find if it produces a non-trivial Berry phase. We studied the case of an electron moving around a triangular plaquette, where the electron interacts with the local magnetic moments. To achieve this, we followed and reproduced meticulously the procedure outlined by S.-S. Zhang, H. Ishizuka, H. Zhang, G. B. Halász, and C. D. Batista, in their article titled "Real-space Berry Curvature of Itinerant Electron Systems with Spin-orbit Interaction".

We did a geometric approach, where we used geodesics in the Bloch sphere. The geodesics showed us how the spin states rotate due to SOC and how the Berry phase, geometrically, is represented. We also did an algebraic approach, where we used the Wilson loop to find that the electrons moving on a close path pick up a non-trivial Berry phase. Then the continuum limit we find that, for systems with finite SOC, a Berry phase exists in collinear configurations. Also a covariant expression for the Berry phase in the presence of SOC was found. The above results are exemplified in an itinerant electron system moving in a kagome lattice, where we found that the SOC modulates the band structures.

# Dedicatoria

*Con todo mi amor, para Rocío, Miguel,*
*Aideé, Angélica, Alejandro y Miztli.*

El mundo y la vida son mejores cuando se comparten con personas tan especiales como ustedes. Muchas gracias por amarme desde el inicio de nuestra historia, por apoyarme durante todo este proyecto y por creer en mí siempre, incluso cuando yo no sabía cómo.

A mi mami, Rocío, porque su amor y apoyo incondicional ha llenado y abrazado mi corazón desde que tengo memoria. Gracias por hacerme sentir suficiente sólo por ser yo, por enseñarme que nos podemos reinventar y encontrar paz, por los cuidados y la fuerza.

A mi papi, Miguel, por cobijarme con su generosidad y amor desde antes de que naciera. Gracias por apoyarme y acompañarme, gracias por enseñarme que el mundo está lleno de diferentes oportunidades.

A Ade, por ser mi confidente, cómplice y compañera de vida. Gracias por darle tanta felicidad a mi vida y por sostener mi mano y no soltarme nunca, desde que éramos niñas y le temía a la oscuridad, hasta este momento.

A Gely, porque desde que llegó con una estrellita pegada en la frente, ha llenado de luz mis días. Gracias por darme ánimo y alegría, por enseñarme nuevas formas de ver el mundo y por inspirarme a crecer como persona.

A Alex, porque desde que entró a mi vida me ha amado de la forma más bonita. Gracias por explicarme temas que no entendía, por acompañarme en los momentos más oscuros, y por ser mi familia elegida. Gracias por enseñarme que los planes pueden cambiar y que eso está bien.

A Miztli, Maya, Vaquis y Nala, por su amor y cariño y compañía. A Lulú, Felipe e Ixchetl les agradezco por su inmenso apoyo y por su maravillosa amistad. Gracias por recordarme que están orgullosos de mí.

Me gustaría agradecer a Fer, Morguis, Mariela, Rubí y Andrea, por todo su apoyo y por escuchar todas mis preocupaciones alrededor de la tesis. A Macarena, María Fernanda y Erika, gracias por enseñarme que soy muchas cosas y ayudarme a sanar. Sin su apoyo, no habría podido culminar este proyecto.

A June, Bren y Mi primer día como científica, por darme un espacio y recordarme porqué me encanta la ciencia. Finalmente, agradezco a las mujeres que me precedieron por abrir el camino y luchar para que personas como yo podamos estar aquí hoy.

# Acknowledgements

I would like to extend my sincere and and deepest acknowledgements to my advisor, Dr. Isaac Pérez Castillo. His guidance, patience, invaluable support, teachings and advises have played a fundamental role in enabling me to understand and finalize this project. I am really thankful with the members of my tutorial committee, Dr. Pablo Barberis Blostein and Dr. Luis Antonio Pérez López, for their understanding and ongoing support during my time as a Master's degree student.

My wholeheartedly gratitude to the examination committee members: Dr. Jorge Gustavo Hirsch, Dr. José Alberto Martín Ruiz, Dr. Luis Alberto Hernández Rosas, and Dr. Miguel Angel Bastarrachea Magnani. Their enlightening review, diverse expertise, and valuable corrections and suggestions improved this thesis.

I would like to acknowledge Dr. Cristian Batista and Dr. Shang-Shun Zhang, for clarifying the questions and doubts that I had about their fantastic investigation. Also, my sincere gratitude to Dr. Joana Avelar Robledo, for her patient explanations and willingness to share her knowledge.

To Dr. Francisco Mireles Higuera, who shared with me his passion for theoretical physics and taught me about spintronics. I would like to thank Dr. David Ruiz Tijerina, for the advice and suggestions during the first semesters of my Master's studies. My profound gratitude to Dr. Alberto Güijosa Hidalgo, for his exceptional understanding and support during these challenging times of the pandemic.

Finally, I would like to acknowledge the Universidad Nacional Autónoma de México, and the CONACyT. To the UNAM, for the opportunities and its invaluable contribution to my academic journey. To the CONACyT, for the financial support, without which this work would not have been possible.

# Contents

# List of Figures

# Chapter 1

# Geometry, Topology and the Berry Phase

## 1.1 A Brief Introduction to Geometry and Topology

In modern quantum physics, two areas of mathematics have become a fundamental part of the theoretical physicist toolbox: geometry and topology [1].

Geometry, from the ancient greek *geo* meaning Earth and *metron* meaning measurement, was invented by the ancients as a tool to measure distances and to survey areas [1]. Notwithstanding its purpose, according to Girvin and Yang [1], the first encounter we have with geometry, as students in elementary school, does not involve distance, but rather it is based on forms that are created using angles and straight segments. These geometric figures and bodies have interesting properties. For example, think of an isosceles triangle, characterized for having two equal edges and two equal angles. If we make this triangle larger and then we rotate it, the resulting triangle is still an isosceles triangle, since its internal angles do not change. In this sense, it can be stated that euclidean plane geometry is characterized as "the study of invariants under linear scale changes and rotations" [1].

On the other hand, topology is a branch of mathematics that studies those properties that do not vary under continuous transformations. An example of this is the transformation of a coffee cup into a torus (i.e. a doughnut): the cup can be continuously transformed to become a torus preserving one hole [1], as it is shown in Figure 1.1. Another example is the transformation of a circle into a triangle: imagine you have a ribbon that forms a circle, if we take two ribbon segments and push them, the circle becomes a triangle [1]. Some quantities are invariant under linear scale change, but only some of them are invariant under continuous arbitrary deformation. These last quantities are called *topological invariants* and have, as we will see later, an important and fundamental role in physics [1].

**Figure 1.1:** The transformation of a coffee cup into a doughnut is a continuous deformation: the bowl of the cup is molded to make it shallower until it becomes a filled cylinder. Now we have a filled cylinder with a handle that, by molding it, it turns into a torus (doughnut) shape. The genus (in this case the hole) is conserved. Image from [2].

In recent years it has been shown that certain physical observables are universal under this type of transformation of the Hamiltonian. This universality is explained by the fact that the observable is represented by a topological invariant that protects the observable from changes in the Hamiltonian [1]. This protection does not work if the Hamiltonian goes under a phase transition. As topological invariants are special and give us information about properties of materials [1], in this thesis we are going to give a brief introduction to two main concepts in topology: homeomorphism and homotopy.

### 1.1.1 Homeomorphism

A homeomorphism is defined as a mapping from one space to another that is continuous and whose inverse exists and it is also continuous [1]. A homeomorphism is a type of topological equivalence, which means that the topological space does not vary under continuous transformations. Indeed, consider two topological spaces: $X$ and $Y$. We say that a function $f : X \to Y$ is a homeomorphism if it is continuous, has a continuous inverse function (the function $f^{-1}$ exists) and it is bijective. The latter means that it is a one-to-one map and that every element in the codomain has at least one element in the domain (even if it is not the only one) [3].

One example of a homeomorphism is the transformation of a coffee cup into a torus that we have already described before (Figure 1.1). In this example, we map a region of the cup into a region in the torus and the homeomorphism tells us exactly which pieces of the torus correspond to pieces of the cup. Notice that a particular homeomorphism describes the range-domain correspondence between spaces but does not describe how the continuous change is made. The

coffee cup, the torus and all the geometric bodies transforming between these two objects belong to the same *topological class*, because the *genus* (in common language in this example, the hole) is preserved under homeomorphism: the number of holes is neither increase nor reduce [1].

Another example of homeomorphism is the transformation of a polyhedron into a sphere. Here, we can think of a regular polyhedron (for example a pentagonal pyramid) with its center of gravity at a point $O$. Any other point of the polyhedron (for example point $x$) can be dragged to a point $f(x)$ on the surface of a sphere. Note that this is a continuous transformation. If we consider the mapping by drawing a line from $O$ to $x$, and follow this path of the point to the surface of the sphere, then the new set of points given by $f(x)$ have their center of gravity also at $O$. This transformation (Figure 1.2) maps curvilinear polygons that are in the sphere's surface [3].

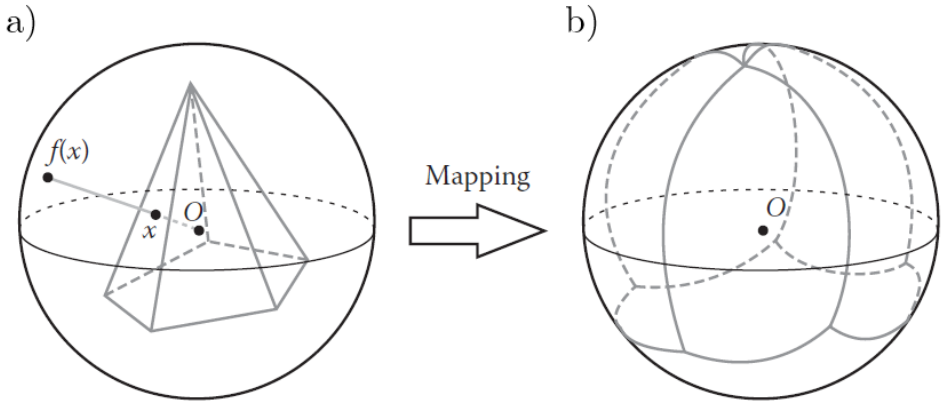


**Figure 1.2:** The homeomorphism from a regular polyhedron to a sphere. a) A regular polyhedron with its center of gravity $O$ can be mapped in to a sphere by mapping the points $x$ into $f(x)$, preserving the center of gravity of the regular polyhedron $O$ (image b). Image from [3].

The quantities that do not change under homeomorphisms, as the genus mentioned in the coffee cup-torus example, are called *topological invariants*. The genus is only one topological invariant, but there are many more. Finally, it is important to say that the topological invariants are not inherently geometric because homeomorphisms do not preserve geometry [1].

### 1.1.2 Homotopy

A homotopy is an equivalence relation among all maps that can be continuously deformed into each other [1]. More precisely, if we suppose that $f, g : X \to Y$ are maps, $F$ is homotopic if there is a map $F : X \times I \to Y$, which satisfies that $F(x, 0) = f(x)$ and $F(x, 1) = g(x)$ [3]. Here, $I = [0, 1]$ is the unit segment in $\mathbb{R}$. Notice that the continuous map $F$ takes as its first entry an element of $X$ and its second input is an interval over time $t \in [0, 1]$, so that for $t = 0$ the map $F$ corresponds to the function $f(x)$, and as the variable $t$ changes, the function continuously changes until it arrives to the map $g(x)$ at $t = 1$ [3].

To understand these concepts, let us consider a mapping of a unit circle into another unit circle. Each circle has a vector position that is defined by its angular position $\theta$ and $\theta'$, respectively. The vectors can be written as:

$$\mathbf{r} = \mathbf{r}_0 + (\cos\theta, \sin\theta), \tag{1.1}$$

$$\mathbf{r}' = (\cos\theta', \sin\theta'). \tag{1.2}$$

Note that $\mathbf{r}_0$ is a vector that describes an arbitrary displacement so that in principle the two circles are not the same. In this example the family of all possible homeomorphisms is given by

$$\theta'(\theta, t) = \theta + t\sin\left(\frac{k\theta}{2}\right), \tag{1.3}$$

where the family is labeled by the parameter $t$ and $k$ is a non-zero integer. Note that if $t = 0$, $\theta' = \theta$, so that $\mathbf{r} = \mathbf{r}_0 + \mathbf{r}'$. Moreover, if we also suppose that $\mathbf{r}_0 = \mathbf{0}$, equation (1.2) now describes the identity map, that is:

$$\mathbf{r} = (\cos\theta, \sin\theta) = \mathbf{r}'. \tag{1.4}$$

Note that for $\theta = 0$ and $\theta = 2\pi$ the term $\sin\left(\frac{k\theta}{2}\right) = 0$, and therefore for any $t$ we have a map from one circle to another and any map of the family can be continuously deformed into another circle if $t$ is varied. These maps are homotopic to each other [1].

### The Winding Number

To fix ideas, let us consider a family of maps defined by

$$\theta'(\theta, t) = m\theta + t\sin\left(\frac{k\theta}{2}\right), \tag{1.5}$$

where $m$ is a non-zero integer. As we can see, equation (1.3) is a particular case ($m = 1$) of equation (1.5). Now we are interested in studying the case with $m = -1$. As we saw before, $m = 1$ is a homeomorphism between two spaces (unit circles). The difference between this mapping and the one described by $m = -1$ is that the path of the latter has opposite direction than the former one. The two maps are not homotopic [1].

The integer parameter $m$ is called the *winding number* and describes the homotopy class for these maps. The rule for a continuous transformation is the following: all maps with the same value of $m$ can be deformed into each other (no matter the value of $k$ and $t$), while the maps with different values of $m$ cannot be continuously deformed into each other. It is important to mention that it is not possible to have a circle with zero radio because the mapping

needs to travel around the circle [1].

For a general map $\theta' = f(\theta)$, the winding number is defined by

$$m = \frac{1}{2\pi} \int_0^{2\pi} d\theta \frac{df}{d\theta}. \tag{1.6}$$

If we go back to the example of mapping unit circles, the distance traveled is $2\pi m$. $\theta$ can be thought of time, and $\frac{df}{d\theta}$ its velocity [1].

In order to give the winding number a meaning, we can think of two unit circles, each one with its own position vector indicating its orientation. One of the circles is a rubber band and the other is a solid circle. Now, suppose that we wrap the solid circle using the rubber band. In this example $m$ represents the number of times that the rubber band wraps around the solid circle. If the orientation of the circles is the same, then $m > 0$, otherwise $m < 0$ [1].

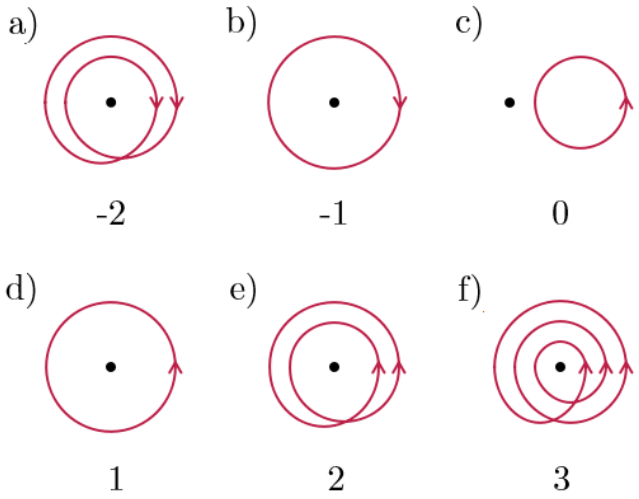


**Figure 1.3:** The winding number can be seen as the number of times that a rubber circumference (red circle) can wrap the rigid circle (black circle). The winding number is positive if the orientation vector of both is in the same direction (images d, e, and, f) and negative if it is not (images a and b). Image from Jim Belk (in public domain).

After this very brief introduction to topology, we have the appropriate tools to understand an important concept that we will explore in this thesis: the Berry phase.

## 1.2 Adiabatic Evolution and the Geometry of the Hilbert Space

The Hilbert space is a linear vector space generated by orthonormal complex vectors, equipped by an inner product [4]. In this section we are interested in studying the geometry of the Hilbert

space, where physical states are represented by *rays*. More precisely, a ray is defined as the equivalence class of non-zero vectors in the Hilbert space related to each other by an overall complex number [1]. That is, we say two vectors $\mathbf{v}$ and $\mathbf{w}$ are equivalent, denoted as $\mathbf{v} \sim \mathbf{w}$, if $\mathbf{v} = \lambda\mathbf{w}$ with $\lambda \in \mathbb{C}$. If the physical states, are chosen to be normalized as they usually are, then $\lambda = \mathrm{e}^{i\theta}$, with $\theta$ a global phase.

One important concept is the *adiabatic evolution* of a given Hamiltonian in its parameter space. In this section, by adiabatic we mean that the Hamiltonian is varied slowly enough, more precisely if $t_\mathrm{e}$ is a time scale related to some external protocol of the time evolution of the Hamiltonian, then we must have that $t_\mathrm{e} \gg t_\mathrm{i}$, where $t_\mathrm{i}$ are the relaxation times related to the eigenenergies of said Hamiltonian. Then, the adiabatic theorem tells us that when an initial Hamiltonian $H_\mathrm{i}$ is adiabatically evolved into a final Hamiltonian $H_\mathrm{f}$, the $n$th eigenstate of $H_\mathrm{i}$ can be transformed into the $n$th eigenstate of $H_\mathrm{f}$ if there are not phase transitions [1].

To study the evolution in the Hilbert space we are going to follow the analysis presented by Girvin and Yang [1]. Let us consider the following Hamiltonian:

$$H(t) = H[\boldsymbol{\mathcal{P}}(t)], \tag{1.7}$$

so that the time dependence is given in terms of a set of parameters $\boldsymbol{\mathcal{P}}$:

$$\boldsymbol{\mathcal{P}} = (\mathcal{P}_1, \mathcal{P}_2, ..., \mathcal{P}_D), \tag{1.8}$$

which can be understood as a vector in a $D$-dimensional parameter space. Note that $D$ is not necessarily related to the spatial dimension $d$ of the physical system. For each $\boldsymbol{\mathcal{P}}$, we can assume that the Hamiltonian given by equation (1.7) has a set of orthonormal eigenstates

$$H(\boldsymbol{\mathcal{P}})\,|n(\boldsymbol{\mathcal{P}})\rangle = \mathcal{E}_n(\boldsymbol{\mathcal{P}})\,|n(\boldsymbol{\mathcal{P}})\rangle\,. \tag{1.9}$$

Let us assume that the spectrum of the Hamiltonian is discrete and non-degenerate. Then, by the adiabatic theorem, if the system is initially in the $n$th eigenstate of the Hamiltonian, that is,

$$|\psi_n(t=0)\rangle = |n[\boldsymbol{\mathcal{P}}(t=0)]\rangle\ , \tag{1.10}$$

then its evolution is given by

$$|\psi_n(t)\rangle = C_n(t)\,|n[\boldsymbol{\mathcal{P}}(t)]\rangle\ . \tag{1.11}$$

Recall that if the Hamiltonian does not depend explicitly on time, $C_n(t)$ becomes:

$$C_n(t) = \mathrm{e}^{-i\mathcal{E}_n t/\hbar}. \tag{1.12}$$

If, however, the Hamiltonian is time-dependent, under adiabatic evolution $C_n(t)$ is

$$C_n(t) = \mathrm{e}^{i\gamma_n(t)}\exp\left[-\frac{i}{\hbar}\int_0^t dt'\mathcal{E}_n(t')\right]. \tag{1.13}$$

Note that in this last equation we have an additional phase $\gamma_n(t)$ (whose origin can be seen in Appendix A). Let us try to understand the physics behind it. In order to do that, we start from the Schrödinger equation:

$$i\hbar\frac{d}{dt}\left|\psi_n(t)\right\rangle = H[\boldsymbol{\mathcal{P}}(t)]\left|\psi_n(t)\right\rangle\,, \tag{1.14}$$

where $|\psi_n(t)\rangle$ is given by equation (1.11). Then, take the inner product on both sides of the last equation, and use the expression for $C_n(t)$ given by equation (1.13), so that

$$\begin{aligned}
\mathcal{E}_n(t) &= \langle n[\boldsymbol{\mathcal{P}}(t)]|\, C_n^*\, H\, C_n\, |n[\boldsymbol{\mathcal{P}}(t)]\rangle \\
&= i\hbar C_n^*(t)\,\langle n[\boldsymbol{\mathcal{P}}(t)]|\,\frac{d}{dt}\,|C_n(t)n[\boldsymbol{\mathcal{P}}(t)]\rangle \\
&= i\hbar\,\langle n[\boldsymbol{\mathcal{P}}(t)]|\,\frac{d}{dt}\,|n[\boldsymbol{\mathcal{P}}(t)]\rangle + i\hbar C_n^*\,\langle n[\boldsymbol{\mathcal{P}}(t)]|\,\frac{dC_n(t)}{dt}\,|n[\boldsymbol{\mathcal{P}}(t)]\rangle \\
&= i\hbar\,\langle n[\boldsymbol{\mathcal{P}}(t)]|\,\frac{d}{dt}\,|n[\boldsymbol{\mathcal{P}}(t)]\rangle - \hbar\frac{d\gamma_n(t)}{dt} + \mathcal{E}_n(t).
\end{aligned} \tag{1.15}$$

Hence,

$$\frac{d}{dt}\gamma_n(t) = i\,\langle n[\boldsymbol{\mathcal{P}}(t)]|\,\frac{d}{dt}\,|n[\boldsymbol{\mathcal{P}}(t)]\rangle\,. \tag{1.16}$$

## 1.3 The Berry Connection and the Geometric Phase

To proceed further in our discussion, let us define the *Berry connection* as:

$$\boldsymbol{\mathcal{A}}^n(\boldsymbol{\mathcal{P}}) = i\,\langle n(\boldsymbol{\mathcal{P}})|\,\frac{\partial}{\partial\boldsymbol{\mathcal{P}}}\,|n(\boldsymbol{\mathcal{P}})\rangle\,. \tag{1.17}$$

This definition is going to be useful when computing the so-called *Berry phase*. Now we can integrate the differential equation that appears in equation (1.16)

$$\int_0^t dt'\frac{d}{dt'}\gamma_n(t') = \int_0^t dt' i\,\langle n[\boldsymbol{\mathcal{P}}(t')]|\,\frac{d}{dt'}\,|n[\boldsymbol{\mathcal{P}}(t')]\rangle\,, \tag{1.18}$$

so that

$$\gamma_n(t) - \gamma_n(0) = i\int_0^t \langle n[\boldsymbol{\mathcal{P}}(t')]|\frac{d}{dt'}|n[\boldsymbol{\mathcal{P}}(t')]\rangle\, dt'\,. \tag{1.19}$$

Notice furthermore that

$$\frac{d\,|n[\boldsymbol{\mathcal{P}}(t')]\rangle}{dt'} = \sum_{\mu} \frac{\partial\,|n(\boldsymbol{\mathcal{P}})\rangle}{\partial \mathcal{P}_{\mu}} \frac{d\mathcal{P}_{\mu}}{dt'} = \frac{\partial\,|n(\boldsymbol{\mathcal{P}})\rangle}{\partial \boldsymbol{\mathcal{P}}} \cdot \frac{d\boldsymbol{\mathcal{P}}}{dt'} \tag{1.20}$$

so that the phase $\gamma_n$ is

$$\gamma_n(t) - \gamma_n(0) = i \int_0^t \langle n(\boldsymbol{\mathcal{P}})|\, \frac{\partial}{\partial \boldsymbol{\mathcal{P}}}\, |n(\boldsymbol{\mathcal{P}})\rangle \cdot d\boldsymbol{\mathcal{P}}\,, \tag{1.21}$$

or in terms of the Berry connection (equation (1.17)) the phase associated to the path $C$ that $\boldsymbol{\mathcal{P}}$ follows in the parameter space can be written as

$$\gamma_n(t) = \int_C \boldsymbol{\mathcal{A}}^n(\boldsymbol{\mathcal{P}}) \cdot d\boldsymbol{\mathcal{P}}\,, \tag{1.22}$$

where we have taken $\gamma_n(0) = 0$ for simplicity [1].

Thus from the two phases that appear in equation (1.13), the first one is given by the equation (1.22) which only depends on the path $C$. This implies that $\gamma_n$ has a *geometric* origin and therefore is usually referred to as the *geometric phase*. The other phase in equation (1.13) depends on the time integral of the energy spectrum. This phase is called the *dynamical phase* [1].

One can show that the geometric phase, given by equation (1.22), has the following properties:

1. It is real.
2. It is related to the Berry connection, which is also real.
3. The geometric phase is gauge-dependent, so it is not an observable.[1]

Following [1], the first property can be proven by noticing first that since $\langle n(\boldsymbol{\mathcal{P}})|n(\boldsymbol{\mathcal{P}})\rangle = 1$, then

$$\begin{aligned} \frac{\partial}{\partial \boldsymbol{\mathcal{P}}} \langle n(\boldsymbol{\mathcal{P}})|n(\boldsymbol{\mathcal{P}})\rangle &= \langle \partial n(\boldsymbol{\mathcal{P}})/\partial \boldsymbol{\mathcal{P}}|n(\boldsymbol{\mathcal{P}})\rangle + \langle n(\boldsymbol{\mathcal{P}})|\partial n(\boldsymbol{\mathcal{P}})/\partial \boldsymbol{\mathcal{P}}\rangle \\ &= 2\,\mathrm{Re}\Big[\, \langle n(\boldsymbol{\mathcal{P}})|\partial n(\boldsymbol{\mathcal{P}})/\partial \boldsymbol{\mathcal{P}}\rangle \,\Big] \\ &= 0. \end{aligned} \tag{1.23}$$

[1] According to Anton Capri [5], in quantum mechanics an *observable* can be defined as: "any physical quantity whose value is obtained by a definite physical operation". The observable $\mathcal{O}$ is represented in Hilbert space by a self-adjoint operator $\mathcal{O}$. If we take the expectation value of this operator in one specific gauge, the result must be equal to the expectation value obtained in some other gauge. If this weren't true, this would mean that the observable depends on the gauge, which cannot be physical accepted [5, 6].

Therefore the Berry connection and the geometric phase are real.

The third property can be shown by doing a phase change to the geometric phase with the purpose of seeing if there is a gauge dependence. More precisely, consider

$$|n(\boldsymbol{\mathcal{P}})\rangle \to \mathrm{e}^{i\zeta(\boldsymbol{\mathcal{P}})}\,|n(\boldsymbol{\mathcal{P}})\rangle \tag{1.24}$$

so that the Berry connection changes as

$$\begin{aligned}\boldsymbol{\mathcal{A}}^n(\boldsymbol{\mathcal{P}}) &\to i\,\langle n(\boldsymbol{\mathcal{P}})|\, i\frac{\partial\zeta(\boldsymbol{\mathcal{P}})}{\partial\boldsymbol{\mathcal{P}}} + \frac{\partial}{\partial\boldsymbol{\mathcal{P}}}\,|n(\boldsymbol{\mathcal{P}})\rangle \\ &= \boldsymbol{\mathcal{A}}^n(\boldsymbol{\mathcal{P}}) - \frac{\partial\zeta(\boldsymbol{\mathcal{P}})}{\partial\boldsymbol{\mathcal{P}}},\end{aligned} \tag{1.25}$$

and, consequently, the geometric phase becomes

$$\begin{aligned}\gamma_n &\to i\int_0^t \langle n(\boldsymbol{\mathcal{P}})|\,\frac{\partial}{\partial\boldsymbol{\mathcal{P}}}\,|\mathrm{e}^{i\zeta(\boldsymbol{\mathcal{P}})}n(\boldsymbol{\mathcal{P}})\rangle\,d\boldsymbol{\mathcal{P}} \\ &= \int_C \boldsymbol{\mathcal{A}}^n(\boldsymbol{\mathcal{P}})\cdot d\boldsymbol{\mathcal{P}} - \int_0^t \langle n(\boldsymbol{\mathcal{P}})|\,\frac{\partial\zeta(\boldsymbol{\mathcal{P}})}{\partial\boldsymbol{\mathcal{P}}}\,|n(\boldsymbol{\mathcal{P}})\rangle\cdot d\boldsymbol{\mathcal{P}} \\ &= \gamma_n - \zeta[\boldsymbol{\mathcal{P}}(0)] + \zeta[\boldsymbol{\mathcal{P}}(t)].\end{aligned} \tag{1.26}$$

This change indicates a gauge dependence in the geometric phase and in the Berry connection, implying that the geometric phase cannot be an observable [1].

## 1.4 The Berry Phase and the Berry Curvature

In the previous section we have shown that the Berry connection and the geometric phase are gauge dependent. In 1984, Berry [7] considered a system that varies under an adiabatic process and for which the initial and final points in the parameter space are the same, so that

$$\boldsymbol{\mathcal{P}}(t_0) = \boldsymbol{\mathcal{P}}(t_f)\,. \tag{1.27}$$

Since the path followed in the parameter space is a loop, we will express the geometric phase, equation (1.22), as follows:

$$\gamma_n = \oint \boldsymbol{\mathcal{A}}^n(\boldsymbol{\mathcal{P}})\cdot d\boldsymbol{\mathcal{P}}\,. \tag{1.28}$$

This is the so-called *Berry phase*. Since the Berry phase is in a closed loop, it is gauge independent. This implies, as we will exemplify below, that interesting physical consequences may appear when $\gamma_n \neq 0$ [1].

Mathematically, the Berry phase can be expressed as a flux passing through a loop in parameter space. From this point of view, the Berry connection is mathematically similar to a magnetic vector potential so one could look for an object that plays a similar role to that of the electromagnetic field tensor, an anti-symmetric rank-two tensor field that lives in the Minkowski space. This is so-called the *Berry curvature* and it is defined as follows:

$$\omega^n_{\mu\nu}(\boldsymbol{\mathcal{P}}) = \partial_{\mathcal{P}_\mu}\mathcal{A}^n_\nu(\boldsymbol{\mathcal{P}}) - \partial_{\mathcal{P}_\nu}\mathcal{A}^n_\mu(\boldsymbol{\mathcal{P}}). \tag{1.29}$$

One can show that the Berry curvature is a rank-two tensor of dimension $D \times D$ [1]. Now, using Stokes' theorem and the Berry curvature we can rewrite the Berry phase as

$$\gamma_n = \int_{\partial S} \boldsymbol{\mathcal{A}}^n(\boldsymbol{\mathcal{P}}) \cdot d\boldsymbol{\mathcal{P}} = \frac{1}{2}\int_S d\mathcal{P}_\mu \wedge d\mathcal{P}_\nu\, \omega^n_{\mu\nu}(\boldsymbol{\mathcal{P}}), \tag{1.30}$$

where $\partial S$ is the loop that encloses the surface $S$ in the parameter space, $d\mathcal{P}_\mu \wedge d\mathcal{P}_\nu$ is an infinitesimal element of surface that is oriented[2], and the factor $\frac{1}{2}$ is necessary to avoid adding twice every element due to Einstein's summation convention [1].

Now that the Berry phase and curvature have been defined, we can explore the different forms that they take depending on the dimension of the parameter space. Clearly, in one dimension, the Berry phase does not exist. On the other hand, in three dimensions the Berry curvature can be nicely written as

$$\begin{aligned} \omega^n_{\mu\nu_{D=3}} &= \Big[\partial_{\mathcal{P}_\mu}\mathcal{A}^n_\nu - \partial_{\mathcal{P}_\nu}\mathcal{A}^n_\mu\Big]_{D=3} = (\delta_{\mu\alpha}\delta_{\nu\beta} - \delta_{\nu\alpha}\delta_{\mu\beta})\partial_{\mathcal{P}_\alpha}\mathcal{A}^n_\beta \\ &= \epsilon_{\lambda\alpha\beta}\,\epsilon_{\lambda\mu\nu}\,\partial_{\mathcal{P}_\alpha}\mathcal{A}^n_\beta = \epsilon_{\lambda\mu\nu}\, b^n_\lambda, \end{aligned} \tag{1.31}$$

where we have introduced

$$b^n_\lambda = \epsilon_{\lambda\mu\nu}\partial_{\mathcal{P}_\mu}\mathcal{A}^n_\nu. \tag{1.32}$$

This vector can be expressed in a three-dimensional ($D = 3$) parameter space as

$$\begin{aligned} \mathbf{b}^n(\boldsymbol{\mathcal{P}}) &= \boldsymbol{\nabla}_{\boldsymbol{\mathcal{P}}} \times \boldsymbol{\mathcal{A}}^n \\ &= i\boldsymbol{\nabla}_{\boldsymbol{\mathcal{P}}} \times \langle n(\boldsymbol{\mathcal{P}})| \frac{\partial}{\partial \boldsymbol{\mathcal{P}}} |n(\boldsymbol{\mathcal{P}})\rangle \ , \end{aligned} \tag{1.33}$$

or more explicitly

$$\begin{aligned} b^n_\lambda &= \epsilon_{\lambda\mu\nu}\partial_{P\mu}\langle n_P|\partial_{P_\nu} n_P\rangle \\ &= \epsilon_{\lambda\mu\nu}\Big(\langle \partial_{P_\mu} n_P|\partial_{P_\nu} n_P\rangle + \langle n_P|\partial_{P_\mu}\partial_{P_\nu} n_P\rangle\Big), \end{aligned} \tag{1.34}$$

[2]The wedge product, also known as exterior product ($\wedge$), of $p$ differentiable forms results in a $p-$form. A $p-$form, is a special tensor that defines a $p-$dimensional and oriented surface element in the manifold and it gives the proper integrand to be used in surface integrals [8].

that is

$$\mathbf{b}^n = \langle \boldsymbol{\nabla}_{\boldsymbol{\mathcal{P}}} n(\boldsymbol{\mathcal{P}}) | \times | \boldsymbol{\nabla}_{\boldsymbol{\mathcal{P}}} n(\boldsymbol{\mathcal{P}}) \rangle \,. \tag{1.35}$$

Furthermore, we see that in a $D = 3$ parameter space it is possible to rewrite the Berry curvature, so that

$$\gamma_n = \int_S \mathbf{b}^n \cdot d\mathbf{S} = \int_S (\boldsymbol{\nabla}_{\boldsymbol{\mathcal{P}}} \times \boldsymbol{\mathcal{A}}^n) \cdot d\mathbf{S}. \tag{1.36}$$

This result invokes a similarity between Berry phase an a magnetic flux. Due to this, in a three-dimensional parameter space, the Berry phase is also known as the *Berry flux*.

Going back to the general case, we are interested on rewriting equation (1.29) as

$$\begin{aligned} \omega^n_{\mu\nu}(\boldsymbol{\mathcal{P}}) &= i\partial_{\mathcal{P}_\mu} \langle n(\boldsymbol{\mathcal{P}}) | \partial_{\mathcal{P}_\nu} n(\boldsymbol{\mathcal{P}}) \rangle + i\partial_{\mathcal{P}_\nu} \langle n(\boldsymbol{\mathcal{P}}) | \partial_{\mathcal{P}_\mu} n(\boldsymbol{\mathcal{P}}) \rangle \\ &= i[\, \langle \partial_{\mathcal{P}_\mu} n(\boldsymbol{\mathcal{P}}) | \partial_{\mathcal{P}_\nu} n(\boldsymbol{\mathcal{P}}) \rangle + \langle n(\boldsymbol{\mathcal{P}}) | \partial_{\mathcal{P}_\mu} \partial_{\mathcal{P}_\nu} n(\boldsymbol{\mathcal{P}}) \rangle \\ &\quad - \langle \partial_{\mathcal{P}_\nu} n(\boldsymbol{\mathcal{P}}) | \partial_{\mathcal{P}_\mu} n(\boldsymbol{\mathcal{P}}) \rangle - \langle n(\boldsymbol{\mathcal{P}}) | \partial_{\mathcal{P}_\nu} \partial_{\mathcal{P}_\mu} n(\boldsymbol{\mathcal{P}}) \rangle \,] \\ &= i[\, \langle \partial_{\mathcal{P}_\mu} n(\boldsymbol{\mathcal{P}}) | \partial_{\mathcal{P}_\nu} n(\boldsymbol{\mathcal{P}}) \rangle - \langle \partial_{\mathcal{P}_\nu} n(\boldsymbol{\mathcal{P}}) | \partial_{\mathcal{P}_\mu} n(\boldsymbol{\mathcal{P}}) \rangle \,] \end{aligned} \tag{1.37}$$

Finally, we are going to derive a formula that allows to compute the Berry curvature easily. This formula does not depend on the eigenstate variation in $\boldsymbol{\mathcal{P}}$. Following [1] we first notice that:

$$\begin{aligned} \left( \frac{\partial H}{\partial \mathcal{P}_\nu} \right) | n(\boldsymbol{\mathcal{P}}) \rangle &= \frac{\partial}{\partial \mathcal{P}_\nu} [H \, | n(\boldsymbol{\mathcal{P}}) \rangle \,] - H \frac{\partial}{\partial \mathcal{P}_\nu} \, | n(\boldsymbol{\mathcal{P}}) \rangle \\ &= \left( \frac{\partial \mathcal{E}_n}{\partial \mathcal{P}_\nu} \right) | n(\boldsymbol{\mathcal{P}}) \rangle + (\mathcal{E}_n - H) \, | \partial_{\mathcal{P}_\nu} n(\boldsymbol{\mathcal{P}}) \rangle \,. \end{aligned} \tag{1.38}$$

Doing the inner product of this result with $\langle n'(\boldsymbol{\mathcal{P}})|$, for $n \neq n'$ we have that

$$\begin{aligned} \langle n'(\boldsymbol{\mathcal{P}})| \left( \frac{\partial H}{\partial \mathcal{P}_\nu} \right) | n(\boldsymbol{\mathcal{P}}) \rangle &= \langle n'(\boldsymbol{\mathcal{P}})| \, \frac{\partial \mathcal{E}_n}{\partial \mathcal{P}_\nu} \, | n(\boldsymbol{\mathcal{P}}) \rangle + \langle n'(\boldsymbol{\mathcal{P}})| \, \mathcal{E}_n - H \, | \partial_{\mathcal{P}_\nu} n(\boldsymbol{\mathcal{P}}) \rangle \\ &= (\mathcal{E}_n - \mathcal{E}_{n'}) \, \langle n'(\boldsymbol{\mathcal{P}}) | \partial_{\mathcal{P}_\nu} n(\boldsymbol{\mathcal{P}}) \rangle \,. \end{aligned} \tag{1.39}$$

Analogously, we can also write

$$\begin{aligned} \langle n(\boldsymbol{\mathcal{P}})| \left( \frac{\partial H}{\partial \mathcal{P}_\mu} \right) | n'(\boldsymbol{\mathcal{P}}) \rangle &= \langle n(\boldsymbol{\mathcal{P}})| \, \mathcal{E}_{n'} - H \, | \partial_{\mathcal{P}_\mu} n'(\boldsymbol{\mathcal{P}}) \rangle \\ &= (\mathcal{E}_{n'} - \mathcal{E}_n) \, \langle n(\boldsymbol{\mathcal{P}}) | \partial_{\mathcal{P}_\mu} n'(\boldsymbol{\mathcal{P}}) \rangle \,, \end{aligned} \tag{1.40}$$

and using these results in the Berry curvature, this can be expressed as

$$\begin{aligned}\omega^n_{\mu\nu} &= i\sum_{n\neq n'} \langle \partial_{\mathcal{P}_\mu} n(\boldsymbol{\mathcal{P}})|n'(\boldsymbol{\mathcal{P}})\rangle \langle n'(\boldsymbol{\mathcal{P}})|\partial_{\mathcal{P}_\nu} n(\boldsymbol{\mathcal{P}})\rangle - c.c. \\ &= i\sum_{n\neq n'} \frac{\langle n(\boldsymbol{\mathcal{P}})|\,\frac{\partial H}{\partial \mathcal{P}_\mu}\,|n'(\boldsymbol{\mathcal{P}})\rangle \langle n'(\boldsymbol{\mathcal{P}})|\,\frac{\partial H}{\partial \mathcal{P}_\nu}\,|n(\boldsymbol{\mathcal{P}})\rangle}{\left(\mathcal{E}_n - \mathcal{E}_{n'}\right)^2} - c.c,\end{aligned} \tag{1.41}$$

where there is no dependence on the variation of the eigenstate $|n(\boldsymbol{\mathcal{P}})\rangle$. This formula is useful because allows us to calculate the Berry curvature for fixed eigenstates [1].

In the next section, we will show a non-trivial example of the Berry phase: the Aharonov-Bohm phase.

### 1.4.1 The Berry Phase in the Aharonov-Bohm Effect

As we have mentioned before, sometimes the Berry phase is non-trivial and it contains interesting physics, as in the case of the Aharonov-Bohm effect. To understand this phenomenon, think of a solid wall barrier that prohibits charge particles to get inside it. Inside the barrier, a magnetic flux $\Phi$ passes through in the $\hat{\mathbf{z}}$ direction. According to classical physics the charged particles are not affected by the magnetic field, as this is inside the wall. Recall also that

$$\mathbf{B} = \boldsymbol{\nabla} \times \mathbf{A}, \tag{1.42}$$

where $\mathbf{B}$ is the magnetic field and $\mathbf{A}$ is the vector potential. A classical charged particle outside the barrier would experience classical free motion because it does not sense the magnetic field, that is, it does not experience a Lorentz force. From a quantum mechanical point of view, however, things are more interesting. There are many possible paths that the charged particle can take and there are certain paths that cannot be transformed into each other continuously: they are topological different. Every non-equivalent path has a different length, corresponding quantum amplitude and winding number. Because of this, the effect between the complex amplitudes related to the path and the magnetic flux is non-trivial, even though we still have that

$$\boldsymbol{\nabla} \times \mathbf{A} = \mathbf{0}, \tag{1.43}$$

but whose contour integral of the vector potential is however

$$\oint d\mathbf{r} \cdot \mathbf{A}(\mathbf{r}) = n\Phi\,. \tag{1.44}$$

Here $n$ is the winding number and $\Phi$ is the magnetic flux inside the barrier [1].

The importance of this phenomenon is the global effect that produces: charged particles

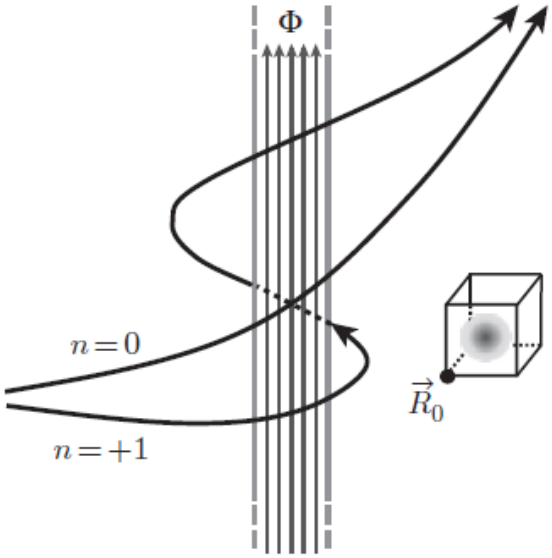


**Figure 1.4:** Schematic diagram of the system. A magnetic field is oriented in to the $\hat{\mathbf{z}}$ direction, around it there is hard wall barrier that keeps the flux confined. In classical physics, if there is a particle outside the barrier it does not perceive the magnetic flux and so, does not experience a Lorentz force. Quantum mechanically, there is a non-trivial effect between the magnetic flux and the complex amplitudes related to every possible different topological path (labeled with a different winding number). The box in the right side of the diagram indicates a box that contains a particle. This box allow us to do an adiabatic analysis of a charged particle traveling around the flux. Image from [1].

are scattered by the flux tube (in classical physics this would not be observed). This scattering is proportional to the charge $q$ and the total magnetic flux $\Phi$. In this case, the path-integral formalism of Feynman is very useful as it accounts for all trajectories. This formalism indicates that any trajectory $\mathbf{r}(t)$ is associated to an amplitude

$$\mathrm{e}^{\frac{i}{\hbar}S[\mathbf{r}]}, \tag{1.45}$$

where $S$ is the *classical action*, defined as

$$S(\mathbf{r}) = \int_0^t d\tau \mathcal{L}(\dot{\mathbf{r}}, \mathbf{r}), \tag{1.46}$$

where $\mathcal{L}$ is the classical Lagrangian. Because of the presence of the vector potential, the Lagrangian must be rewritten as

$$\mathcal{L} \to \mathcal{L} + [-e\mathbf{A}(\mathbf{r}) \cdot \dot{\mathbf{r}}], \tag{1.47}$$

and, as a consequence, the amplitude is

$$\exp\left[\frac{i}{\hbar}\int d\tau[\mathcal{L} - e\mathbf{A}(\mathbf{r}) \cdot \dot{\mathbf{r}}]\right], \tag{1.48}$$

which has a phase that depends on the vector potential, that is

$$\theta = -\frac{e}{\hbar}\int \mathbf{A}(\mathbf{r})\cdot d\mathbf{r}, \tag{1.49}$$

and following equation (1.44), it can bee seen that this phase depends in the winding number. Using that the quantum flux is

$$\Phi_0 = \frac{h}{e}, \tag{1.50}$$

the Aharonov-Bohm phase becomes

$$\theta = -\frac{e}{\hbar}\oint d\mathbf{r}\cdot\mathbf{A}(\mathbf{r}) = -\frac{e}{\hbar}n\Phi = -\frac{2\pi e}{h}n\Phi = -2\pi n\frac{\Phi}{\Phi_0}. \tag{1.51}$$

In this example the Aharonov-Bohm phase is equal to the Berry phase that arises from the adiabatic transport of an electron around a flux tube [1].

To do the analysis of the adiabatic transport of a electron around the flux tube, an excitation gap in the Hamiltonian is necessary. This gap can be introduced by supposing that either the electron is inside a box with hard walls or that it is inside another confining potential. The Hamiltonian of the model is

$$H = \frac{1}{2m_\mathrm{e}}\left[\mathbf{p} + \frac{e}{c}\mathbf{A}(\mathbf{r})\right]^2 + V(\mathbf{r}-\mathbf{R}_0), \tag{1.52}$$

where $\mathbf{R}_0$ indicates the position of one of the box's corner. To simplify the derivation, let us assume that the box orientation is fixed, this neglects any relation between the potential and $\mathbf{R}_0$. In this model, $\boldsymbol{\mathcal{P}} = \mathbf{R}_0$ [1]. Assume also, that the box, and as a consequence the particle, is always outside the magnetic flux tube, so the magnetic field is zero, $\boldsymbol{\nabla}\times\mathbf{A} = \mathbf{0}$, but the vector potential is not $\mathbf{A} \neq \mathbf{0}$. If the vector potential is proportional to a gradient function, both conditions are followed, so

$$\mathbf{A}(\mathbf{r}) = \frac{\Phi_0}{2\pi}\boldsymbol{\nabla}\chi(\mathbf{r}), \tag{1.53}$$

and must satisfy that

$$\oint d\mathbf{r}\cdot\mathbf{A} = \frac{\Phi_0}{2\pi}\oint d\mathbf{r}\cdot\boldsymbol{\nabla}\chi(\mathbf{r}) \equiv n\Phi. \tag{1.54}$$

A possible expression

$$\chi(\mathbf{r}) = \frac{\Phi}{\Phi_0}\varphi(\mathbf{r}), \tag{1.55}$$

where $\varphi(\mathbf{r})$ is the azimuthal angle of the point $\mathbf{r}$.

In the case that the quantum ground state wave function is $\xi_0(\mathbf{r}-\mathbf{R}_0)$ when $\mathbf{A} = 0$ in all

the space, the Schrödinger equation is

$$\psi(\mathbf{r}) = \mathrm{e}^{-i\chi_{\mathbf{R}_0}(\mathbf{r})}\xi_0(\mathbf{r}-\mathbf{R}_0), \tag{1.56}$$

where

$$\chi_{\mathbf{R}_0}(\mathbf{r}) \equiv \frac{2\pi}{\Phi_0}\int_{\mathbf{R}_0}^{\mathbf{r}} d\mathbf{r}'\cdot\mathbf{A}(\mathbf{r}'). \tag{1.57}$$

Note that the integral has $\mathbf{r}$ as the upper limit, $\mathbf{R}_0$ as the lower limit and so, it is evaluated for a path that is inside the box. As the vector potential has zero curl inside the box, this function is well-defined. Due to all the possible combinations, this function must be multiplied by a phase $\mathrm{e}^{i\theta}$. Different choices can be taken for $\theta(\mathbf{R}_0)$ (in the parameter space) that correspond to different gauges for $\chi(\mathbf{r})$. For this analysis we choose the values so that

$$\psi(\mathbf{r}) = \mathrm{e}^{i\theta(\mathbf{R}_0)}\mathrm{e}^{-i\chi_{\mathbf{R}_0}(\mathbf{r})}\xi_0(\mathbf{r}-\mathbf{R}_0) \tag{1.58}$$

is real and positive at a point inside the box and different from the corner. This point is $\mathbf{R}_0+\boldsymbol{\Delta}$, and satisfies that $\xi_0(\boldsymbol{\Delta})\neq 0$. We can assume that $\xi_0(\mathbf{r}-\mathbf{R}_0)\in\mathbb{R}$ and that $\xi_0(\boldsymbol{\Delta})>0$. Due to these considerations

$$\theta(\mathbf{R}_0) = \chi_{\mathbf{R}_0}(\mathbf{R}_0+\boldsymbol{\Delta}). \tag{1.59}$$

It can be calculated that

$$\begin{aligned}\boldsymbol{\nabla}_{\mathbf{R}_0}\theta(\mathbf{R}_0) &= \boldsymbol{\nabla}_{\mathbf{R}_0}\chi_{\mathbf{R}_0}(\mathbf{R}_0+\boldsymbol{\Delta})\\ &= \frac{2\pi}{\Phi_0}\boldsymbol{\nabla}_{\mathbf{R}_0}\int_{\mathbf{R}_0}^{\mathbf{R}_0+\boldsymbol{\Delta}} d\mathbf{r}'\cdot\mathbf{A}(\mathbf{r}')\\ &= \frac{2\pi}{\Phi_0}\left[\mathbf{A}(\mathbf{R}_0+\boldsymbol{\Delta})-\mathbf{A}(\mathbf{R}_0)\right],\end{aligned} \tag{1.60}$$

and

$$\begin{aligned}\boldsymbol{\nabla}_{\mathbf{R}_0}\chi_{\mathbf{R}_0}(\mathbf{r}) &= \frac{2\pi}{\Phi_0}\boldsymbol{\nabla}_{\mathbf{R}_0}\int_{\mathbf{R}_0}^{\mathbf{r}} d\mathbf{r}'\cdot\mathbf{A}(\mathbf{r}')\\ &= -\frac{2\pi}{\Phi_0}\mathbf{A}(\mathbf{R}_0).\end{aligned} \tag{1.61}$$

Using this, we find that

$$\begin{aligned}\boldsymbol{\mathcal{A}}(\mathbf{R}_0) &= i\,\langle\psi|\nabla_{\mathbf{R}_0}|\psi\rangle\\ &= i\,\langle\psi|\nabla_{\mathbf{R}_0}|\mathrm{e}^{i\theta(\mathbf{R}_0)}\mathrm{e}^{-i\chi_{\mathbf{R}_0}(\mathbf{r})}\xi_0(\mathbf{r}-\mathbf{R}_0)\rangle\\ &= i^2\,\langle\psi|\nabla_{\mathbf{R}_0}\theta(\mathbf{R}_0)-\nabla_{\mathbf{R}_0}\chi_{\mathbf{R}_0(\mathbf{r})}|\psi\rangle + i\,\langle\psi|\boldsymbol{\nabla}_{\mathbf{R}_0}\xi_0(\mathbf{r}-\mathbf{R}_0)|\mathrm{e}^{i\theta}\mathrm{e}^{-i\chi_{\mathbf{R}_0}}\rangle\\ &= -\frac{2\pi}{\Phi_0}\Big[\mathbf{A}(\mathbf{R}_0+\boldsymbol{\Delta})-\mathbf{A}(\mathbf{R}_0)\Big] + \frac{2\pi}{\Phi_0}\mathbf{A}(\mathbf{R}_0) + \langle\xi_0(\mathbf{r}-\mathbf{R}_0)\boldsymbol{\nabla}_{\mathbf{R}_0}\xi_0(\mathbf{r}-\mathbf{R}_0)\rangle\\ &= -\frac{2\pi}{\Phi_0}\mathbf{A}(\mathbf{R}_0+\boldsymbol{\Delta}) + i\int d^3\mathbf{r}\xi_0(\mathbf{r}-\mathbf{R}_0)\boldsymbol{\nabla}_{\mathbf{R}_0}\xi_0(\mathbf{r}-\mathbf{R}_0).\end{aligned} \tag{1.62}$$

Notice that

$$\begin{aligned} i\int d^3\mathbf{r}\xi_0(\mathbf{r}-\mathbf{R}_0)\boldsymbol{\nabla}_{\mathbf{R}_0}\xi_0(\mathbf{r}-\mathbf{R}_0) &= \frac{i}{2}\int d^3\mathbf{r}\boldsymbol{\nabla}_{\mathbf{R}_0}\xi_0^2(\mathbf{r}-\mathbf{R}_0) \\ &= -\frac{i}{2}\int d^3\mathbf{r}\boldsymbol{\nabla}_{\mathbf{r}}\xi_0^2(\mathbf{r}-\mathbf{R}_0), \end{aligned} \tag{1.63}$$

and if we use the divergence theorem

$$\oint_S \psi\, d\mathbf{S} = \int_V \boldsymbol{\nabla}\psi\, dV, \tag{1.64}$$

we get that

$$i\int d^3\mathbf{r}\xi_0(\mathbf{r}-\mathbf{R}_0)\boldsymbol{\nabla}_{\mathbf{R}_0}\xi_0(\mathbf{r}-\mathbf{R}_0) = -\frac{i}{2}\oint_S \xi_0^2(\mathbf{r}-\mathbf{R}_0)d\mathbf{S} = 0. \tag{1.65}$$

This integral is equal to zero for the surface integral, since the function $\xi_0$ vanishes outside the box. We can write that

$$\boldsymbol{\mathcal{A}}(\mathbf{R}_0) = -\frac{2\pi}{\Phi_0}\mathbf{A}(\mathbf{R}_0+\boldsymbol{\Delta}), \tag{1.66}$$

which indicates that the Berry connection and, as a consequence, the Berry phase are related to the vector potential which in turn is related to a magnetic field [1]. We want to explicitly calculate the Berry phase using equation (1.36)

$$\begin{aligned} \gamma &= \oint d\mathbf{R}_0\cdot\boldsymbol{\mathcal{A}}(\mathbf{R}_0) \\ &= -\frac{2\pi}{\Phi_0}\oint d\mathbf{R}_0\cdot\mathbf{A}(\mathbf{R}_0+\boldsymbol{\Delta}) \\ &= -\frac{2\pi}{\Phi_0}n\Phi. \end{aligned} \tag{1.67}$$

In this case we have shown that the Aharonov-Bohm phase (equation (1.51)) is equal to the Berry phase.

Let us finalize this chapter by introducing another concept: the Chern number.

### 1.4.2 The Chern Number

New quantum phases have arisen with the study of topological quantum matter. These phases differ from the conventional phases: they posses neither symmetry breaking nor a local order parameter. Because of that, topological phases are classified by integer indices that do not change because they are protected, and only change their value when the gap energy is closed. In two-dimensional lattice systems, the topology of the filled bands is given by the *Chern number*. The Chern number is defined as the integral of the Berry curvature in $k$-space ($\mathbf{b}^n(\mathbf{k})$)

in the first Brillouin zone (1BZ):

$$\mathcal{C}_n = \frac{1}{2\pi} \int_{\mathbf{k}\in 1\mathrm{BZ}} \mathbf{b}^n(\mathbf{k}) dk_x dk_y, \tag{1.68}$$

and gives us the eigenvectors winding number. Note that if the band structure changes smoothly, the Berry curvature changes too, but the Chern number remains unchanged [1, 9].

After this chapter, we have the tools to understand the importance of the Berry phase, which is essential in this work. In the next chapter we are seeking to introduce the electron's physics and to explore the physics behind the behaviour of different magnetic materials.

# Chapter 2

# Electron's Physics and Magnetism

## 2.1 A Brief History of Magnetism

To talk about the beginnings of magnetism we need to go back in time 6,000 years, when magnetite was discovered, as the first written records point out, in China. In the period that comprises from 3,000 to 2,500 B.C., the first known primitive compass, made with a magnetite object that had the shape of a spoon, was already developed. There is a military manual (1044 A.D.) where an illustration of a magnetized iron piece, with the shape of a fish, is floating and points to the South. Some years later, a compass made with a magnetic needle was described [10].

In Europe, the most ancient findings about magnetism and descriptions were made by the Greeks. Back then, the discoveries of magnetism were due to people's curiosity to understand the ability of some materials in manipulating objects from a distance [10]. In ancient Greece three main magnetism breakthroughs were made: Plato discovered the magnetic induction, which explains why some magnetized materials can attract others; Lucretius found out that two or more magnetic materials can also repeal each other; moreover they found the existence of two magnetic poles [10].

Other important experiments were made by Gilbert and Descartes, that changed the world. Gilbert (1544-1603) wrote *Magnet*, a book where he reproduced magnetic experiments done before him and introduced his own experiments, observations and results. Also, reproducing Peregrinus' experiments with a terrella (a small magnetized sphere), Gilbert proposed that the Earth is actually a magnet [10].

The first extensive theory of magnetism was done by René Descartes (1596-1650), who wrote his ideas and discoveries in Part IV (sections 133-183) of his *Principia*. He called *threaded parts* to the *effluvia*, a known concept at the time that refers to different magnetic fluids and

explained magnetism [10].

Gilbert and Descartes were great thinkers of their time, whose work touched many areas like physics and philosophy. Gilbert did huge discoveries in magnetism and thought of its philosophical implications. On the other hand, Descartes was a more rigorous man, scientifically speaking, and his work was better grounded. A century latter (1750, approximately), the first signs of what we understand now as modern science appeared [10]. This new era was characterized by the interplay between experimental data and theory. One of the most important scientist of this period was Charles Coulomb (1736-1806), who discovered that the attraction or repulsion forces between two charges is proportional to the inverse of the squared distance between them. He also found that magnetism can be thought of as a magnetic fluid bounded to the molecules due to the polarization it induces by its motion. Then, Siméon Denis Poisson (1781-1840), the mathematician who first studied the static potential, introduced the magnetostatic theory which allowed him to find solutions to many problems. After this, George Green (1793-1841) extended Poisson's work [10].

The path of magnetism changed with the study of the correlation between magnetism and electricity. This opened the door to a new subject: Electrodynamics. The first scientist who worked on this new topic was Hans Christian Oersted (1777-1851) who discovered that a current that passes close to a suspended and magnetized needle moves the needle. After this, André Marie Ampère (1775-1836) found out that the magnetization depends on the direction of electric loop. Then, Michael Faraday (1791-1867) used for the first time the term *magnetic field* and discovered that when polarized light passes through a medium whose magnetization direction is the same than the light beam, the polarization plane rotates, and this change is proportional to the magnetic field. Faraday's research was summarized and extended by James Clerk Maxwell (1831-1879) [10].

Faraday and Maxwell did important contributions to the study of magnetism. Both of them realized that the charge is always present in discrete units. In 1874 Johnstone Stoney suggested the existence of a minimum unit of charge, and in 1891 he coined the term *electron* and used it to name the unit of charge [10] . In 1895 Jean Perrin discovered that an electron beam, also known as the cathode ray, is made of charged particles with negative charge. After this, Thomson estimated accurately the ratio between the charge of the electron and its rest mass. These three discoveries just described, revolutionized the way that Physics was studied, because of the consequences that the existence of the electron produces [10].

As time passed by, scientists focused more to understand the properties of the electron and the physics behind it. Its spin was first detected in 1921 and quantum mechanics started to play an important role in describing magnetism. Throughout this chapter we will introduce some

basic properties of the electron and the role they play to understand the magnetic behaviour of some materials.

## 2.2 Basic Properties of the Electron to Understand Magnetism

In solid materials, some magnetic properties are related to the electrons, whose nature as a particle with negative charge changed how magnetism was studied [11, 12]. In 1924, Louis de Broglie proposed that the wave-particle duality, originally introduced to a photon of light, can be extended to material particles, so that they have an associated wavelength $\lambda$ given by

$$\lambda = \frac{h}{\gamma_{\mathrm{r}} m v}, \tag{2.1}$$

in which $m$ is the mass of the particle, $v$ is its velocity and $\gamma_{\mathrm{r}}$ is the relativistic factor given by

$$\gamma_{\mathrm{r}} = \frac{1}{\sqrt{1 - \frac{v^2}{c^2}}}. \tag{2.2}$$

Notice that $\gamma_{\mathrm{r}} m v = p$ is the particles momentum. Equation (2.1) is referred to as the de Broglie wavelenght [11, 12].

Before this, Niels Bohr postulated the quantization of the electron's angular momentum, that states that the magnitude of this momentum in an atom is quantized in multiples of $\hbar$, that is,

$$|\mathbf{L}| = |\mathbf{r} \times \mathbf{p}| = n\hbar, \tag{2.3}$$

where $\mathbf{L}$ is the angular momentum, $\mathbf{r}$ is the vector between the origin and the position of the particle and $n$ is an integer. This result, together with the de Broglie's wavelength proposition, led to the idea that the electron's allowed orbits are in fact "stationary states with an integral number of de Broglie wavelengths" [12], as it can be seen in Figure 2.1a. Note that a fractional number of de Broglie's wavelengths would result in a destructive pattern of interference [11] (Figure 2.1b).

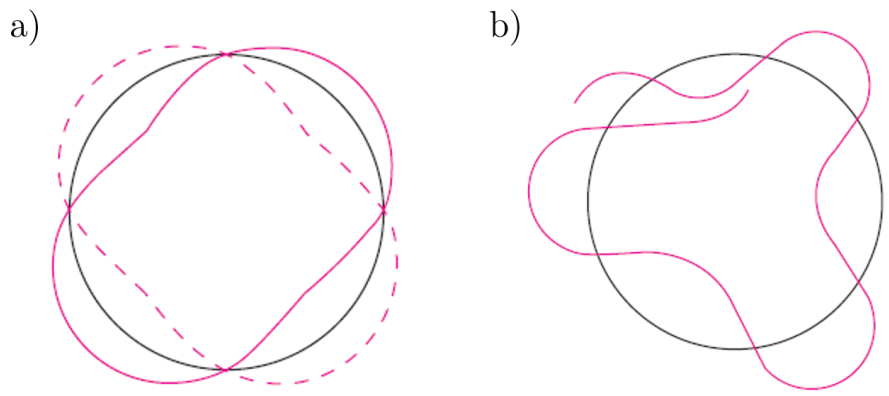


**Figure 2.1:** The electron's orbit are stationary states. a) These states have to be multiple of an integer de Broglie's wavelengths. b) If the number were not a integer, the wave would interfere destructively with itself. Image from [11].

Since the electron's angular momentum is quantized, it is appropriate to study magnetism using quantum theory. With this in mind we are interested on understanding better the two sources of the momentum of the electron: the orbital momentum, that is related to the electron's movement around the nucleus, and the electron's intrinsic momentum: the spin [11].

### 2.2.1 The Orbital Momentum

The orbital momentum can be understood using the Bohr model (see Figure 2.2), in which electrons rotate around the nucleus in circular orbits, whose electric charge is $Ze$, with $Z$ the atomic number. The electrons orbit the nucleus under an electric potential given by

$$\phi_{\mathrm{e}} = -\frac{Ze}{4\pi\epsilon_0 r}, \tag{2.4}$$

where $\epsilon_0$ is the vacuum permittivity [12]. On the other hand, the motion of the electron produces a current loop, that has an associated magnetic momentum, viz.

$$\mathbf{m} = -\frac{e\mathbf{L}}{2m_{\mathrm{e}}}. \tag{2.5}$$

Here $m_{\mathrm{e}}$ is the electron mass and $\mathbf{L} = \mathbf{r} \times \mathbf{p}$ is the angular momentum [12].

Using that the allowed electron orbit has to be proportional to a integer number of de Broglie wavelengths and by the arbitrary consideration of using $\hat{\mathbf{z}}$ as the chosen direction of the spin, the magnetic momentum in this direction is

$$m_z = -\frac{e}{2m_{\mathrm{e}}} m_l \hbar = -\mu_{\mathrm{B}} m_l, \tag{2.6}$$

where $m_l$ is the orbital magnetic quantum number that takes values $m_l = 0, \pm 1, \pm 2, \ldots$ and

$\mu_B = \frac{e\hbar}{2m_e}$ is the Bohr magneton [12].

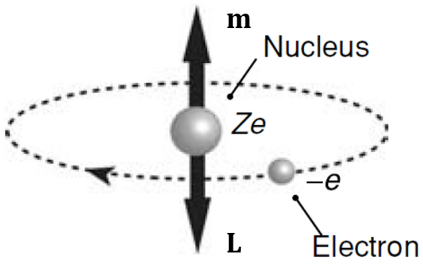


**Figure 2.2:** A schematic representation of an atom. The nucleus with charge $Ze$ is in the center of the atom and, traveling around it, is the electron. The angular momentum points in the direction perpendicular to the electron's orbit, and the magnetic momentum is in the opposite direction [12]. Image from [12].

### 2.2.2 Electron's Spin

The other important property of the electron is its spin, which is an intrinsic angular momentum not related to its motion [12].

At the beginnings of the 1900s, Bohr's theory of the electron, predicted that the electron's angular momentum $\mathbf{L}$ was quantized. Choosing, say, $\hat{\mathbf{z}}$ as a direction of quantization we know that

$$L_z = m_l \hbar, \tag{2.7}$$

where

$$m_l = 0, \pm 1, \pm 2, ..., \pm l, \tag{2.8}$$

where $l$ is the quantum orbital number related to the $|\mathbf{L}|$ by the formula

$$L = \sqrt{l(l+l)}\hbar, \tag{2.9}$$

and $L > L_z$ [11, 12].

Notice that, due to the uncertainty principle, nothing deterministic can be said about the $x$ and $y$ components of $\mathbf{L}$. Thus, according to this principle, the angular momentum can classically be visualized as moving in a cone, so that $L_z$ is determined by the arbitrary choice of the quantization axis, while $L_x$ and $L_y$ remained undetermined [11].

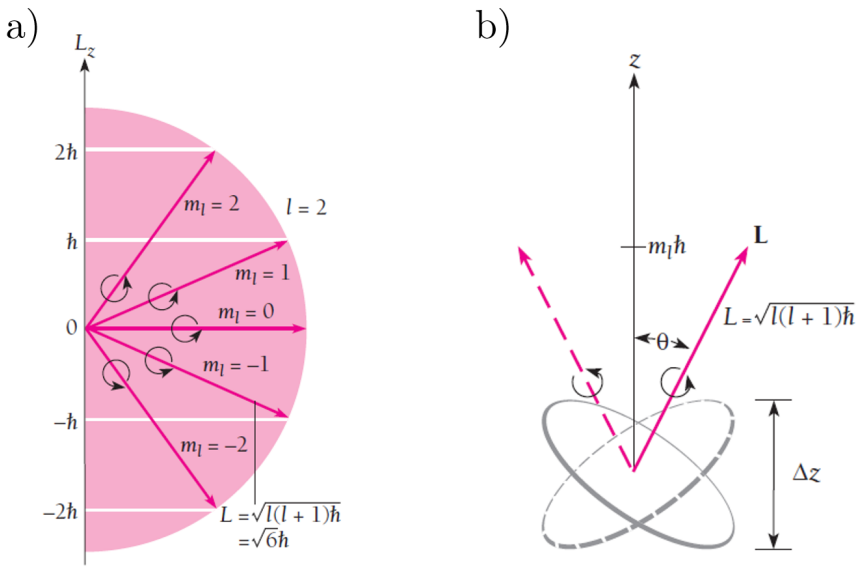


**Figure 2.3:** a) Space quantization of orbital angular momentum to the quantum number $l = 2$. b) The angular momentum must live in a cone due to the uncertainty principle. Image from [11].

In 1921, Otto Stern and Walter Gerlach were trying to assertain experimentally Bohr's theory. Their experiment was made of a beam of silver atoms, that came from a hot oven approximately at 1000 °C. This beam traveled under the effect of a non-homogeneous external magnetic field until the beam stroked a photographic plate that recorded the beam shape. This experiment was designed under the assumption that an electron orbiting around a nucleus produces a magnetic moment that is proportional to the orbital angular momentum. They thought that the silver atoms had a non-zero magnetic momentum and that the magnetic field would generate a torque in the magnetic dipole, so that the atoms would experience a force in the beam direction. What they observed (in the now called Stern-Gerlach experiment) was that the silver atoms stroke the plate only at two points, and they thought that this was the experimental confirmation of Bohr's theory [11].

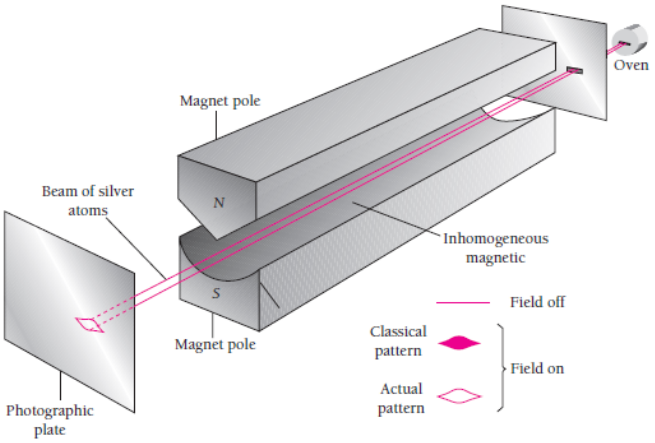


**Figure 2.4:** Schematic diagram of the Stern-Gerlach experiment. A silver beam that comes from a hot oven passes though an non-homogeneous magnetic field and strikes in to a plate. When there is no magnetic field the pattern in the plate should be a straight line. When there is an external magnetic field, they observed that the beam splits in two different points [11]. Image from [11].

However, Stern and Gerlach made a mistake in the interpretation of their results. They had predicted that because of space quantization, the silver beam would split in two components because they thought that the silver atoms have a non-zero angular momentum. In reality silver has a magnetic moment related to the spin (that was not even proposed at that time), because the electronic configuration of silver is

$$\mathrm{Ag}^{47} = [\mathrm{Kr}]4\mathrm{d}^{10}5\mathrm{s}^{1}, \tag{2.10}$$

so it is the spin of the electron in the 5s shell that contributes to the atom's magnetic moment [11, 13].

Four years later, the first idea of the existence of the electron spin was made. Even when the interpretation was later refuted, it had a huge importance because that was the first time (1925) that the idea of the spin was introduced. The authors of this idea were Samuel Goudsmit and George Uhlenbeck. They proposed that every electron had an intrinsic magnetic moment (the spin) that was related to the rotation of the electron (that was thought of as a rigid ball) around its own axis. Even when this approach managed to explain some physical phenomena, when the electron's rotation velocity was computed, they found out that their ideas could not be correct, because the electron would had to rotate with a velocity bigger than $c$ [11].

The idea of the spin saw again the light four years later, when, in 1929, Paul Dirac worked with both quantum mechanics and special relativity to introduce a new theory: relativistic quantum mechanics, which allowed him to explain that there should be a spin associated to

the electron, which is an electron intrinsic magnetic momentum [11].

The spin magnetic quantum number $m_s$ describes the electron's space quantization and can take two different values. The quantum number $m_s = \frac{1}{2}$ for the *spin up* and $m_s = -\frac{1}{2}$ for the *spin down* [11]. The component on $\hat{\mathbf{z}}$ of the spin angular momentum is

$$S_z = m_s\hbar = \pm\frac{1}{2}\hbar. \tag{2.11}$$

The spin magnetic moment $\boldsymbol{\mu}_s$ is

$$\boldsymbol{\mu}_s = -\frac{e}{m_\mathrm{e}}\mathbf{S}, \tag{2.12}$$

where $\mathbf{S}$ is the spin angular momentum. If we are only interested in the $z$ component, the the magnetic moment is

$$\mu_{s_z} = \pm\frac{e\hbar}{2m_\mathrm{e}} = \pm\mu_\mathrm{B}. \tag{2.13}$$

The orbital momentum and spin momentum of the electron are the main sources of the total angular momentum and both interact with each other through the spin-orbit coupling [11].

## 2.3 The Spin-Orbit Coupling

The first quantum atomic models explained most of the hydrogen atom's properties correctly, but in other cases the answers given by quantum mechanics were incorrect. Some of the unexplained phenomena were the splitting of spectral lines and the anomalous patterns found in the Zeeman effect. In the first case, the theory predicted that for the hydrogen Balmer series a spectral line would appear for a wavelength at 656.3 nm. Instead of this, two lines appeared, separated only by 0.14 nm. The existence of two lines instead of one suggested that the existent theory was incomplete [11]. In the Zeeman effect, it was expected that the spectral lines of an atom should split into three components due to the effect of the magnetic field, but in some case was observed that more than three spectral lines appeared. The nature of the "extra" spectral lines was successfully explained by the spin-orbit coupling (SOC), also called the spin-orbit interaction [11].

The SOC is present in most of the atoms due to the electron's orbital $\mathbf{l}$ and spin momentum $\mathbf{s}$, giving raise to a total electronic angular momentum $\mathbf{j} = \mathbf{s} + \mathbf{l}$[1] that is proportional to the magnetic moment $\mathbf{m}$ [12].

[1] In this paragraph we use $\mathbf{l}$, $\mathbf{s}$ and $\mathbf{j}$ in lowercase letters because we are talking about atoms with one electron. For atoms with more than one electron, we use capital letters $\mathbf{L}$, $\mathbf{S}$ and $\mathbf{J}$.

In order to understand the SOC, it is helpful to use a semi-classical model. Thinking in terms of Bohr's electron model, we have that the electron is moving in a circular orbit around a charged $Ze$ nucleus (Figure 2.5a). If we change the nucleus' framework to the electron's framework, the electron "sees"a charged particle around itself, while the electron is fixed [12]. The circular movement of a charge particle, in this case the nucleus, produces a current loop

$$I = \frac{Zev}{2\pi r}, \tag{2.14}$$

where $r$ is the orbit's radius. The current loop produces an effective (non-external) magnetic field $\mathbf{B}_{\text{eff}}$, normal to the plane of the orbit (see Figure 2.5b) and given by

$$\mathbf{B}_{\text{eff}} = \frac{\mu_0 I}{2r} = \frac{\mu_0 Zev}{4\pi r^2}, \tag{2.15}$$

where $\mu_0$ is the vacuum permeability. The effective magnetic field is responsible of the SOC, because interacts with the electron intrinsic magnetic moment: the spin. In the ground state, the spin is oppositely aligned with the angular electron's momentum [12].

Recalling magnetostatic theory, when a magnetic moment is in the presence of a magnetic field, a torque $\mathbf{\Gamma}$ appears

$$\mathbf{\Gamma} = \mathbf{m} \times \mathbf{B}, \tag{2.16}$$

which is related to a magnetic energy

$$\mathcal{E}_m = -\mathbf{m} \cdot \mathbf{B}. \tag{2.17}$$

In the case of the SOC, this magnetic energy reads

$$\mathcal{E}_{\text{SOC}} = -\mu_{\text{B}} B_{\text{eff}} = -\frac{\mu_{\text{B}} \mu_0 Zev}{4\pi r^2}. \tag{2.18}$$

Notice that $\mathcal{E}_{\text{SOC}}$ is proportional to the atomic number $Z$. So the SOC effect becomes more important as $Z$ increases [11, 12].

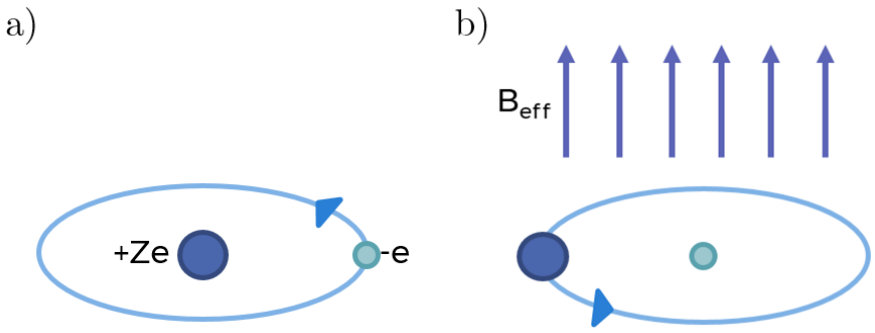


**Figure 2.5:** Semi-classical model of atomic SOC. a) Schematic representation of Bohr's model and b) the schematic representation from the framework of a fixed electron that *sees* that the nucleus moves around itself, creating an effective magnetic field $\mathbf{B}_{\text{eff}}$ that is normal to the orbit plane. Image from [14].

Let us analyze the SOC a bit more thoroughly. To achieve this purpose, we followed the procedure done by Strange [15], where he used a non-relativistic Hamiltonian in which the spin particle interacts with a magnetic field. [15]. Starting from Schrödinger's equation for this case (also called Pauli's equation)

$$i\hbar\frac{\partial\Psi(\mathbf{r},\,t)}{\partial t} = \left[\frac{1}{2m_{\text{e}}}\left(\frac{\hbar}{i}\boldsymbol{\nabla} - e\mathbf{A}(\mathbf{r})\right)^2 - \hat{\boldsymbol{\mu}}\cdot\mathbf{B}(\mathbf{r}) + U(\mathbf{r})\right]\Psi(\mathbf{r},\,t), \tag{2.19}$$

where $\Psi(\mathbf{r},\,t)$ is the wavefunction, $m_{\text{e}}$ is the electron mass, $\mathbf{A}(\mathbf{r})$ is the vector potential, $\hat{\boldsymbol{\mu}}$ is the magnetic momentum, $\mathbf{B} = \boldsymbol{\nabla}\times\mathbf{A}$ is the magnetic field, $U(\mathbf{r}) = eV(\mathbf{r})$ is the electrostatic potential energy, and $V(\mathbf{r})$ is the electrostatic potential [15].

Recall that in the electron's framework, the electron "sees" a magnetic field due to the nucleus. The nucleus generates a loop current that is

$$\mathbf{I} = -Ze\mathbf{v}, \tag{2.20}$$

where $\mathbf{v}$ is the nucleus relative velocity to the electron [15]. Recall further that the nucleus electric field is

$$\mathbf{E}(\mathbf{r}) = \frac{Ze}{4\pi\epsilon_0 r^3}\mathbf{r}, \tag{2.21}$$

and that an electric current generates a magnetic field given by the Biot-Savart law

$$\mathbf{B}(\mathbf{r}) = \frac{\mu_0}{4\pi}\frac{\mathbf{I}\times\mathbf{r}}{r^3}. \tag{2.22}$$

From the latter, together with equations (2.20) and (2.21), and recalling that $c = \frac{1}{\sqrt{\mu_0\epsilon_0}}$, the

magnetic field can be rewritten as

$$\begin{aligned}\mathbf{B}(\mathbf{r}) &= \frac{-\mu_0 Ze}{4\pi r^3}\mathbf{v}\times\mathbf{r} \\ &= -\mu_0\epsilon_0\mathbf{v}\times\left(\frac{Ze\mathbf{r}}{4\pi\epsilon_0 r^3}\right) \\ &= \frac{-1}{c^2}\mathbf{v}\times\mathbf{E}.\end{aligned} \tag{2.23}$$

Going back from the electron's framework to the nucleus one, adding a factor of $\frac{1}{2}$ due to the Thomas precession, the part of the Pauli equation containing the magnetic field can be rewritten as follows [15]:

$$\begin{aligned}H_1 &= -\hat{\boldsymbol{\mu}}\cdot\mathbf{B} \\ &= \frac{e}{2m}\hat{\mathbf{S}}\cdot\mathbf{B} \\ &= \frac{-e}{2mc^2}\hat{\mathbf{S}}\cdot(\mathbf{v}\times\mathbf{E}),\end{aligned} \tag{2.24}$$

With this in mind, we use that

$$\mathbf{F} = e\mathbf{E} = -e\frac{dV(r)}{dr}\hat{\mathbf{r}}, \tag{2.25}$$

and then, substituting the last two equations into (2.24), one can finally obtain a formula for the coupling between the spin and the orbital angular momentum.

$$\begin{aligned}H_1 &= \frac{1}{2mc^2}\frac{1}{r}\left(\frac{dV(r)}{dr}\right)\hat{\mathbf{S}}\cdot(\mathbf{v}\times\mathbf{r}) \\ &= \frac{-1}{2m^2c^2}\frac{1}{r}\frac{dV(r)}{dr}\hat{\mathbf{S}}\cdot\hat{\mathbf{L}},\end{aligned} \tag{2.26}$$

It is also important to mention that in order to have $H_1 \neq 0$ it is necessary that $\frac{dV(r)}{dr} \neq 0$. Finally note that in a Hamiltonian with a SOC present, only the total angular momentum is a conserved quantity [15].

## 2.4 Main Types of Magnetic Behaviour

In materials, the different combinations of electronic spin and orbital momentum give rise to different magnetic behaviours [16]. Here we discuss the four main kinds of magnetic behaviour in materials: diamagnetism, paramagnetism, ferromagnetism and antiferromagnetism. In this section we are interested in giving a brief introduction to them.

### 2.4.1 Diamagnetism

Diamagnetism only occurs when an external field is present. Before and after the presence of the magnetic field there is no magnetization in the material. Its origin is the change in the orbital moment that is produced when a external magnetic field is applied [16].

Diamagnetism is the reaction that some materials experience when an external field is present. Here there is an overall alignment of the electrons orbital momenta with the whole purpose to generate an effective field that cancels the external one [16].

In general, the magnetic susceptibility per volume is

$$\chi = \frac{\mu_0 M}{B} \tag{2.27}$$

where $M$ is the magnetization magnitude and $B$ is the external magnetic field magnitude. For a diamagnetic material the magnetic susceptibility is always negative [16]. This is due to Lenz's law, that states that "when the flux through and electrical circuit is changed, an induced current is set up in such a direction as to oppose the flux change" [16]. That is, the induced current is in a direction opposite to the external magnetic field. In a diamagnetic material, the relative permeability, $\mu_r = \frac{\mu}{\mu_0}$, is less than a unit [16].

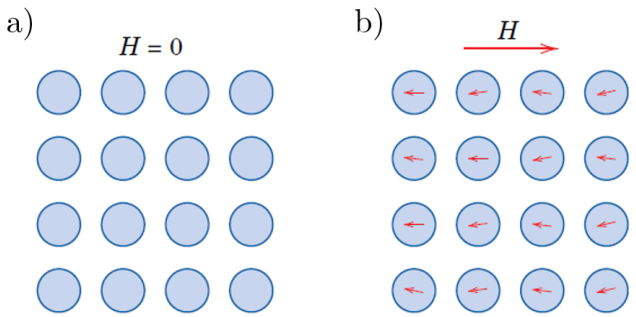


**Figure 2.6:** A diamagnetic system, a) when there is not external magnetic field and b) when a magnetic field is applied. Note that the induced current has an opposite direction to the external magnetic field. Image from [16].

### 2.4.2 Paramagnetism

It is a phenomenon originated due to the presence of both, the orbital and spin momenta. In such materials, this results into a non-zero magnetic dipole associated to each atom, but randomly oriented in the material sample. When an external magnetic field is applied, the atoms rotate and reorder themselves in the same orientation to the magnetic field. The magnetic susceptibility, equation (2.27), is small and positive, while the relative permeability is bigger than the unit [16].

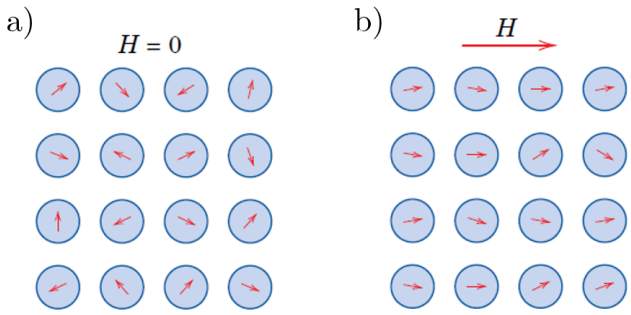


**Figure 2.7:** Paramagnetic behaviour. a) When $H \neq 0$ the dipole moments do not have specific direction, b) when an external field is applied the atoms acquires the same orientation that the field. Image from [16].

Diamagnetic and paramagnetic materials are considered non-magnetic materials, because both of them show magnetic properties only when an external field is applied.

### 2.4.3 Ferromagnetism

Ferromagnetism is an ability present in some materials to show a permanent magnetization even in the absence of an external magnetic field. This permanent magnetization may be due to both orbital and spin momenta contributions, but usually the spin part contributes more to this effect than the orbital part. In these materials, the exchange interactions result into creating local domains in the material having a non-zero macroscopic magnetization. These are usually called magnetic domains [16].

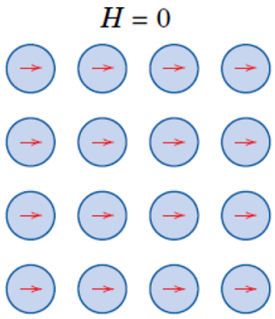


**Figure 2.8:** Ferromagnetic behaviour, the electrons are oriented without an external field. Image from [16].

From the magnetic theory we know that, in general, the magnetic field is

$$\mathbf{B} = \mu_0 \mathbf{H} + \mu_0 \mathbf{M}. \tag{2.28}$$

In ferromagnetic materials the magnetic susceptibility can take values of the order of $10^6$, and as a consequence of this, due to equation (2.27), $M \gg H$ [16] and then the equation (2.28) can

be approximated by

$$\mathbf{B} \approx \mu_0 \mathbf{M}. \tag{2.29}$$

### 2.4.4 Antiferromagnetism

In some magnetic materials, the exchange coupling between adjacent ions results into the spins moments to be aligned antiparallel. This phenomenon is called antiferromagnetism [16].

An example of a material that presents antiferromagnetism is Manganese Oxide (MnO), which composed of two ions: $Mn^{+2}$ and $O^{-2}$. The oxygen atoms do not contribute with a magnetic moment, because both spin and orbital momentum are cancelled. On the other hand, the manganese ions have a magnetic momentum, whose origin is predominantly from the electron's spin. So, the magnetic configuration for these ions is antiparallel as it is shown in figure 2.9. It is important to note that while each manganese ion does possess a magnetic momentum, overall magnetization of the material does not, because these momenta cancelled out macroscopically [16].

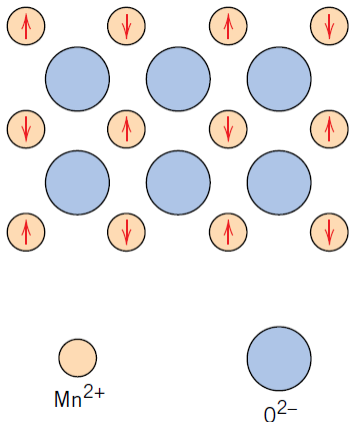


**Figure 2.9:** Antiferromagnetic behaviour in MnO. The oxygen ions (blue) do not possess any magnetic momenta, while the manganese ions (red) do possess a magnetic momenta whose origin comes mainly from the spins [16]. The alignment of manganese ions is antiparallel. Image from [16].

In this chapter we explored some of the most important behaviours of magnetic materials and the most important ingredients: the electron role, the angular momentum, the spin momentum and the spin orbit coupling. This information is going to be useful in the exploration of striking physical phenomena, where the electrons, the magnetic field, and (in some cases) the spins take an important role: the Hall effects.

# Chapter 3

# Hall Effects

The Hall effects are a set of physical phenomena that comprise the behaviour of two-dimensional systems in which a longitudinal density current flows in the presence of an orthogonal magnetic field either external or effective. Different kinds of Hall effects appear depending on the material or the magnetic field properties. Our goal in this chapter is to give a brief introduction to the Classical, Spin and Quantum Integer Hall effects and then to proceed to study in more detailed the Anomalous Hall effect.

## 3.1 The Classical Hall Effect

The Classical Hall Effect (CHE) was discovered in 1879 by Edwin Hall while he was a PhD student [17]. The CHE consists on the generation of a transverse voltage due to the presence of a longitudinal electric current in a *Hall bar* (a thin plate of a metal or semiconductor) immerse in an external magnetic field, normal to the Hall bar surface [18].

To explain further the CHE, let us consider the case of a conducting material Hall bar with negative electric carriers: electrons. Suppose that, initially we subject the material to an electric field along the sample, say, in the $\hat{\mathbf{x}}$ direction $\mathbf{E} = E_x\hat{\mathbf{x}}$. This generates a current $\mathbf{J} = J_x\hat{\mathbf{x}}$ which after a transient regime, results into a drift velocity, $\mathbf{v}_\mathrm{d} = -v_\mathrm{d}\hat{\mathbf{x}}$, for the electrons. Suppose then, that we switch on a magnetic field in the orthogonal direction to the plane, $\mathbf{B} = B_z\hat{\mathbf{z}}$ (see Figure 3.1a). The moving electrons now feel a magnetic force

$$\mathbf{F}_m = |q|\,\mathbf{v}_\mathrm{d} \times \mathbf{B} = qv_\mathrm{d}B_z\hat{\mathbf{x}} \times \hat{\mathbf{z}} = -qv_\mathrm{d}B_z\hat{\mathbf{y}}, \tag{3.1}$$

that deflects the electrons in the $-\hat{\mathbf{y}}$ direction. The accumulation of negative charges at the bottom edge of the Hall bar produces an excess of positive charges at the opposite edge (Figure 3.1c). This charge polarization between the edges produces, in turn, an electrostatic field that

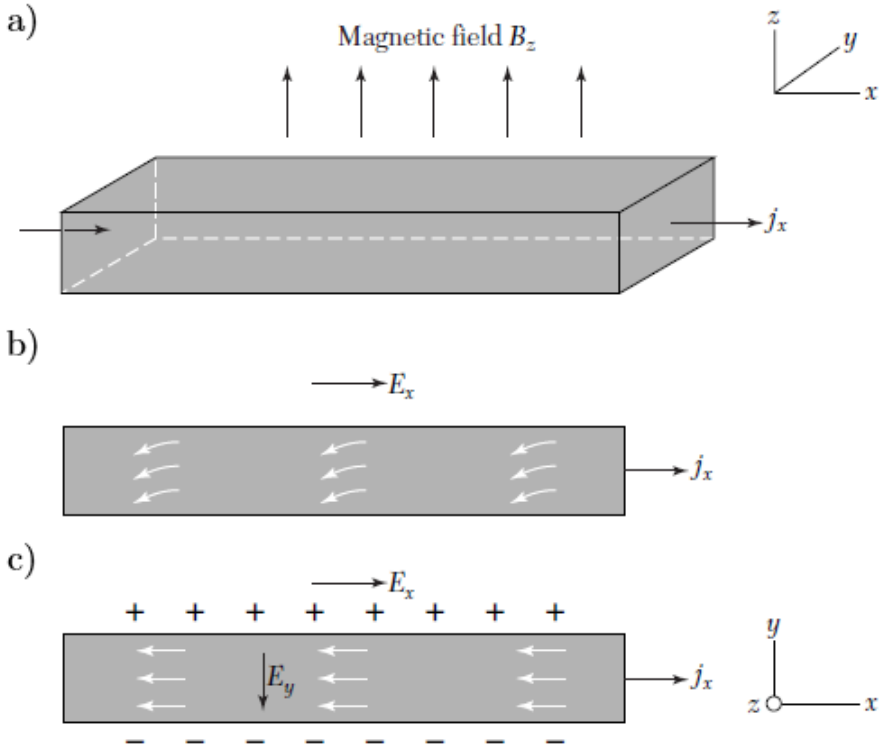


**Figure 3.1:** Classical Hall effect. a) The Hall bar is crossed by a longitudinal current density and there is an external magnetic field normal to the plate. b) When the longitudinal electric field is turned on, immediately the electrons acquire a drift velocity in the opposite direction. c) The negative current chargers are deflected to one side of the Hall bar because of the magnetic force, leaving an accumulation of positive current chargers in the opposite edge, resulting in an electrostatic field. Assuming that the system reaches mechanical equilibrium, then the new electrostatic force has the same magnitude but opposite direction than the magnetic force [17, 19]. Image from [19].

generates another electrostatic force

$$\mathbf{F}_{\mathrm{e}} = |q|\,\mathbf{E}_{\mathrm{e}} = -q(-E_{\mathrm{e}})\hat{\mathbf{y}} = qE_{\mathrm{e}}\hat{\mathbf{y}}, \tag{3.2}$$

which is equal in magnitude and opposite in direction to the magnetic force, assuming of course, mechanical equilibrium (equation (3.1)). As a result of this, the $y$ component of the Lorentz force is zero [17, 19]

$$|q|\,(\mathbf{E}_{\mathrm{e}} + \mathbf{v}_{\mathrm{d}} \times \mathbf{B})_y = 0\,. \tag{3.3}$$

Thus, after the electrostatic force is generated, the system is in a stationary state, and therefore there is not a force that deflects the charge current in the $\hat{\mathbf{y}}$ direction. Due to the polarization, there exists a voltage between the opposite edges of the Hall bar, the so-called the Hall voltage [17, 19]. It is possible to write the conductivity and resistivity in its tensorial

form, which is (Nb. Einstein's summation convention applies here)

$$J_\mu = \sigma_{\mu\nu} E_\nu, \tag{3.4}$$

$$E_\mu = \rho_{\mu\nu}\, J_\nu. \tag{3.5}$$

In this case the resistivity is given by

$$\rho_{yx} = \frac{B_z}{nq}\,, \tag{3.6}$$

thus $\rho_{yx}$ is proportional to the magnetic field intensity and inversely proportional to the charge $q$ and the carrier density $n$ [1].

The CHE provides the basic mechanisms to understand the other Hall effects that occur under different conditions. An example of this is the integer quantum Hall effect that is present when the sample is a two-dimensional electron gas and when the external magnetic field is strong.

## 3.2 The Integer Quantum Hall Effect

The Integer Quantum Hall Effect (IQHE) was discovered in 1980 by von Klitzing, Dorda, and Pepper [20]. In 1982, Paalanen, Tsui, and Gossard [21] measured its Hall resistance. Their experimental setup consisted on a two-dimensional electron gas (2DEG) trapped between two crystals: a GaAs and a GaAlAs one [22].

In the IQHE, a 2DEG is under the effect of a large external magnetic field. In this experiment the main observation is that the resistance spectrum as a function of the magnetic field has "horizontal steps", which means that for different values of the external magnetic field, the resistance has the same value (see Figure 3.2), instead of having a linear dependence as is observed in the CHE [1]. Moreover, at these specific points the resistance is quantized and the "horizontal steps" are known as *quantum Hall plateaux* [1,22]. The Hall resistance (considering the same direction for the magnetic field and the current density as in the previous description of the CHE) is

$$R_{\mathrm{H}} = \frac{V_y}{I_x} = \frac{1}{\nu}\frac{h}{e^2}, \tag{3.7}$$

where $V_y$ is the magnitude of the voltage, $I_x$ is the electron current magnitude, $e$ is the electron charge and $\nu$ takes integer values ($\nu = 1, 2, 3, ...$). Note that the formula for $R_{\mathrm{H}}$ implies that the quantization is universal, independent of the sample or the magnetic field [1].

In 1981, Robert Laughlin [23] presented his *thought experiment*, where he used the rela-

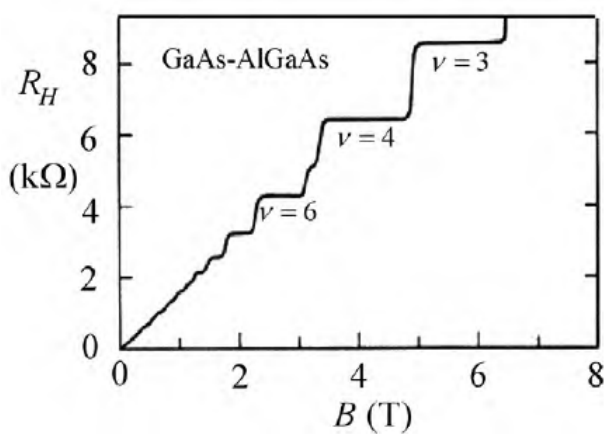


**Figure 3.2:** Hall resistance versus external magnetic field for a 2DEG trapped between a GaAs and a GaAlAs crystals. The quantum Hall plateaux can be seen for different $\nu$ values, the Hall plateaux are bigger as the magnetic field increases. Note that for non-large external magnetic field, the Hall resistance has a linear behaviour [22]. Image from [22].

tionship between the electric current $I$ and the total magnetic energy $U_{\mathrm{B}}$

$$I_\mu = \left( \frac{\partial U_{\mathrm{B}}}{\partial \Phi_\mu} \right)_{\Phi', \mathbf{R}'}, \tag{3.8}$$

where $\Phi$ is a magnetic flux related to $N$ current loops and $\mathbf{R}$ is the center of mass coordinate of each loop. In addition, Laughlin used gauge invariance and the solutions of the Schrödinger equation for a two-dimensional system of free electrons in a perpendicular magnetic field [22], to show that the smallest increment in magnetic flux that can be accommodated by a 2DEG carrying a current is $\Delta\Phi = h/e$. As a consequence of this, there is a change in the energy

$$\Delta U_{\mathrm{B}} = \nu e V_{\mathrm{H}}, \tag{3.9}$$

so that an expression for the Hall resistance can be justified as follows:

$$R_{\mathrm{H}} = \frac{V_{\mathrm{H}}}{I} = V_{\mathrm{H}} \frac{\Delta\Phi}{\Delta U_{\mathrm{B}}} = V_{\mathrm{H}} \frac{h/e}{e\nu V_{\mathrm{H}}} = \frac{h}{e^2 \nu}. \tag{3.10}$$

From this equation it can be noticed that the Hall resistance in the IQHE depends only on universal constants and is indeed quantized [22].

The semi-classical interpretation of the current on the IQHE is that some electrons are moving in *skipping orbits*. Indeed, in principle electrons should have a circular cyclotron motion, but for those electrons close to the edges their motion is interrupted by the collisions with the boundaries. This means that the bulk electrons are localized in circular orbits while the edge electrons are the ones that effectively produce an electric current (Figure 3.3) [1].

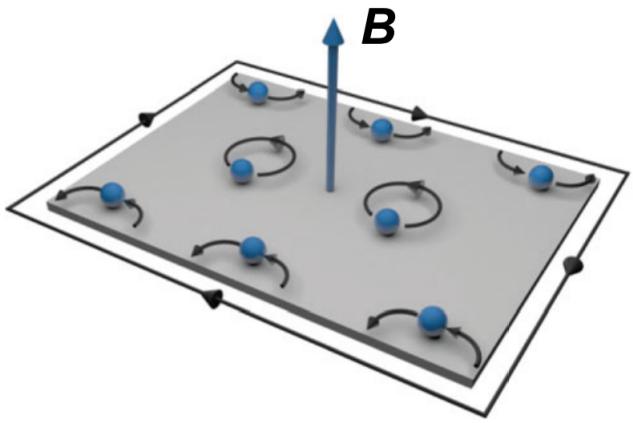


**Figure 3.3:** Semi-classical representation of the IQHE. In a two-dimensional sample under a intense magnetic field **B**, the electrons at the boundaries move in skipping orbits, while the motion is circular at the bulk of the sample. These skipping orbits solely contribute to the electric current transport [1]. Image from [24].

So far we have seen that these Hall effects produce a Hall voltage; but not all Hall effects are characterized by this. The paradigmatic case is the so-called the spin Hall effect.

## 3.3 The Spin Hall Effect

In 1971 D'yakonov and Perel made the theoretical prediction of the Spin Hall Effect (SHE) [25, 26], which was named in 1999 by Hirsch [27], who chose this name due to its similarity with the CHE [28].

The SHE is based on the linear response of a system with a strong SOC. In this case, the sample is a two-dimensional system that, as in CHE, is crossed by a longitudinal electric field, but there is no external magnetic field. Assuming that the system has strong SOC, this produces an effective magnetic field $\mathbf{B}_{\text{eff}}$ that deflects the electrons associated to the electric current density. More precisely, electrons with *spin up* are deflected to one edge of the sample, while electrons with *spin down* are deflected to the other side. As a consequence of this, each edge of the sample has a different spin polarization [24, 28].

While in the previous sections we have seen that the Hall effect produces a Hall voltage due to charge current polarization, in the SHE there is no transverse voltage, because the probability of having a spin up electron is exactly the same one as having a spin down. That is, there is the same amount of electrons at each boundary of the sample, but with different spin polarization. This results into a net *spin current* at the edges [24, 28].

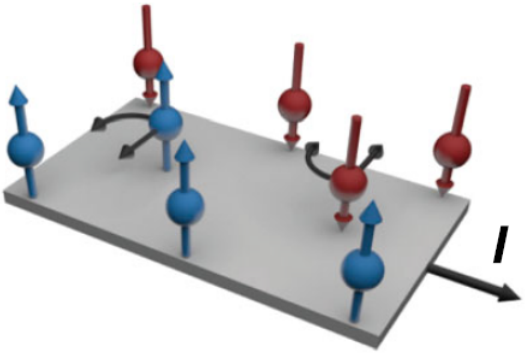


**Figure 3.4:** A schematic draw of SHE. The electrons are injected into the sample, which is a two-dimensional system with strong SOC. The spin up electrons are deflected to one side of the sample, while the spin down electrons are deflected to the opposite side. This produces a spin polarization in the sample's edges, and as a consequence a spin current appears [24, 28]. Image from [24].

While measuring experimentally the presence of the CHE is easy (just use a voltmeter connected to the edges of the sample), verifying the presence of the SHE is not that simple since there is no apparatus that could measure the polarization of electron spin. Therefore, the experimental test of the SHE arrived almost 30 years after its theoretical prediction. Its first successful measurement was done by Kato, Myers, Gossard and Awschalom in 2004 [29] using the static Kerr rotation. In their experiment, the sample were GaAs layers with silicon impurities. An electric field $\mathbf{E} = -E\hat{\mathbf{z}}$ is applied and an in-plane magnetic field $\mathbf{B}_{\text{ext}}$ is present to promote the emergence of spin accumulation. A linear polarized laser beam is focused on normal direction to the sample plane. The rotation axis is known. When the beam is reflected its polarization changes due to the spin polarization of the sample, with a rotation angle that depends on the magnetization [24, 28]. The results of these experiments can be seen in the Figure 3.5.

In Figure 3.5b we can see two different results: on the left plot there is a spin density where a spin accumulation is notable at the edges of the sample (in the figure the spin orientations are highlighted using blue and red colors), that have opposite spin polarization. On the figure to the right, we show a reflectivity image, where the spin accumulation can also be seen. Figure 3.5c shows the result of the Kerr rotation, highlighting the opposite polarization of the spin accumulation at the edges of the sample [24, 29].

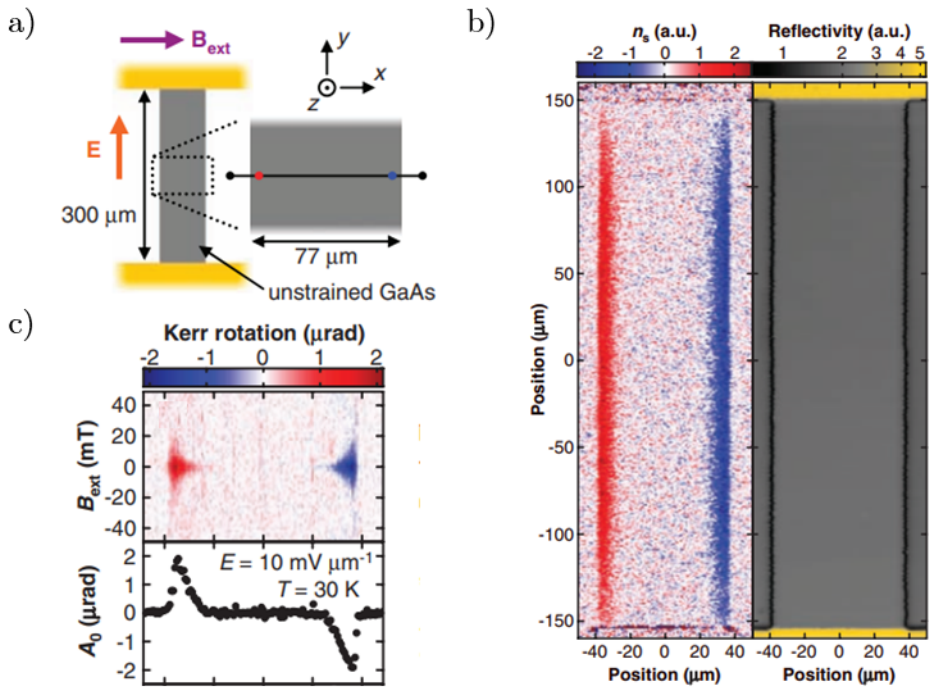


**Figure 3.5:** a) The schematic representation of the system. b) The spin density (left) and the reflectivity (right). In the spin density, spin up electrons are in one color and spin down electrons in another one. As it can be seen there are more electrons at the boundaries and the spin polarization is opposite at the edges. c) Kerr rotation in microradians in terms of the magnetic field (up) and in terms of $A_0$, a measure of the spin density (down) [24, 29]. Image from [29].

Let us move on now to introduce another striking Hall effect that shares some features withe the SHE: the so-called anomalous Hall effect.

## 3.4 The Anomalous Hall Effect

In 1880, one year after Edwin Hall discovered the Classical Hall effect, he found out that the Hall voltage was larger, approximately ten times larger, when the Hall bar was made of iron instead of gold. He found out that, in general, this effect is an order of magnitude larger in ferromagnetic materials. This is the so-called Anomalous Hall Effect (AHE). The experimental setup to study the AHE is the same to the one used for the CHE, but instead of having a conducting plate, we have a ferromagnetic material whose magnetic domains provide a net magnetization in the absence of an external magnetic field [30].

In 1929 Smith and Sears [31] proposed that the relationship between the resistivity $\rho_{xy}$, the normal Hall coefficient $R_0$, the anomalous Hall coefficient $R_S$ (typically at least an order of magnitude larger than $R_0$), the magnitude of the magnetization $\mathbf{M}$ and the external magnetic

field **H** in ferromagnetic materials are related by the following formula

$$\rho_{xy} = R_0(\mu_0 H) + R_S M,$$

where the magnetization component, which plays an important role in this effect, is absent in the CHE. The magnetization appears here due to the electron spin and therefore it influences the transport process. Another key ingredient of the AHE is the SOC, as we will see later. Note that when $\mathbf{H} = \mathbf{0}$, $\rho_{xy} \neq 0$ due to the magnetization [30].

As we described previously, the CHE is a direct consequence of the Lorentz force. On the other hand, the origin of the AHE was unveiled in the 1950's [32]. The AHE may be described by three main mechanisms that can be classified as either intrinsic or extrinsic. The intrinsic mechanism considers the interaction between the angular momentum **L** and the spin of itinerant electrons **s** (Figure 3.6a), whose energy levels follow a band structure. On the other hand, the extrinsic mechanism assumes a scattering process between the localised spins of ions $\boldsymbol{\sigma}$ and electron's orbital momentum **L** (Figure 3.6b). This extrinsic mechanism can further be subdivided into two main processes: skew scattering and side jump mechanism [24, 30]. From these contributions, the anomalous Hall conductivity $\sigma_{xy}^{\mathrm{A}}$ can be expressed as

$$\sigma_{xy}^{\mathrm{A}} = \sigma_{xy}^{\mathrm{int}} + \sigma_{xy}^{\mathrm{skew}} + \sigma_{xy}^{\text{side-jump}}, \tag{3.11}$$

where $\sigma_{xy}^{\mathrm{int}}$ is the intrinsic mechanism contribution to the conductivity, and $\sigma_{xy}^{\mathrm{skew}}$ and $\sigma_{xy}^{\text{side-jump}}$ correspond to the skew scattering and the side-jump mechanisms, respectively [30]. In the next sections, we are going to present in more detail both the intrinsic and extrinsic mechanisms.

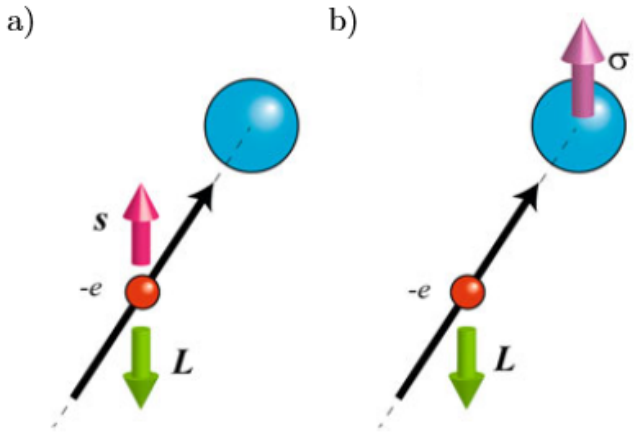


**Figure 3.6:** The AHE has its origin in the a) intrinsic mechanism, where the spin interacts with the angular momentum and b) in the extrinsic mechanism, where the electron's angular momentum interacts with the ion's momentum [24, 30]. Image from [30].

### 3.4.1 The Intrinsic Mechanism

The intrinsic mechanism was initially studied by Karplus and Luttinger in 1954 [33]. It is called intrinsic because it depends on the band structure and it is independent of scattering processes. Karplus and Luttinger discovered that when an external electric field is applied, the group velocity of the electrons acquires an additional term that is perpendicular to the electric field. This is called *anomalous velocity*. The total contribution of the anomalous velocity in ferromagnetic materials with SOC is non-zero, when it is summed over all occupied band states, so it contributes to the Hall effect [30, 32, 34]. The intrinsic AHE resistivity is given approximately by the relation

$$\rho_{xy} \approx \frac{\sigma_{xy}}{\sigma_{xx}^2} \propto \rho_{xx}^2. \tag{3.12}$$

In order to understand the nature and the contribution of intrinsic mechanism to the AHE conductivity, we start by considering the equations of motion of an electron in a solid. The Lorentz force is given by

$$\mathbf{F} = \hbar\dot{\mathbf{k}} = -e(\mathbf{E}(\mathbf{r}) - \dot{\mathbf{r}} \times \mathbf{B}(\mathbf{r})), \tag{3.13}$$

and recall also that crystal with band structure having time reversal and inversion symmetry results into the following expression for the group velocity

$$\mathbf{v} = \dot{\mathbf{r}} = \frac{1}{\hbar}\frac{\partial \mathcal{E}_n(\mathbf{k})}{\partial \mathbf{k}}. \tag{3.14}$$

When we consider that the system is under a perturbation given by $H' = e\mathbf{E}\cdot\mathbf{r}$, using perturbation theory up to first order, we can find that the previous formula for the group velocity is changed to:

$$\mathbf{v} = \frac{1}{\hbar}\frac{\partial \mathcal{E}_n(\mathbf{k})}{\partial \mathbf{k}} + \underbrace{\frac{e}{\hbar}\mathbf{E}\times\mathbf{b}^n(\mathbf{k})}_{\mathbf{v}_a(n,\,\mathbf{k})}, \tag{3.15}$$

where, as we saw in Chapter 1, $\mathbf{b}^n$ is the Berry curvature which can be interpreted as a fictitious magnetic flux associated to the electrons [1, 34]. The second term in equation (3.15) represents the anomalous velocity $\mathbf{v}_a(n, \mathbf{k})$, which is proportional to the Berry curvature of the band, and it is always perpendicular to the electric field (the complete derivation of the anomalous velocity is shown in Appendix B). In equation (3.14) there is no additional contribution to the velocity because in crystals with both time reversal and spatial inversion symmetry the Berry curvature vanishes in the Brillouin zone [30, 34]. Using that $-e\mathbf{E} = \hbar\dot{\mathbf{k}}$[1], we can write that

$$\hbar\dot{\mathbf{r}} = \frac{\partial \mathcal{E}_n(\mathbf{k})}{\partial \mathbf{k}} + e\mathbf{E}\times\mathbf{b}^n(\mathbf{k}) = \frac{\partial \mathcal{E}_n(\mathbf{k})}{\partial \mathbf{k}} - \hbar\dot{\mathbf{k}}\times\mathbf{b}^n(\mathbf{k}). \tag{3.16}$$

[1]The relation $-e\mathbf{E} = \hbar\dot{\mathbf{k}}$ is obtained from a semiclassical analysis. Let us think on a wave package that represents a semiclassical particle with position $\mathbf{R}$, momentum $\hbar\mathbf{K}$, and energy $\mathcal{E}_{n\mathbf{K}}$. The velocity of this particle is the group velocity of the wave package, so $\mathbf{v}_n(\mathbf{K}) = \frac{d\mathbf{R}}{dt} = \frac{1}{m^*}\hbar\mathbf{K} = \frac{1}{\hbar}\boldsymbol{\nabla}_{\mathbf{K}}\mathcal{E}_{n\mathbf{K}}$, and because the Hamiltonian $H = \mathcal{E}_{n\mathbf{K}} + U(\mathbf{R})$ is a constant of motion $\frac{dH}{dt} = 0 = \frac{d\mathbf{K}}{dt}\cdot\boldsymbol{\nabla}_{\mathbf{K}}\mathcal{E}_{n\mathbf{K}} + \frac{d\mathbf{R}}{dt}\cdot\boldsymbol{\nabla}U(\mathbf{R})$, then we can arrive to $\hbar\dot{\mathbf{K}} = -\boldsymbol{\nabla}U(\mathbf{R}) = -e\mathbf{E}(\mathbf{R})$ [1].

The intrinsic contribution to the Hall conductivity, which depends on the bands and not on the defects, can be calculated from Kubo's formula [34–36] given by

$$\sigma_{xy}^{\mathrm{A}} = e^2\hbar \sum_{n\neq n'} \int [f(\mathcal{E}_n(\mathbf{k})) - f(\mathcal{E}_{n'}(\mathbf{k}))] \mathrm{Im} \left\{ \frac{\langle n(\mathbf{k})|v_x(\mathbf{k})|n'(\mathbf{k})\rangle \langle n'(\mathbf{k})|v_y(\mathbf{k})|n(\mathbf{k})\rangle}{[(\mathcal{E}_n(\mathbf{k})) - (\mathcal{E}_{n'}(\mathbf{k}))]^2} \right\}, \quad (3.17)$$

expression that, using the definition of the Berry curvature, reduces to

$$\sigma_{xy}^{A} = -\frac{e^2}{\hbar} \sum_n \int \frac{d\mathbf{k}}{(2\pi)^3} f(\mathcal{E}_n(\mathbf{k})) b_z^n(\mathbf{k}). \quad (3.18)$$

We would like to emphasize that this last equation is known as the intrinsic conductivity since it only depends on the band structure of the material and not on the concentration of the impurities [30, 34].

### 3.4.2 The Extrinsic Mechanism

The extrinsic mechanism is related to scattering processes in a periodic crystal. In order to understand this, think of an electron wave packet getting closer to a scattering center. Before the scattering process occurs, the wave packet is not perturbed, and so it travels in a straight line. After scattering, the wave packet is no longer a packet, and becomes a set of spherical waves whose center of mass also travels in a straight line. If the electron's spin is pointing in a direction orthogonal to the paper (Figure 3.7), the set of waves will change its trajectory due to spin-orbit coupling. If the trajectory after the scattering differs from an angle to the original one (Figure 3.7a), the electron is gaining a transverse momentum. This effect is known as skew scattering. If the direction of both the before and after trajectories is the same but is displaced from the origin, the side jump mechanism is present (Figure 3.7b) [30].

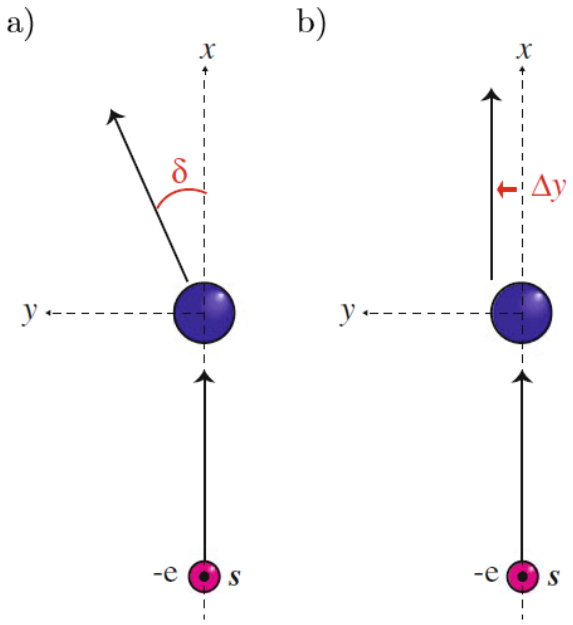


**Figure 3.7:** The extrinsic mechanism of the AHE can be separated in the a) skew scattering mechanism, where the trajectory of the wave packet has changed from an angle to the original trajectory and; the b) side jump mechanism, where the direction of the trajectory is the same after scattering but it is displaced [30]. Image from [30].

### The Skew Scattering Mechanism

The skew scattering mechanism was first described by Smith in 1958 [37] for electrons that interact via a short-range potential so that the spin-orbit Hamiltonian can be written as

$$H_{\mathrm{SO}} = -\lambda_{\mathrm{SO}}(\mathbf{k} \times \mathbf{s}) \cdot \boldsymbol{\nabla} V \,, \tag{3.19}$$

where $\lambda_{\mathrm{SO}}$ is the coupling parameter. The existence of spin-orbit interaction induces a *transverse polarization* that can be seen as an impact parameter in the collision process and is the source of the skew scattering [30].

This mechanism is related to the lifetime of the Bloch state transport, so its contribution is larger when the crystal does not have impurities. As consequence of that, the Hall resistivity for this mechanism can be described by

$$\rho_{xy}^{skew} \approx \sigma_{xy}^{skew} \rho_{xx}^2 \sim \rho_{xx}. \tag{3.20}$$

### The Side Jump Mechanism

The semi-classical argument for this mechanism is that the Gaussian packet undergoes a spatial displacement. This displacement was first noticed by Smith (1958) [37] but was studied in more detail a few years later by Berger (1964) [38]. Using the first Born approximation it can be

calculated that the spatial displacement in, say, the $\hat{\mathbf{y}}$ direction is given by:

$$\Delta y = -\lambda_{\mathrm{SO}} s_z k_x, \tag{3.21}$$

where $s_z = \pm 1/2$ is the spin of the itinerant electron.

In a weak spin-orbit interacting system the side jump contribution can be computed only by considering the disorder of the scattering potential. For strong SOC it is necessary to consider the contribution from the scattering that arises from the part of the wave packet that does not have SOC [30].

### 3.4.3 The Berry Phase and the AHE

As we mentioned before, Karplus and Luttinger discovered the anomalous velocity in the AHE that arises from the inter-band matrix elements. This phenomenom was understood more deeply thanks to the analysis that Thouless [39] did for the Hall conductivity and the QHE. He proposed that one can trace the origin of the AHE to a Berry phase. Later it was found that the Berry phase can arise from two different mechanisms [40].

The first mechanism was described by Jinwu Ye and collaborators [41]. They presented a new theory for the AHE which is a generalization of the so-called colossal magnetoresistance. This generalization allowed them to apply the existing theory into a system of conventional ferromagnets. Their theory is based on the motion of a charged particle in a "topologically non-trivial spin background". The motion of the carrier is affected because the emergence of a Berry phase, which affects the motion similarly as a magnetic field does. If the system also has SOC, the AHE appears in the same magnitude and temperature dependence that the effect that has been studied in the colossal magnetoresistance [40].

The other mechanism was described in 2002 by T. Jungwirth and collaborators [42]. They found that non-coplanar ordering is not necessary in order for the AHE to appear. In this study the Berry phase is in momentum space (instead of a Berry phase in real space that was studied in the work of Ye; et al.). The AHE in this kind of systems is related to a ground state property and depends on how the Bloch wave function coupled to the SOC evolves with respect to the wave vector [40].

The explanation of this Berry phase can be understood considering that there is a total spin magnetization in a ferromagnetic system, which is responsible for inducing an orbital current through the SOC. The joint total spin magnetization and the SOC create an effective magnetic field. This field induces a polarization in the electrons' spins degrees of freedom [40].

In addition to the non-coplanar or coplanar ordering there is a main difference between these mechanisms. While the mechanism described by Jungwirth et al. [42] requires a SOC relativistic contribution, the mechanism described by Ye et al. [41] appears even when the relativistic contribution of the SOC is absent [40].

To understand more thoroughly this last mechanism, in the next chapter we are going to describe the tight-binding method and to explore the double exchange mechanism.

# Chapter 4

# Berry Phases in Itinerant Magnetic Systems: The Model

In this thesis we seek to find that for coplanar and collinear spin configurations, a Berry phase different from 0 or $\pi$ is acquired when an electron is moving along a closed path. These calculations are going to be done for an extended double-exchange model that considers spin-orbit coupling and for SU(2) invariant systems. In this chapter we introduce the model and some concepts that are going to be useful in this work. First, we are going to present the tight-binding approximation, then we describe the double exchange mechanism and remind the concept of gauge invariance, and after that we are going to present the model of interacting electrons.

## 4.1 The Tight-binding Method

The tight-binding method is a useful tool to calculate energy bands. To understand it, let us consider, say, two hydrogen atoms in the ground state, originally well separated from each other. Both atoms, denoted here as A and B has the same wavefunction: $\psi_{\mathrm{A}}$ (Figure 4.1a) and $\psi_{\mathrm{B}}$ (Figure 4.1b), respectively [19], the label only indicates to which atom the same wavefunction corresponds to.

When the two atoms get closer we expect electrons to be able to tunnel between them. Since electrons are indistinguishable now one electron will have an associated wavefunction $\psi_{\mathrm{A}} + \psi_{\mathrm{B}}$, while the other one will be in the wavefunction $\psi_{\mathrm{A}} - \psi_{\mathrm{B}}$. In this very crude approximation we are assuming that there are no corrections to the atomic wavefunctions [1, 19].

The wavefunction in the combination $\psi_{\mathrm{A}} + \psi_{\mathrm{B}}$ (Figure 4.1c), is non-zero in the midway between the two protons, whilst in $\psi_{\mathrm{A}} - \psi_{\mathrm{B}}$ (Figure 4.1d) the wavefunction vanishes at this point. This means that $\psi_{\mathrm{A}} + \psi_{\mathrm{B}}$ corresponds to a bonding orbital (Figure 4.1e), while the

$\psi_A - \psi_B$ case, for which the electron probability is zero between the two protons, gives rise to an anti-bonding orbital (Figure 4.1f) [19].

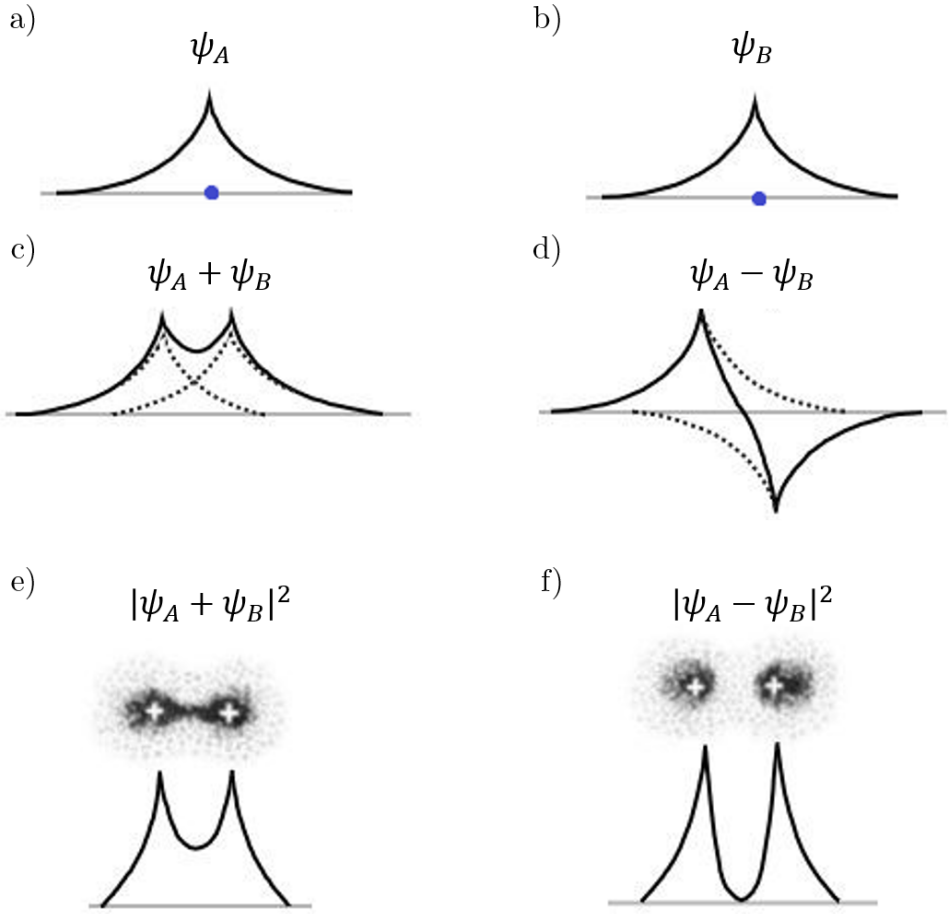


**Figure 4.1:** a) The wavefunction $\psi_A$, b) the wavefunction $\psi_B$, c) the overlap $\psi_A + \psi_B$ and d) $\psi_A - \psi_B$, e) the electron probability distribution $|\psi_A + \psi_B|^2$ and f) $|\psi_A - \psi_B|^2$. Image from Review of the Universe [43].

Now, we are interested in analyzing the case of group of atoms forming a crystal. Suppose that the distance between the atoms is large enough so that they do not interact with each other, so that their spectrum is unchanged. The spectrum of the whole system is highly degenerate. As the atoms get closer, they will start to interact among them. The firs effect of this will be to break the spectrum degeneracy, resulting in energy bands [19].

The tight-binding method tries to capture in a first approximation the aforementioned phenomena: overlapping wavefunctions and the appearance of energy bands. The main idea of this method is to use the non-interacting atoms wavefunctions to describe a crystal wavefunction [44]. This approximation is useful when the wavefunction superposition needs corrections with respect to the non-interacting wavefunction, but in many cases of interest these corrections are rather small. Indeed, the tight-binding method is very powerful and has been used to de-

scribe, for instance, the energy bands that emerge from partially full $d$ shells, which correspond to transition metals, allowing also to describe the insulator energy bands [19, 45].

The general formulation of this approximation is going to be developed. Let us suppose that the periodic crystal Hamiltonian $H$ can be approximated by the atomic Hamiltonian $H_{\text{at}}$ near a lattice point $\mathbf{R}$, that is

$$H = H_{\text{at}} = \sum_{\mathbf{R}} H_{\text{at},\,\mathbf{R}}, \tag{4.1}$$

where

$$H_{\text{at},\,\mathbf{R}}\psi_n = \mathcal{E}_n\psi_n. \tag{4.2}$$

Here $H_{\text{at},\,\mathbf{R}}$ is the atomic Hamiltonian at $\mathbf{R}$. We are somewhat assuming that $|\psi_n(\mathbf{r}-\mathbf{R})|^2$ is very small when $|\psi_n(\mathbf{r}-\mathbf{R})|$ is larger than the lattice parameter. If we want to incorporate interactions between the atoms, one can rewrite the crystal Hamiltonian as follows

$$H = \sum_{\mathbf{R}} H_{\text{at},\,\mathbf{R}} + \Delta U(\mathbf{r}), \tag{4.3}$$

where $\Delta U(\mathbf{r})$ is a correction to the atomic potential. Since the system is periodic, the wavefunction must satisfy the Bloch condition:

$$\psi_{n\mathbf{k}}(\mathbf{r}) = \sum_{\mathbf{R}} \mathrm{e}^{i\mathbf{k}\cdot\mathbf{R}}\psi_n(\mathbf{r}-\mathbf{R}), \tag{4.4}$$

where $\mathbf{k}$ takes values through the first Brillouin zone [19, 45].

To show that $\psi_{n\mathbf{k}}(\mathbf{r})$ has indeed the periodicity of the crystal, first recall that the sum of two vectors of the Bravais lattice, say $\mathbf{R}-\mathbf{R}'$, is also a vector of the Bravais lattice. Then,

$$\psi_{n\mathbf{k}}(\mathbf{r}+\mathbf{R}) = \sum_{\mathbf{R}'} \mathrm{e}^{i\mathbf{k}\cdot\mathbf{R}'}\psi_n(\mathbf{r}+\mathbf{R}-\mathbf{R}') = \mathrm{e}^{i\mathbf{k}\cdot\mathbf{R}}\left(\sum_{\mathbb{R}} \mathrm{e}^{i\mathbf{k}\cdot\mathbb{R}}\psi_n(\mathbf{r}-\mathbb{R})\right) = \psi_{n\mathbf{k}}(\mathbf{r})\mathrm{e}^{i\mathbf{k}\cdot\mathbf{R}}. \tag{4.5}$$

Note that, independently of the crude approximation we have discussed here for the crystal Hamiltonian, a general solution for a latter, disregarding any approximation, must be of the following form

$$\psi(\mathbf{r}) = \sum_{\mathbf{R}} \mathrm{e}^{i\mathbf{k}\cdot\mathbf{R}}\phi(\mathbf{r}-\mathbf{R}), \tag{4.6}$$

where now $\phi(\mathbf{r})$ is not necessarily an atomic wavefunction, but nevertheless it can be expanded in terms of them

$$\phi(\mathbf{r}) = \sum_{n} b_n\psi_n(\mathbf{r}), \tag{4.7}$$

so that

$$H\psi(\mathbf{r}) = \left( \sum_{\mathbf{R}} H_{\mathrm{at},\mathbf{R}} + \Delta U(\mathbf{r}) \right) \psi(\mathbf{r}) = \mathcal{E}(\mathbf{k})\psi(\mathbf{r}). \tag{4.8}$$

Due to equation (4.7), sometimes the tight-binding method is also referred to as *the method of linear combinations of atomic orbitals*, because within this approximation we are considering a set of atomic levels [45].

In summary, the tight-binding approximation considers the atom as a system that is isolated and with its own atomic levels and takes into account the moving of the electrons between the atomic potentials [45].

### 4.1.1 Itinerant Electrons

When the outermost atomic shell is not closed, the remaining electrons in that shell can be either localized or itinerant. Their properties are the result of which of the four following energies dominates the electron: thermal, intraatomic, interatomic or electron-lattice [46].

In the case of localized electrons, the intraatomic energy dominates their behaviour, while in itinerant electrons, the energy that dominates is the interatomic one [46]. The itinerant electrons move from one atom to another, with a transition amplitude that may also depend on the spin state of the electron. For instance, in most transition metals, the electrons coming from the d-shells become itinerant ones in the crystal [47].

In the model of this work we are considering itinerant electrons that interact with a background magnetic moments [40]. In this thesis, we are going to mention two important concepts: the double exchange mechanism and the *sd* model.

## 4.2 The Double Exchange Mechanism

The double exchange mechanism was first proposed by Zener [48] to explain the ferromagnetism in mixed valence manganites. A few years later Anderson and Hasegawa [49] used this mechanism to solve a system of mixed valence dimers. The double exchange interaction relates two localized magnetic moments with an itinerant electron that travels between them [10].

More precisely, the double exchange mechanism considers two magnetic ions, denoted here as 1 and 2, and a mobile electron between the two ions. The model supposes that the electron and ion spins interact say antiferromagnetically, so that they want to align in opposite directions. Of course, if the physical effect is the opposite, the sign of the coupling constant

ought to be negative. The corresponding Hamiltonian that considers both cases is:

$$H = -t \sum_{m=\uparrow,\downarrow} (c^{\dagger}_{1,m} c_{2,m} + \text{H.C.}) + J(\boldsymbol{\sigma}_1 \cdot \mathbf{S}_1 + \boldsymbol{\sigma}_2 \cdot \mathbf{S}_2), \tag{4.9}$$

where $t$ is the hopping between sites 1 and 2, $c^{\dagger}_{i,m}$ and $c_{i,m}$ are the electron creation and annihilation operators at site $i$, with the spin degree of freedom, $\boldsymbol{\sigma}_i$ is the electron spin operator at site $i$, and $\mathbf{S}_i$ is the orientation of the ion spin. Here $i$ only takes values 1 and 2 [10, 50]. The first term in equation (4.9) describes how the electron moves between the ion cores, so an electron with spin up or down is annihilated at one site and create at the other. The second term represents how the spin of the itinerant electron aligns with the fixed spin. In this first approach, it is considered that each ion spin, which in this model are supposed to be fixed, carries spin $\frac{1}{2}$ [10]. There are sixteen basis states which are represented by

$$c^{\dagger}_{i,m} |0\rangle \otimes \gamma_1^{+} \gamma_2^{+} |{\downarrow\downarrow}\rangle , \tag{4.10}$$

where $i = 1, 2$ represents the position of the itinerant electron and $m = \uparrow\downarrow$ the spin direction. Also $\gamma_i^{+}$ are operators that take different values depending on the ion fixed spin polarization (at position $i$). For spin down $\gamma_i^{+} = 1$ and for spin up $\gamma_i^{+} = S_i^{+}$, where $S_i^{+}$ is the raising spin operator [1]. Using these basis states we can calculate

$$M_{i\,j} = \langle i|H|j\rangle , \tag{4.11}$$

and from there, the eigenvalues and eigenvectors of the corresponding model [10].

To simplify the model, we will consider (as was also done in [40]) that the ion spins are modeled as a classical ones

$$\mathbf{S}_j = S\mathbf{n}_j \tag{4.12}$$

Notice that the Hamiltonian (equation (4.9)) captures two distinct physical regimes for $J \gg t$ or $J \ll t$. In the first case, the Hamiltonian corresponds to the double exchange model and it is used to describe ferromagnetism in manganites. On the other hand, the weak coupling limit $J \ll t$ also called the $sd-$model, successfully explains ferromagnetism due to itinerant electrons [51].

We will see that in this system, an electron moving in a closed path acquires a Berry phase, which is gauge invariant. Let us brief recall about the latter concept.

[1] Note that the operators $\gamma_i^{+}$ and $S_i^{+}$ have as super index a plus sign (+), which is different to the dagger (†) symbol.

### 4.2.1 Gauge Invariance

In quantum mechanics, if $\psi(\mathbf{x}, t)$ describes the quantum state of a physical system, so does $\psi(\mathbf{x}, t)\mathrm{e}^{-i\theta}$. Note that $\theta$ is usually referred to as a global phase and it is constant. Thus quantum states have a *global symmetry*

$$\psi(\mathbf{x}, t) \to \psi(\mathbf{x}, t)\mathrm{e}^{-i\theta}, \tag{4.13}$$

and this, inturn, automatically implies that the equation of motion is invariant under this global symmetry.

There are other cases in which physical systems are invariant under a local phase transformation. That is, if the phase is a function $\theta = f(\mathbf{x}, t)$, the previous transformation becomes indeed local:

$$\psi(\mathbf{x}, t) \to \psi(\mathbf{x}, t)\mathrm{e}^{-if(\mathbf{x}, t)}. \tag{4.14}$$

Now, we have the basic concepts to present the details of the model.

## 4.3 Real-space Berry Phases in Itinerant Magnetic Systems: The Model

The model of this thesis is based on the work done by [40]. We consider itinerant electrons that interact with magnetic moments. This interaction is made through an exchange coupling $J$. Given the normalized vector field

$$\mathbf{n}_j = (\sin\theta_j \cos\varphi_j, \sin\theta_j \sin\varphi_j, \cos\theta_j), \tag{4.15}$$

the classical spin of the ion $j$ is given by equation (4.12).

The Hamiltonian that describes the system is

$$H = H_{\mathrm{t}} + H_{\mathrm{J}}, \tag{4.16}$$

where

$$H_{\mathrm{t}} = \sum_{j,\,k} (t_{kj}\mathbf{c}_k^{\dagger}\, U_{kj}\, \mathbf{c}_j + t_{kj}^{*}\mathbf{c}_j^{\dagger}\, U_{kj}^{\dagger}\, \mathbf{c}_k), \tag{4.17}$$

is the tight-binding Hamiltonian that considers SOC and

$$H_{\mathrm{J}} = \frac{-JS}{2} \sum_j \mathbf{c}_j^{\dagger} \boldsymbol{\sigma} \mathbf{c}_j \cdot \mathbf{n}_j, \tag{4.18}$$

is the Hamiltonian that models the exchange coupling between electrons and ions.

The tight-binding Hamiltonian (equation (4.17)), corresponds to the kinetic energy of the conduction electrons. This Hamiltonian considers the SOC by introducing the matrix $U_{kj}$. When the electron is moving from site $k$ to site $j$, the spin orientation changes due to the SOC. On the other hand, the exchange coupling Hamiltonian describes the interaction between the spin of the electron and that of the ion via Hund's coupling.

To understand better both Hamiltonians, we present the definition of each element presented in equations (4.17) and (4.18). The creation and annihilation operators in spinor notation are

$$\mathbf{c}_k = \begin{bmatrix} c_{k\uparrow} \\ c_{k\downarrow} \end{bmatrix}, \tag{4.19}$$

$$\mathbf{c}_k^\dagger = \begin{bmatrix} c_{k\uparrow}^\dagger & c_{k\downarrow}^\dagger \end{bmatrix}, \tag{4.20}$$

and

$$U_{kj} = \exp\left[ -\frac{i\alpha_{kj}}{2}(\mathbf{a}_{kj}\cdot\boldsymbol{\sigma})\right], \tag{4.21}$$

in which $\alpha_{kj}$ is the rotation angle that is induced by a finite SOC, $\mathbf{a}_{kj}$ is the unitary vector that indicates the direction of the rotation axis, and $\boldsymbol{\sigma} = (\sigma_x, \sigma_y, \sigma_z)$ is the vector of the Pauli matrices. The parameter that gives the hopping amplitude is

$$t_{kj} = |t_{kj}|\mathrm{e}^{i\beta_k}. \tag{4.22}$$

Note that if we choose $\alpha_{kj} = 0$, the Hamiltonian models a system in the absence of SOC, so that there is no rotation angle induced, and the Hamiltonian becomes SU(2) invariant.

It is necessary to assume that the exchange interaction is of the order or larger than the itinerant electrons' bandwidth. This is called *the double exchange limit*. This model gives us a low energy Hamiltonian that is a tight-binding model with spinless fermions whose hopping amplitudes are

$$\tilde{t}_{kj} = \tau_{kj}\mathrm{e}^{i\gamma_{kj}}, \tag{4.23}$$

in which the underlying magnetic moments are

$$\tau_{kj} = t_{kj}\sqrt{\frac{1+\mathbf{n}_k\cdot\mathbf{R}_{kj}\cdot\mathbf{n}_j}{2}}, \tag{4.24}$$

where

$$\mathbf{R}_{kj} = \exp[\alpha_{kj}(\mathbf{a}_{kj}\cdot\mathbf{L})], \tag{4.25}$$

is a rotation matrix of the SO(3) group, which is related to the rotation given by $U_{kj}$ and

$\mathbf{L} = (L_x, L_y, L_z)$, both belonging to the group SU(2) .

When the electron is moving through the triangle $jkl$, it acquires a net phase given by

$$\Phi_{jkl} = \beta_{jkl} + \gamma_{jkl}, \tag{4.26}$$

where each contribution has a different origin. The contribution given by

$$\beta_{jkl} = \beta_{jl} + \beta_{lk} + \beta_{kj}, \tag{4.27}$$

is a phase due to the complex hopping amplitudes $t_{kj}$ that can only take two values, 0 or $\pi$ because the Hamiltonian is time reversal invariant. On the other hand, the contribution given by

$$\gamma_{jkl} = \gamma_{jl} + \gamma_{lk} + \gamma_{kj}, \tag{4.28}$$

is the Berry phase. It appears due to the strong interaction between the local moments and the electronic spin.

In the computing of the real-space Berry curvature, we will consider an adiabatic process because it makes the analysis simpler and allows us to compare the Berry curvature with a fictitious magnetic field that is coupled to the orbital motion of the itinerant electrons [40]. In the presence of finite SOC the Berry connection is

$$\gamma_{kj} = \arg[\langle \mathbf{n}_k | U_{kj} | \mathbf{n}_j \rangle]. \tag{4.29}$$

In the following chapter we are interested in understanding how the spin rotation induced by the SOC changes the effective magnetic field. We also present the derivation of Berry phase for this type of systems.

# Chapter 5

# Real-space Berry Phases in Itinerant Magnetic Systems

In this chapter we will calculate the Berry phase under different approaches. First, we are going to take a geometric approach, then an algebraic approach and finally we will derive it in the continuum limit. In these three approaches, we are going to obtain the Berry phase for a SU(2) invariant system and for the case with SOC. This section presents in minute detail the procedure done by Cristian Batista and collaborators in [40].

## 5.1 Geometric Approach

This section's goal is to find a geometric description to the Berry phase. We are considering a model that changes the spin direction along a geodesic.

### 5.1.1 Geodesic Spin Rotations

For any two unit and non-collinear vectors $\mathbf{p}$ and $\mathbf{q}$ there are two spin states associated with them, that we denote as $|\mathbf{p}\rangle$ and $|\mathbf{q}\rangle$. We are interested in studying how the spin direction changes from $\mathbf{p}$ to $\mathbf{q}$ through a geodesic in the Bloch sphere. This procedure is done using a matrix $\tilde{U}_{\mathbf{q},\,\mathbf{p}}$, that for a geodesic, understood to be the shortest path possible, is

$$\tilde{U}_{\mathbf{q},\,\mathbf{p}} = \exp\left[-\frac{i\chi_{\mathbf{q},\,\mathbf{p}}}{2}(\mathbf{u}_{\mathbf{q},\,\mathbf{p}}\cdot\boldsymbol{\sigma})\right]. \tag{5.1}$$

This matrix rotates the spin direction from $\mathbf{p}$ to the $\mathbf{q}$ direction. Note that

$$\mathbf{p}\cdot\mathbf{q} = \cos\chi_{\mathbf{q},\,\mathbf{p}}, \tag{5.2}$$

so $\chi_{\mathbf{q},\mathbf{p}} = \arccos(\mathbf{p}\cdot\mathbf{q}) < \pi$. The rotation axis is given by the unit vector

$$\mathbf{u}_{\mathbf{q},\mathbf{p}} = \frac{\mathbf{p}\times\mathbf{q}}{|\mathbf{p}\times\mathbf{q}|} = \frac{\mathbf{p}\times\mathbf{q}}{\sin\chi_{\mathbf{q},\mathbf{p}}}. \tag{5.3}$$

Using that

$$\exp\left[i\theta(\mathbf{v}\cdot\boldsymbol{\sigma})\right] = \cos(\theta) + i(\mathbf{v}\cdot\boldsymbol{\sigma})\sin(\theta), \tag{5.4}$$

where $\theta$ is an angle and $\mathbf{v}$ is any vector, and also that

$$\begin{aligned} \sin(2\theta) &= 2\sin(\theta)\cos(\theta), \\ \frac{\sin(\theta)}{\sin(2\theta)} &= \frac{1}{2}\left[\cos\left(\frac{\theta}{2}\right)\right]^{-1}, \end{aligned} \tag{5.5}$$

we can do the following derivation

$$\begin{aligned} \langle\mathbf{q}|\,\tilde{U}_{\mathbf{q},\mathbf{p}}\,|\mathbf{p}\rangle &= \langle\mathbf{q}|\exp\left[-\frac{i\chi_{\mathbf{q},\mathbf{p}}}{2}(\mathbf{u}_{\mathbf{q},\mathbf{p}}\cdot\boldsymbol{\sigma})\right]|\mathbf{p}\rangle \\ &= \langle\mathbf{q}|\cos\left(\frac{-\chi_{\mathbf{q},\mathbf{p}}}{2}\right) + i(\mathbf{u}_{\mathbf{q},\mathbf{p}}\cdot\boldsymbol{\sigma})\sin\left(\frac{-\chi_{\mathbf{q},\mathbf{p}}}{2}\right)|\mathbf{p}\rangle \\ &= \cos\left(\frac{\chi_{\mathbf{q},\mathbf{p}}}{2}\right)\langle\mathbf{q}|\mathbf{p}\rangle - i\,\langle\mathbf{q}|\frac{(\mathbf{p}\times\mathbf{q})\cdot\boldsymbol{\sigma}}{\sin(\chi_{\mathbf{q},\mathbf{p}})}\sin\left(\frac{-\chi_{\mathbf{q},\mathbf{p}}}{2}\right)|\mathbf{p}\rangle \\ &= \cos\left(\frac{\chi_{\mathbf{q},\mathbf{p}}}{2}\right)\langle\mathbf{q}|\mathbf{p}\rangle - \frac{i}{2}\left[\cos\left(\frac{\chi_{\mathbf{q},\mathbf{p}}}{2}\right)\right]^{-1}\langle\mathbf{q}|[(\mathbf{p}\times\mathbf{q})\cdot\boldsymbol{\sigma}]|\mathbf{p}\rangle\,, \end{aligned} \tag{5.6}$$

where

$$\langle\mathbf{q}|\,[(\mathbf{p}\times\mathbf{q})\cdot\boldsymbol{\sigma}]\,|\mathbf{p}\rangle = 2i\sin^2\left(\frac{\chi_{\mathbf{q},\mathbf{p}}}{2}\right)\langle\mathbf{q}|\mathbf{p}\rangle\,, \tag{5.7}$$

so that

$$\begin{aligned} \langle\mathbf{q}|\,\tilde{U}_{\mathbf{q},\mathbf{p}}\,|\mathbf{p}\rangle &= \cos\left(\frac{\chi_{\mathbf{q},\mathbf{p}}}{2}\right)\langle\mathbf{q}|\mathbf{p}\rangle + \left[\cos\left(\frac{\chi_{\mathbf{q},\mathbf{p}}}{2}\right)\right]^{-1}\sin^2\left(\frac{\chi_{\mathbf{q},\mathbf{p}}}{2}\right)\langle\mathbf{q}|\mathbf{p}\rangle \\ &= \cos\left(\frac{\chi_{\mathbf{q},\mathbf{p}}}{2}\right)\left[1+\tan^2\left(\frac{\chi_{\mathbf{q},\mathbf{p}}}{2}\right)\right]\langle\mathbf{q}|\mathbf{p}\rangle \\ &= \cos\left(\frac{\chi_{\mathbf{q},\mathbf{p}}}{2}\right)\sec^2\left(\frac{\chi_{\mathbf{q},\mathbf{p}}}{2}\right)\langle\mathbf{q}|\mathbf{p}\rangle \\ &= \left[\cos\left(\frac{\chi_{\mathbf{q},\mathbf{p}}}{2}\right)\right]^{-1}\langle\mathbf{q}|\mathbf{p}\rangle = \frac{\langle\mathbf{q}|\mathbf{p}\rangle}{|\langle\mathbf{q}|\mathbf{p}\rangle\,|}. \end{aligned} \tag{5.8}$$

It is important to note that since $|\langle\mathbf{q}|\mathbf{p}\rangle\,|$ by definition is real and positive, the argument of $\langle\mathbf{q}|\tilde{U}_{\mathbf{q},\mathbf{p}}|\mathbf{p}\rangle$ is actually the argument of $\langle\mathbf{q}|\mathbf{p}\rangle$ [40]. This result is going to be useful in the derivation of an expression of the Berry curvature in the following section.

### 5.1.2 SU(2) Invariant Case

The Berry connection in the presence of the SOC is given by equation (4.29). The electron spin is not rotated as it hops between different sites $\alpha_{kj} = 0$, and so $U_{kj} = \mathrm{e}^0 = 1$. This implies that

$$\gamma_{kj} = \arg[\langle \mathbf{n}_k | \mathbf{n}_j \rangle]. \tag{5.9}$$

Note that using the result shown in equation (5.8) we can write

$$\begin{aligned} \gamma_{kj} &= \arg[\langle \mathbf{n}_k | U_{\mathbf{n}_k, \mathbf{n}_j} | \mathbf{n}_j \rangle] = \arg[\langle \mathbf{n}_k | (U^{1/N}_{\mathbf{n}_k, \mathbf{n}_j})^N | \mathbf{n}_j \rangle] \\ &= \arg[\langle \mathbf{n}_k | U_{\mathbf{n}_k, \mathbf{n}_{kj}^{(N-1)}} ... U_{\mathbf{n}_{kj}{}^{(2)}, \mathbf{n}_{kj}{}^{(1)}} U_{\mathbf{n}_{kj}{}^{(1)}, \mathbf{n}_j} | \mathbf{n}_j \rangle], \end{aligned} \tag{5.10}$$

where $\mathbf{n}_{kj}^{(n)}$, with $n = 1, 2, ..., N-1$ are unit vectors along the circle that contains the vectors $\mathbf{n}_j$ and $\mathbf{n}_k$ (Figure 5.2a). Using the orthogonality relation $\langle -\mathbf{p} | \mathbf{p} \rangle = 0$ and the resolution of the identity

$$\mathbb{I} = |\mathbf{p}\rangle \langle \mathbf{p}| + |-\mathbf{p}\rangle \langle -\mathbf{p}|, \tag{5.11}$$

and identifying $|\mathbf{p}\rangle = |\mathbf{n}_{kj}^{(n)}\rangle$ at each intermediate step in the expression of the geodesic matrix element that was found in the previous section (equation (5.8)), it can be obtained that

$$\begin{aligned} \gamma_{kj} &= \arg\left[ \langle \mathbf{n}_k | \tilde{U}_{\mathbf{n}_k, \mathbf{n}_{kj}^{(N-1)}} | \mathbf{n}_{kj}^{(N-1)} \rangle \langle \mathbf{n}_{kj}^{(N-1)} | ... | \mathbf{n}_{kj}^{(2)} \rangle \langle \mathbf{n}_{kj}^{(2)} | \tilde{U}_{\mathbf{n}_{kj}^{(2)}, \mathbf{n}_{kj}^{(1)}} | \mathbf{n}_{kj}^{(1)} \rangle \langle \mathbf{n}_{kj}^{(1)} | \tilde{U}_{\mathbf{n}_{kj}^{(1)}, \mathbf{n}_j} | \mathbf{n}_j \rangle \right] \\ &= \arg\left[ \frac{\langle \mathbf{n}_k | \mathbf{n}_{kj}^{(N-1)} \rangle}{|\langle \mathbf{n}_k | \mathbf{n}_{kj}^{(N-1)} \rangle|} ... \frac{\langle \mathbf{n}_{kj}^{(2)} | \mathbf{n}_{kj}^{(1)} \rangle}{|\langle \mathbf{n}_{kj}^{(2)} | \mathbf{n}_{kj}^{(1)} \rangle|} \frac{\langle \mathbf{n}_{kj}^{(1)} | \mathbf{n}_j \rangle}{|\langle \mathbf{n}_{kj}^{(1)} | \mathbf{n}_j \rangle|} \right]. \end{aligned} \tag{5.12}$$

Note that using

$$\arg(xyz) = \arg(x) + \arg(y) + \arg(z), \tag{5.13}$$

we can rewrite the Berry phase when the electron spin is not rotated as it hops between the sites of the triangle as follows

$$\gamma_{kj} = \arg\left[ \langle \mathbf{n}_k | \mathbf{n}_{kj}^{(N-1)} \rangle \right] + ... + \arg\left[ \langle \mathbf{n}_{kj}^{(2)} | \mathbf{n}_{kj}^{(1)} \rangle \right] + \arg\left[ \langle \mathbf{n}_{kj}^{(1)} | \mathbf{n}_j \rangle \right]. \tag{5.14}$$

The last equation is really important because it shows that the Berry phase for this system can be written as a sum of a very large number of infinitesimal Berry connections (Nb. when $N \to \infty$) that are in a closed loop in the Hilbert space. This allows to express the Berry phase as a surface integral of the Berry curvature whose boundary is the closed loop mentioned before [40].

It is important to note that if we consider a triangle, the Berry phase (in this close path) can be computed using equation (4.28). This Berry phase corresponds to half the solid angle generated by the triangle formed by the three vectors $\mathbf{n}_j$, $\mathbf{n}_k$ and $\mathbf{n}_l$ [40]. The diagram of the

triangular plaquette with the spin direction vectors and the SOC vector can be seen in Figure 5.1.

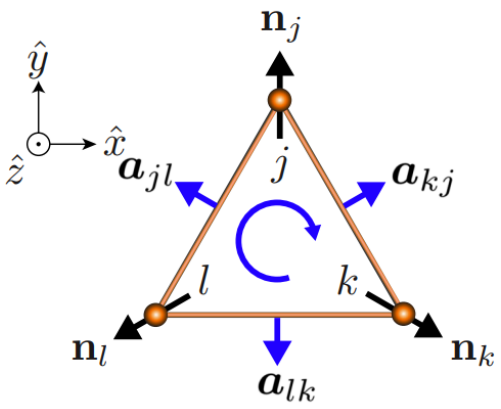


**Figure 5.1:** Triangular plaquette for an electron that picks a non-trivial Berry phase. The configuration is coplanar, the spin vectors are depicted in black arrows, the SOC vectors are in blue arrows and inside the triangle the direction of the bond orientation is shown. Image from [40].

### 5.1.3 General Case with Spin-orbit Interaction

In this section we are interested on computing the Berry phase of this model with finite SOC. Recall first the following useful results

$$\begin{aligned} &U_{kj}\left|\mathbf{n}_j\right\rangle \propto \left|R_{kj}\cdot\mathbf{n}_j\right\rangle, \\ &\left|\mathbf{p}\right\rangle = \left|R_{kj}\cdot\mathbf{n}_j\right\rangle, \\ &\mathbb{I} = \left|R_{kj}\cdot\mathbf{n}_j\right\rangle\left\langle R_{kj}\cdot\mathbf{n}_j\right| + \left|-R_{kj}\cdot\mathbf{n}_j\right\rangle\left\langle -R_{kj}\cdot\mathbf{n}_j\right|. \end{aligned} \tag{5.15}$$

Note that we are now considering that the system possesses SOC. Then, the Berry connection in this case can be written as follows

$$\begin{aligned} \gamma_{kj} &= \arg\left[\left\langle\mathbf{n}_k\right| U_{kj}\left|\mathbf{n}_j\right\rangle\right] \\ &= \arg\left[\left\langle\mathbf{n}_k|R_{kj}\cdot\mathbf{n}_j\right\rangle\left\langle R_{kj}\cdot\mathbf{n}_j|U_{kj}|\mathbf{n}_j\right\rangle\right] \\ &= \arg\left[\left\langle\mathbf{n}_k|\tilde{U}_{\mathbf{n}_k,\,R_{kj}\cdot\mathbf{n}_j}|R_{kj}\cdot\mathbf{n}_j\right\rangle\left\langle R_{kj}\cdot\mathbf{n}_j|U_{kj}|\mathbf{n}_j\right\rangle\right] \\ &= \arg\left[\left\langle\mathbf{n}_k|\tilde{U}_{\mathbf{n}_k,\,R_{kj}\cdot\mathbf{n}_j}U_{kj}|\mathbf{n}_j\right\rangle\right]. \end{aligned} \tag{5.16}$$

In this representation the electron spin is rotated first around $\mathbf{a}_{kj}$ (due to the SOC) and then along the circle that contains $R_{kj}\cdot\mathbf{n}_j$ and $\mathbf{n}_k$. We then use

$$U_{kj}^{-1}\tilde{U}_{\mathbf{n}_k,\,R_{kj}\cdot\mathbf{n}_j}U_{kj} = \tilde{U}_{R_{kj}^{-1}\cdot\mathbf{n}_k,\,\mathbf{n}_j}, \tag{5.17}$$

to get that

$$\gamma_{kj} = \arg\left[\langle \mathbf{n}_k | \tilde{U}_{\mathbf{n}_k,\, R_{kj}\cdot\mathbf{n}_j} U_{kj} | \mathbf{n}_j \rangle\right] = \arg\left[\langle \mathbf{n}_k | U_{kj} \tilde{U}_{R_{kj}^{-1}\cdot\mathbf{n}_k,\, \mathbf{n}_j} | \mathbf{n}_j \rangle\right], \tag{5.18}$$

where the order of the spin rotation has changed. We are interested to compute the Berry connection, for which the following identity is useful

$$U_{kj}\tilde{U}_{R_{kj}^{-1}\cdot\mathbf{n}_k,\,\mathbf{n}_j} = \pm U_{kj}\tilde{U}_{R_{kj}^{-1}\cdot\mathbf{n}_k,\,\boldsymbol{\nu}_{kj}}\tilde{U}_{\boldsymbol{\nu}_{kj},\,\mathbf{n}_j} = \pm\tilde{U}_{\mathbf{n}_k,\,R_{kj}\cdot\boldsymbol{\nu}_{kj}}U_{kj}\tilde{U}_{\boldsymbol{\nu}_{kj},\,\mathbf{n}_j}, \tag{5.19}$$

where $\boldsymbol{\nu}_{kj}$ is an unit vector along the circle that contains $\mathbf{n}_j$ and $R_{kj}^{-1}\cdot\mathbf{n}_k$, and is also in the great circle perpendicular to $\mathbf{a}_{kj}$. The sign $\pm$ shows that the left and the right side of the equation differs for a spin rotation of $2\pi$, so that $\mathrm{e}^{i\pi} = -1$.

The spin rotation mentioned before $U_{kj}$ becomes a geodesic spin rotation $\tilde{U}_{\boldsymbol{\omega}_{kj},\boldsymbol{\nu}_{kj}}$ where

$$\boldsymbol{\omega}_{kj} = R_{kj}\cdot\boldsymbol{\nu}_{kj}. \tag{5.20}$$

Thus, the previous identity given in equation (5.19) becomes

$$U_{kj}\tilde{U}_{R_{kj}^{-1}\cdot\mathbf{n}_k,\,\mathbf{n}_j} = \pm\tilde{U}_{\mathbf{n}_k,\,\boldsymbol{\omega}_{kj}}\tilde{U}_{\boldsymbol{\omega}_{kj},\,\boldsymbol{\nu}_{kj}}\tilde{U}_{\boldsymbol{\nu}_{kj},\,\mathbf{n}_j}. \tag{5.21}$$

Notice that since $\boldsymbol{\nu}_{kj}$ is then along the great circle that is perpendicular to $\mathbf{a}_{kj}$, and, more over, the great circle contains $\mathbf{n}_j$ and $R_{kj}^{-1}\cdot\mathbf{n}_k$, and so $\boldsymbol{\nu}_{kj}$ can be expressed as follows

$$\boldsymbol{\nu}_{kj} = \frac{\mathbf{a}_{kj}\times\left[\mathbf{n}_j\times(R_{kj}^{-1}\cdot\mathbf{n}_k)\right]}{\left|\mathbf{a}_{kj}\times\left[\mathbf{n}_j\times(R_{kj}^{-1}\cdot\mathbf{n}_k)\right]\right|}, \tag{5.22}$$

and from here

$$\boldsymbol{\omega}_{kj} = R_{kj}\cdot\boldsymbol{\nu}_{kj} = \frac{\mathbf{a}_{kj}\times[(R_{kj}\cdot\mathbf{n}_j)\times\mathbf{n}_k]}{|\mathbf{a}_{kj}\times[(R_{kj}\cdot\mathbf{n}_j)\times\mathbf{n}_k]|}. \tag{5.23}$$

Please note that $\boldsymbol{\nu}_{kj}$ and $\boldsymbol{\omega}_{kj}$ are in the intersection of the great circles, and the negative of these vectors ($-\boldsymbol{\nu}_{kj}$ and $-\boldsymbol{\omega}_{kj}$) are along these intersections too. Then, the Berry connection becomes

$$\begin{aligned}
\gamma_{kj} &= \arg\left[\langle \mathbf{n}_k | U_{kj}\tilde{U}_{R_{kj}^{-1}\cdot\mathbf{n}_k,\,\mathbf{n}_j} | \mathbf{n}_j\rangle\right] \\
&= \arg\left[\langle \mathbf{n}_k | \pm\tilde{U}_{\mathbf{n}_k,\,\boldsymbol{\omega}_{kj}}\tilde{U}_{\boldsymbol{\omega}_{kj},\,\boldsymbol{\nu}_{kj}}\tilde{U}_{\boldsymbol{\nu}_{kj},\,\mathbf{n}_j} | \mathbf{n}_j\rangle\right] \\
&= \arg\left[\pm\langle \mathbf{n}_k | \tilde{U}_{\mathbf{n}_k,\,\boldsymbol{\omega}_{kj}} | \boldsymbol{\omega}_{kj}\rangle\langle\boldsymbol{\omega}_{kj} | \tilde{U}_{\boldsymbol{\omega}_{kj},\,\boldsymbol{\nu}_{kj}} | \boldsymbol{\nu}_{kj}\rangle\langle\boldsymbol{\nu}_{kj} | \tilde{U}_{\boldsymbol{\nu}_{kj},\,\mathbf{n}_j} | \mathbf{n}_j\rangle\right] \\
&= \arg\left[\langle \mathbf{n}_k | \boldsymbol{\omega}_{kj}\rangle\right] + \arg\left[\langle\boldsymbol{\omega}_{kj} | \boldsymbol{\nu}_{kj}\rangle\right] + \arg\left[\langle\boldsymbol{\nu}_{kj} | \mathbf{n}_j\rangle\right] \pmod{\pi}.
\end{aligned} \tag{5.24}$$

As it can be seen, the sign $\pm$ disappears in the last step. This is a consequence of choosing the same sign in order to avoid that the contribution vanishes because of the condition $\langle -\mathbf{p}|\mathbf{p}\rangle = 0$. The importance of the last equation is that it shows that the Berry phase is the sum of nine

different Berry connections that have the form that we saw in the SU(2) invariant case but with an important difference. In the SU(2) invariant case, the system does not posses SOC, and we found that the Berry phase is half the solid angle formed by the three vectors $\mathbf{n}$. In this case, were SOC is present, the Berry phase is half the solid angle of the nonagon created with the three vectors $\mathbf{n}$, the three vectors $\boldsymbol{\nu}$ and the three vectors $\boldsymbol{\omega}$ [40].

Also, the importance of the Berry curvature computed in equation (5.24) is that it shows that for a system with SOC, it is possible to have an effective magnetic field if the spin configuration is collinear or coplanar.

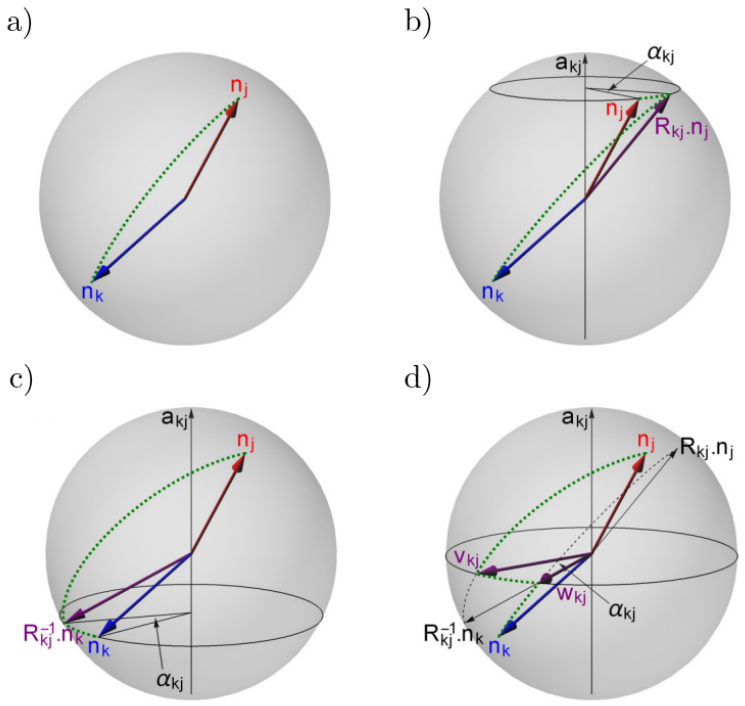


**Figure 5.2:** Geometric approach for the Berry phase. a) Schematic representation of the geodesic (green line) that connects the unit vectors $\mathbf{n}_j$ and $\mathbf{n}_k$. b) Geometric representation of equation (5.16): the spin direction is rotated due to the SOC around the vector $\mathbf{a}_{kj}$, and then is rotated along the geodesic that connects to $\mathbf{R}_{kj} \cdot \mathbf{n}_k$. c) Geometric representation of equation (5.18): in this equation, the spin direction is rotated along the geodesic that connects $\mathbf{n}_j$ with $R_{kj}^{-1} \cdot \mathbf{n}_k$ and around the vector $\mathbf{a}_{kj}$. d). Geometric representation of the spin rotation $\tilde{U}_{\boldsymbol{\omega}_{kj},\boldsymbol{\nu}_{kj}}$ [40]. Image from [40].

## 5.2 Algebraic Approach

In this section, we are seeking to show the same results we got in the geometric approach, but using an algebraic one.

### 5.2.1 SU(2) Invariant Case

In absence of the SOC the Berrry phase acquired by an electron moving along three sites ($j$, $k$, and $l$) forming a triangle is

$$\gamma_{jkl} = \frac{\Omega_{jkl}}{2}. \tag{5.25}$$

We introduce an arbitrary unit vector that is parallel to the quantization axis: $\mathbf{n} = \hat{\mathbf{z}}$. The spin state at site $j$ in this frame is given by

$$|\mathbf{n}_j\rangle = \cos\frac{\theta_j}{2}|\uparrow\rangle + \mathrm{e}^{i\phi_j}\sin\frac{\theta_j}{2}|\downarrow\rangle. \tag{5.26}$$

When there is no SOC, we have that the Berry connection is

$$\begin{aligned}\gamma_{kj} &= \arg\left[\langle\mathbf{n}_k|\mathbf{n}_j\rangle\right] \\ &= \arg\left[\left(\langle\uparrow|\cos\frac{\theta_k}{2} + \langle\downarrow|\,\mathrm{e}^{-i\phi_k}\sin\frac{\theta_k}{2}\right)\left(\cos\frac{\theta_j}{2}|\uparrow\rangle + \mathrm{e}^{i\phi_j}\sin\frac{\theta_j}{2}|\downarrow\rangle\right)\right] \\ &= \\ &= \arg\left[\cos\frac{\theta_k}{2}\cos\frac{\theta_j}{2} + \mathrm{e}^{i(\phi_j-\phi_k)}\sin\frac{\theta_k}{2}\sin\frac{\theta_j}{2}\right].\end{aligned} \tag{5.27}$$

Using that

$$\mathrm{e}^{i(\phi_j-\phi_k)} = \cos(\phi_j-\phi_k) + i\sin(\phi_j-\phi_k), \tag{5.28}$$

and that

$$\arg(z) = \arctan\left(\frac{y}{x}\right), \tag{5.29}$$

where $z = x+iy$, it can be derived that the real and imaginary parts inside the argument above are:

$$x = \cos\frac{\theta_k}{2}\cos\frac{\theta_j}{2} + \cos(\phi_j-\phi_k)\sin\frac{\theta_k}{2}\sin\frac{\theta_j}{2}, \tag{5.30}$$

and

$$y = \sin(\phi_j-\phi_k)\sin\frac{\theta_k}{2}\sin\frac{\theta_j}{2}. \tag{5.31}$$

Substituting these expressions into the Berry connection we arrive at the following:

$$\begin{aligned}\tan\gamma_{kj} &= \frac{\sin(\phi_j-\phi_k)\sin\frac{\theta_k}{2}\sin\frac{\theta_j}{2}}{\cos\frac{\theta_k}{2}\cos\frac{\theta_j}{2} + \cos(\phi_j-\phi_k)\sin\frac{\theta_k}{2}\sin\frac{\theta_j}{2}} \\ &= \frac{\sin(\theta_j-\theta_k)}{\cot\frac{\theta_j}{2}\cot\frac{\theta_k}{2} + \cos(\phi_j-\phi_k)}.\end{aligned} \tag{5.32}$$

Recall further that for 3 generic vectors, let's say $\mathbf{a}$, $\mathbf{b}$ and $\mathbf{c}$:

$$\tan\left(\frac{1}{2}\Omega\right) = \frac{\mathbf{a}\cdot(\mathbf{b}\times\mathbf{c})}{abc + (\mathbf{a}\cdot\mathbf{b})c + (\mathbf{a}\cdot\mathbf{c})b + (\mathbf{b}\cdot\mathbf{c})a}, \tag{5.33}$$

where $\Omega$ is the solid angle subtended by the surface of the triangle $ABC$, and notation $a = |\mathbf{a}|$. In spherical coordinates:

$$\mathbf{n}_j = (\sin\theta_j \cos\phi_j,\, \sin\theta_j \sin\phi_j,\, \cos\theta_j), \tag{5.34}$$

$$\mathbf{n}_k = (\sin\theta_k \cos\phi_k,\, \sin\theta_k \sin\phi_k,\, \cos\theta_k), \tag{5.35}$$

and

$$\mathbf{n} = \hat{\mathbf{z}}. \tag{5.36}$$

Using these vectors we compute all the ingredients that appear in equation (5.33)

$$\begin{aligned} \mathbf{n} \cdot (\mathbf{n}_j \times \mathbf{n}_k) &= \hat{\mathbf{z}} \cdot \hat{\mathbf{z}}(\sin\theta_j \cos\phi_j \sin\theta_k \sin\phi_k - \sin\theta_k \cos\phi_k \sin\theta_j \sin\phi_j) \\ &= \sin\theta_j \sin\theta_k(\cos\theta_j \sin\phi_k - \cos\phi_k \sin\theta_j) \\ &= \sin\theta_j \sin\theta_k \sin(\phi_k - \phi_j), \end{aligned} \tag{5.37}$$

$$n n_j n_k = 1, \tag{5.38}$$

$$(\mathbf{n} \cdot \mathbf{n}_j) n_k = \cos\theta_j, \tag{5.39}$$

$$(\mathbf{n} \cdot \mathbf{n}_k) n_j = \cos\theta_k, \tag{5.40}$$

$$(\mathbf{n}_j \cdot \mathbf{n}_k) n = \sin\theta_j \cos\phi_j \sin\theta_k \sin\phi_k + \sin\theta_j \sin\phi_j \sin\theta_k \sin\phi_k + \cos\theta_j \cos\theta_k, \tag{5.41}$$

$$\cos(\phi_j - \phi_k) = \cos\phi_j \cos\phi_k + \sin\phi_j \sin\phi_k, \tag{5.42}$$

All in all, the Berry connection is

$$\tan\gamma_{kj} = \tan\frac{\Omega(\phi_j - \phi_k,\, \theta_j,\, \theta_k)}{2} = \frac{\sin\theta_j \sin\theta_k \sin(\phi_k - \phi_j)}{1 + \cos\theta_j + \cos\theta_k + \sin\theta_j \sin\theta_k \cos(\phi_j - \phi_k) + \cos\theta_j \cos\theta_k}.$$

Note further

$$\frac{1 + \cos\theta_j + \cos\theta_k + \cos\theta_j \cos\theta_k}{\sin\theta_j \sin\theta_k} = \left(\frac{1 + \cos\theta_j}{\sin\theta_j}\right)\left(\frac{1 + \cos\theta_k}{\sin\theta_k}\right) = \cot\frac{\theta_j}{2}\cot\frac{\theta_k}{2}, \tag{5.43}$$

and

$$\frac{\sin\theta_j \sin\theta_k \cos(\phi_j - \phi_k)}{\sin\theta_j \sin\theta_k} = \cos(\phi_j - \phi_k), \tag{5.44}$$

so that the Berry connection can be alternatively written as

$$\tan\gamma_{kj} = \frac{\sin\phi_j - \phi_k}{\cot\frac{\theta_j}{2}\cot\frac{\theta_k}{2} + \cos(\phi_j - \phi_k)} = \tan\frac{\Omega(\phi_j - \phi_k,\, \theta_j,\, \theta_k)}{2}, \tag{5.45}$$

$$\gamma_{kj} = \frac{\Omega(\phi_j - \phi_k,\, \theta_j,\, \theta_k)}{2}, \tag{5.46}$$

where $\Omega(\phi_j - \phi_k,\, \theta_j,\, \theta_k)$ is the solid angle subtended by the vectors $\mathbf{n}$, $\mathbf{n}_k$ and $\mathbf{n}_j$. The Berry

phase, according to equation (5.25) is [40]

$$\gamma_{jkl} = \frac{\Omega_{jkl}}{2}, \tag{5.47}$$

which agrees with expected when the Berry connections of the form of equation (5.46) are summed to form the triangular plaquette.

### 5.2.2 General Case with Spin-orbit Interaction

Recall that in this case we have

$$\gamma_{jkl} = \arg\left[\langle \mathbf{n}_k | U_{kj} | \mathbf{n}_j \rangle \langle \mathbf{n}_l | U_{lk} | \mathbf{n}_k \rangle \langle \mathbf{n}_j | U_{jl} | \mathbf{n}_l \rangle\right]. \tag{5.48}$$

Under local rotations of the spin reference frame, the Berry phase is invariant:

$$\begin{array}{lll} |\mathbf{n}'_j\rangle = \mathcal{U}_j |\mathbf{n}_j\rangle, & |\mathbf{n}'_k\rangle = \mathcal{U}_k |\mathbf{n}_k\rangle, & |\mathbf{n}'_l\rangle = \mathcal{U}_l |\mathbf{n}_l\rangle, \\ \mathbf{n}'_j = \mathcal{R}_j \cdot \mathbf{n}_j, & \mathbf{n}'_k = \mathcal{R}_k \cdot \mathbf{n}_k, & \mathbf{n}'_l = \mathcal{R}_l \cdot \mathbf{n}_l, \end{array} \tag{5.49}$$

where $\mathcal{R}$ is the SO(3) rotation matrix associated with the SU(2) matrix $\mathcal{U}_j$ if

$$\begin{array}{l} U'_{kj} = \mathcal{U}_k U_{kj} \mathcal{U}_j^\dagger, \\ U'_{lk} = \mathcal{U}_l U_{lk} \mathcal{U}_k^\dagger, \\ U'_{jl} = \mathcal{U}_j U_{jl} \mathcal{U}_l^\dagger. \end{array} \tag{5.50}$$

Let us now introduce the Wilson loop operator [52, 53]

$$\mathcal{A}_{jkl} = U_{jl} U_{lk} U_{kj} = \exp\left[-\frac{i\alpha_{jkl}}{2}(\mathbf{a}_{jkl} \cdot \boldsymbol{\sigma})\right], \tag{5.51}$$

which is gauge-invariant [40].

To find a useful expression for $\gamma_{jkl}$, we rotate to a local reference frame of two spins (for example $k$ and $l$), so that the unit operator transforms into the identity on two out of three bonds. Consider that the bonds that are going to become the identity are $kj$ and $jl$. Then, the local unit transformations that perform this local rotation are:

$$\begin{array}{llll} \mathcal{U}_j = \mathbb{I}, & \mathcal{U}_k = U_{kj}^\dagger, & \mathcal{U}_l = U_{jl}, \\ \mathcal{R}_j = \mathbb{I}, & \mathcal{R}_k = R_{kj}^T, & \mathcal{R}_l = R_{jl}. \end{array} \tag{5.52}$$

Note that if we compute this transformation, the Wilson loop $\mathcal{A}_{jkl}$ does not change, and so, the unit operator of the bond $lk$ has to be the Wilson loop, as we will see below [40].

Finally, we need to align the global quantization axis $\hat{\mathbf{n}}$ with $\mathbf{a}_{jkl}$, which represents the Wil-

son loop's rotation axis. In this new reference frame it is necessary to compute again the Berry connections using that, in the presence of the SOC, the connection is $\gamma_{xy} = \arg[\langle \mathbf{n}_x | U_{xy} | \mathbf{n}_\mathbf{y} \rangle]$. The new expression of the Berry connection is

$$\gamma_{kj} = \arg[\langle \mathbf{n}_k | U_{kj} | \mathbf{n}_j \rangle] = \arg[\langle \mathbf{n}'_k | \mathcal{U}_k U_{kj} \mathcal{U}_j^\dagger | \mathbf{n}'_j \rangle] = \arg[\langle \mathbf{n}'_k | U_{kj}^\dagger U_{kj} \mathbb{I} | \mathbf{n}'_j \rangle] = \arg[\langle \mathbf{n}'_k | \mathbf{n}'_j \rangle], \quad (5.53)$$

which, similarly to the last result in the previous section, can be written as

$$\gamma_{kj} = \arg[\langle \mathbf{n}'_k | \mathbf{n}'_j \rangle] = \frac{\Omega(\phi'_j - \phi'_k,\, \theta'_j,\, \theta'_k)}{2}. \quad (5.54)$$

Of course, the same expression is obtained for $\gamma_{jl}$, that is:

$$\gamma_{jl} = \arg[\langle \mathbf{n}'_j | \mathbf{n}'_l \rangle] = \frac{\Omega(\phi'_l - \phi'_j,\, \theta'_l,\, \theta'_j)}{2}. \quad (5.55)$$

For the bond that contains the two spins whose local reference frames have been rotated, the Berry connection is, in turn,

$$\begin{aligned} \gamma_{lk} &= \arg[\langle \mathbf{n}_l | U_{lk} | \mathbf{n}_k \rangle] = \arg[\langle \mathbf{n}'_l | \mathcal{U}_l U_{lk} \mathcal{U}_k^\dagger | \mathbf{n}'_k \rangle] = \arg[\langle \mathbf{n}'_l | U_{jl} U_{lk} U_{kj} | \mathbf{n}'_k \rangle] \\ &= \arg[\langle \mathbf{n}'_k | \mathcal{A}_{jkl} | \mathbf{n}'_j \rangle] = \arg[\langle \mathbf{n}'_k | \exp\left[\frac{-i\alpha_{jkl}}{2}(\mathbf{a}_{jkl} \cdot \boldsymbol{\sigma})\right] | \mathbf{n}'_j \rangle] \\ &= \arg[\langle \mathbf{n}'_k | \mathrm{e}^{-i\alpha_{jkl}/2} \cos\frac{\theta'_k}{2} \cos\frac{\theta'_l}{2} + \mathrm{e}^{i(\phi'_k - \phi_l + \frac{1}{1}\alpha_{jkl})} \sin\frac{\theta'_k}{2} \sin\frac{\theta'_l}{2} | \mathbf{n}'_j \rangle], \end{aligned} \quad (5.56)$$

and, using the result that we got before, the last expression can be written as

$$\gamma_{lk} = \frac{-\alpha_{jkl}}{2} + \frac{\Omega(\phi'_k - \phi_l + \alpha_{jkl},\, \theta'_k,\, \theta'_l)}{2}. \quad (5.57)$$

The Berry phase that the electron acquires while moving along the triangle given by $jkl$ is then:

$$\begin{aligned} \gamma_{jkl} &= \gamma_{kj} + \gamma_{jl} + \gamma_{lk} \\ &= \frac{\Omega(\phi'_j - \phi'_k,\, \theta'_j,\, \theta'_k)}{2} + \frac{\Omega(\phi'_l - \phi'_j,\, \theta'_l,\, \theta'_j)}{2} - \frac{\alpha_{jkl}}{2} + \frac{\Omega(\phi'_k - \phi_l + \alpha_{jkl},\, \theta'_k,\, \theta'_l)}{2}. \end{aligned} \quad (5.58)$$

Using the result of the Berry phase in the previous section, we can define

$$\frac{\Omega'_{jkl}}{2} \equiv \frac{\Omega(\phi'_j - \phi'_k,\, \theta'_j,\, \theta'_k)}{2} + \frac{\Omega(\phi'_l - \phi'_j,\, \theta'_l,\, \theta'_j)}{2} + \frac{\Omega(\phi'_k - \phi'_l,\, \theta'_k,\, \theta'_l)}{2}, \quad (5.59)$$

and also

$$\delta\Omega'_{jkl} \equiv \Omega(\phi'_k - \phi'_l + \alpha_{jkl},\, \theta'_k,\, \theta'_l) - \Omega(\phi'_k - \phi'_l,\, \theta'_k,\, \theta'_l), \quad (5.60)$$

which allows us to finally express the Berry phase as

$$\gamma_{jkl} = \frac{\Omega'_{jkl}}{2} + \hat{\gamma}_{jkl}, \tag{5.61}$$

where

$$\hat{\gamma}_{jkl} = -\frac{\alpha_{jkl}}{2} + \frac{\delta\Omega'_{jkl}}{2}. \tag{5.62}$$

It is important to notice that the Berry phase has acquired a new term given by $\hat{\gamma}_{jkl}$. This contribution is due to the Wilson loop. Equation (5.61) is a generalization of equation (5.25) which can be used only in SU(2) invariant systems because of the restrictions that we used.

In order to show that the collinear and the coplanar configurations induce a Berry phase which is neither 0 nor $\pi$, and that this Berry phase acts as a magnetic flux, we are going to think about a collinear ferromagnet. This means that, given a reference frame the spins point in the same direction, and therefore, the solid angle contribution becomes zero. As a consequence of this the Berry phase for this system simplifies to

$$\gamma_{jkl} = -\frac{\alpha_{jkl}}{2}, \tag{5.63}$$

This is the proof that a ferromagnetic system with SOC has a Berry phase in real space that is proportional to the rotation angle of Wilson's loop. This result reproduces that reported in 1954 by Karplus and Luttinger [33].

### 5.2.3 Limit of Small Spin-orbit Interaction

In this section we are going to explore the Berry phase for systems with small SOC, which implies that $\alpha_{kj} \ll 1$ for all the bonds labeled as $kj$ which are connected by hopping amplitudes. These hopping amplitudes $t_{kj}$ are finite and because of the exponential decay of the atomic orbitals we have considered that they vanished beyond a characteristic distance that is given by a few lattice spaces.

At first, we expand the unit operator $U_{kj}$ and the Wilson loop operator up to first order in $\alpha_{kj}$ and $\alpha_{jkl}$, respectively, so that

$$U_{kj} = 1 - \frac{i\alpha_{kj}}{2}(\mathbf{a}_{kj} \cdot \boldsymbol{\sigma}) + \mathcal{O}(\alpha^2), \tag{5.64}$$

and

$$\begin{aligned}\mathcal{A}_{kjl} = U_{jl}U_{lk}U_{kj} &= \left[1 - \frac{i\alpha_{jl}}{2}(\mathbf{a}_{jl}\cdot\boldsymbol{\sigma})\right]\left[1 - \frac{i\alpha_{lk}}{2}(\mathbf{a}_{lk}\cdot\boldsymbol{\sigma})\right]\left[1 - \frac{i\alpha_{kj}}{2}(\mathbf{a}_{kj}\cdot\boldsymbol{\sigma})\right] + \mathcal{O}(\alpha^2) \\ &= 1 - \frac{i}{2}\left[(\alpha_{lk}\mathbf{a}_{lk} + \alpha_{jl}\mathbf{a}_{jl} + \alpha_{kj}\mathbf{a}_{kj})\cdot\boldsymbol{\sigma}\right] + \mathcal{O}(\alpha^2),\end{aligned} \tag{5.65}$$

where we have defined the following

$$\begin{aligned}\alpha_{jkl} &= |\boldsymbol{\nu}_{jkl}|, \\ \mathbf{a}_{jkl} &= \frac{\nu_{jkl}}{|\boldsymbol{\nu}_{jkl}|}, \\ \boldsymbol{\nu}_{jkl} &= \alpha_{kj}\mathbf{a}_{kj} + \alpha_{lk}\mathbf{a}_{lk} + \alpha_{jl}\mathbf{a}_{jl}.\end{aligned} \tag{5.66}$$

The Berry phase in equation (5.62), when expanded up to second order is

$$\begin{aligned}\hat{\gamma}_{jkl} &\approx \left[\frac{-\alpha}{2} + \frac{\Omega(\phi'_k - \phi'_l + \alpha,\, \theta'_k,\, \theta'_l)}{2} - \frac{\Omega(\phi'_k - \phi'_l,\, \theta'_k,\, \theta'_l)}{2}\right]\Bigg|_{\alpha=0} \\ &\quad + \alpha_{jkl}\left[-\frac{1}{2} + \frac{1}{2}\frac{\partial}{\partial\alpha}\Omega(\phi'_k - \phi'_l + \alpha,\, \theta'_k,\, \theta'_l)\Big|_{\alpha=0}\right] \\ &= \frac{\alpha_{jkl}}{2}\left[-1 + \frac{\partial}{\partial\alpha}\Omega(\phi'_k - \phi'_l + \alpha,\, \theta'_k,\, \theta'_l)\Big|_{\alpha=0}\right].\end{aligned} \tag{5.67}$$

Following the same procedure that we did in equation (5.32), we know that

$$\tan\frac{\Omega(\phi'_k - \phi'_l + \alpha,\, \theta'_k,\, \theta'_l)}{2} = \frac{\sin(\phi'_k - \phi'_l + \alpha)}{\cot\frac{\theta'_k}{2}\cot\frac{\theta'_l}{2} + \cos(\phi'_k - \phi'_l + \alpha)}, \tag{5.68}$$

from which we can get that

$$\frac{\Omega(\phi'_k - \phi'_l + \alpha,\, \theta'_k,\, \theta'_l)}{2} = \arctan\left[\frac{\sin(\phi'_k - \phi'_l + \alpha)}{\cot\frac{\theta'_k}{2}\cot\frac{\theta'_l}{2} + \cos(\phi'_k - \phi'_l + \alpha)}\right], \tag{5.69}$$

and using

$$\frac{d}{dx}\arctan(u) = \frac{u'}{1+u^2}, \tag{5.70}$$

we can painfully write

$$\begin{aligned}\frac{\partial}{\partial\alpha}\left(\frac{\Omega(\phi'_k-\phi'_l+\alpha,\,\theta'_k,\,\theta'_l)}{2}\right) &= \frac{\frac{\cos(\prime_k-\phi'_l+\alpha)\left[\cot\frac{\theta'_k}{2}\cot\frac{\theta'_l}{2}+\cos(\prime_k-\phi'_l+\alpha)\right]+\sin^2(\phi'_k-\phi'_l+\alpha)}{\left[\cot\frac{\theta'_k}{2}\cot\frac{\theta'_l}{2}+\cos(\prime_k-\phi'_l+\alpha)\right]^2}}{1+\left[\frac{\sin(\phi'_k-\phi'_l+\alpha)}{\cot\frac{\theta'_k}{2}\cot\frac{\theta'_l}{2}+\cos(\phi'_k-\phi'_l+\alpha)}\right]^2} \\ &= \frac{\cos(\phi'_k-\phi'_l+\alpha)\cot\frac{\theta'_k}{2}\cot\frac{\theta'_l}{2}+1}{\left(\cot\frac{\theta'_k}{2}\cot\frac{\theta'_l}{2}\right)^2+2\cot\frac{\theta'_k}{2}\cot\frac{\theta'_l}{2}\cos(\phi'_k-\phi'_l+\alpha)+1},\end{aligned} \tag{5.71}$$

so that

$$\frac{\partial}{\partial\alpha}\left(\frac{\Omega(\phi'_k-\phi'_l+\alpha,\,\theta'_k,\,\theta'_l)}{2}\right)\Bigg|_{\alpha=0} = \frac{\cos(\phi'_k-\phi'_l)\cot\frac{\theta'_k}{2}\cot\frac{\theta'_l}{2}+1}{\left(\cot\frac{\theta'_k}{2}\cot\frac{\theta'_l}{2}\right)^2+2\cos(\phi'_k-\phi'_l)\cot\frac{\theta'_k}{2}\cot\frac{\theta'_l}{2}+1}. \tag{5.72}$$

The Berry phase is then

$$\begin{aligned}\hat{\gamma}_{jkl} &= \alpha_{jkl}\left[\frac{-1}{2}+\frac{\cos(\phi'_k-\phi'_l p\cot\frac{\theta'_k}{2}\cot\frac{\theta'_l}{2}+1}{\left(\cot\frac{\theta'_k}{2}\cot\frac{\theta'_l}{2}\right)^2+2\cos(\phi'_k-\phi'_l)\cot\frac{\theta'_k}{2}\cot\frac{\theta'_l}{2}+1}\right] \\ &= \alpha_j kl\left[\frac{1-\left(\cot\frac{\theta'_k}{2}\cot\frac{\theta'_l}{2}\right)^2}{2\left[1+\left(\cot\frac{\theta'_k}{2}\cot\frac{\theta'_l}{2}\right)^2+2\cos(\phi'_k-\phi'_l)\cot\frac{\theta'_k}{2}\cot\frac{\theta'_l}{2}\right]}\right].\end{aligned} \tag{5.73}$$

Using the trigonometric identity

$$\tan\frac{\theta}{2} = \pm\sqrt{\frac{1-cos\theta}{1+\cos\theta}}, \tag{5.74}$$

we get

$$\left(\cot\frac{\theta'_k}{2}\cot\frac{\theta'_l}{2}\right)^2 = \frac{1+\cos(\theta'_k)+\cos(\theta'_l)+\cos(\theta'_k)\cos(\theta'_l)}{1-\cos(\theta'_k)-\cos(\theta'_l)+\cos(\theta'_k)\cos(\theta'_l)}, \tag{5.75}$$

so that

$$1-\left(\cot\frac{\theta'_k}{2}\cot\frac{\theta'_l}{2}\right)^2 = \frac{-2(\cos\theta'_k+\cos\theta'_l)}{1-\cos\theta'_k-\cos\theta'_l+\cos\theta'_k\cos\theta'_l}, \tag{5.76}$$

and

$$1+\left(\cot\frac{\theta'_k}{2}\cot\frac{\theta'_l}{2}\right)^2 = \frac{2(1+\cos\theta'_k\cos\theta'_l)}{1-\cos\theta'_k-\cos\theta'_l+\cos\theta'_k\cos\theta'_l}. \tag{5.77}$$

Utilizing

$$\tan\frac{\theta}{2} = \frac{1-\cos\theta}{\sin\theta}, \tag{5.78}$$

we obtain that

$$2\cos\left(\phi'_k-\phi'_l\right)\cot\frac{\theta'_k}{2}\cot\frac{\theta'_l}{2}=\frac{2\cos\left(\phi'_k-\phi'_l\right)\sin\theta'_k\sin\theta'_l}{1-\cos\theta'_l-\cos\theta'_k+\cos\theta'_k\cos\theta'_l}. \tag{5.79}$$

From these, we can get that the additional contribution due to Wilson loop to the Berry phase is

$$\hat{\gamma}_{jkl}=\frac{-\alpha_{jkl}(\cos\theta'_k+\cos\theta'_l)}{2[1+\cos\theta'_k\cos\theta'_l+\cos\left(\phi'_k-\phi'_l\right)\sin\theta'_k\sin\theta'_l]}. \tag{5.80}$$

Note that when the directions of the spins are close to a ferromagnetic configuration, which implies that $\theta'_k\approx\theta'_l\approx\theta'$ and that $\phi'_k\approx\phi'_l\approx\phi'$, the additional contribution to the Berry phase reduces to the following expression

$$\hat{\gamma}_{jkl}=\frac{-2\alpha_{jkl}\cos\theta'}{2(1+\cos^2\theta'+\sin^2\theta')}=\frac{-\alpha_{jkl}\cos\theta'}{2}, \tag{5.81}$$

which is the projection of the spin-orbit total rotation to the common direction in which spins are oriented.

If the spin-orbit rotation angle is zero ($\alpha_{jkl}=0$), the Wilson loop operator is the identity. In this case, the additional contribution to the Berry phases $\hat{\gamma}_{jkl}$ vanishes, so that the Berry phase reduces to

$$\gamma_{jkl}=\frac{\Omega'_{jkl}}{2}. \tag{5.82}$$

The solid angle is the one subtended by the three magnetic moments in the local reference frame where is required to gauge away the SOC. Even in the antiferromagnetic ordering, that is coplanar in the original reference frame, in a rotated reference frame could exist a finite real space Berry curvature.

Focusing in the $C_3$ invariant system, the three angles are identical and fulfill that

$$\alpha_{kj}=\alpha_{lk}=\alpha_{jl}=\alpha\ll 1, \tag{5.83}$$

and the three vectors ($\mathbf{a}_{kj}$, $\mathbf{a}_{lk}$, $\mathbf{a}_{jl}$) are related by $\frac{2\pi}{3}$ rotations around the $\hat{\mathbf{z}}$ axis. If the $z$ component in the vector $\mathbf{a}_{kj}$ disappears, this implies that

$$\boldsymbol{\nu}_{jkl}=\alpha(\mathbf{a}_{kj}+\mathbf{a}_{lk}+\mathbf{a}_{jl})=\mathbf{0}. \tag{5.84}$$

In other words, up to first order in the SOC, the Wilson loop is equal to the identity since $\alpha_{jkl}=|\boldsymbol{\nu}_{jkl}|=|\mathbf{0}|=0$. We are interested to get the three spin directions in the new reference

frame. We can use that

$$\begin{aligned} \mathbf{n}'_j &= \mathcal{R}_j \cdot \mathbf{n}_j, \\ \mathbf{n}'_k &= \mathcal{R}_k \cdot \mathbf{n}_k, \\ \mathbf{n}'_l &= \mathcal{R}_l \cdot \mathbf{n}_l, \end{aligned} \tag{5.85}$$

with

$$\begin{aligned} \mathcal{R}_j &= \mathbb{I}, \\ \mathcal{R}_k &= \mathbb{R}^T_{kj}, \\ \mathcal{R}_l &= \mathbb{R}_{jl}, \end{aligned} \tag{5.86}$$

where the matrices $\mathbb{R}$ up to first order in $\alpha$ are

$$\begin{aligned} \mathbb{R}_{kj} &= 1 + \alpha(\mathbf{a}_{kj} \cdot \mathbf{L}) + \mathcal{O}(\alpha^2), \\ \mathbb{R}_{jl} &= 1 + \alpha(\mathbf{a}_{jl} \cdot \mathbf{L}) + \mathcal{O}(\alpha^2). \end{aligned} \tag{5.87}$$

where $\mathbf{L} = (L_x,\, L_y,\, L_z)$ is the vector containing the SO(3) generators, whose irreducible matrix representations are:

$$L_x = \begin{pmatrix} 0 & 0 & 0 \\ 0 & 0 & -1 \\ 0 & 1 & 0 \end{pmatrix}, \qquad L_y = \begin{pmatrix} 0 & 0 & 1 \\ 0 & 0 & 0 \\ -1 & 0 & 0 \end{pmatrix}, \qquad L_z = \begin{pmatrix} 0 & -1 & 0 \\ 1 & 0 & 0 \\ 0 & 0 & 0 \end{pmatrix}. \tag{5.88}$$

Using these, we can compute that in the new reference frame

$$\mathbf{n}'_j = \mathcal{R}_j \cdot \mathbf{n}_j = \mathbb{I} \cdot \mathbf{n}_j = \mathbf{n}_j, \tag{5.89}$$

$$\begin{aligned} \mathbf{n}'_k &= \mathcal{R}_k \cdot \mathbf{n}_k = \mathbb{R}^T_{kj} \cdot \mathbf{n}_k \approx \left[1 + \alpha(\mathbf{a}_{kj} \cdot \mathbf{L})\right]^T \cdot \mathbf{n}_k \\ &= \mathbf{n}_k + \alpha \left(-a^y_{kj} \cos\theta'_k,\, a^x_{kj} \cos\theta'_k,\, a^y_{kj} \sin\theta'_k \cos\phi'_k - a^x_{kj} \sin\theta'_k \sin\phi'_k\right) \\ &= \mathbf{n}_k - \alpha(\mathbf{a}_{kj} \times \mathbf{n}_k), \end{aligned} \tag{5.90}$$

$$\begin{aligned} \mathbf{n}'_l &= \mathcal{R}_l \cdot \mathbf{n}_l = \mathbb{R}_{jl} \cdot \mathbf{n}_l \approx \left[1 + \alpha(\mathbf{a}_{jl} \cdot \mathbf{L})\right] \cdot \mathbf{n}_l \\ &= \mathbf{n}_l + \alpha \left(a^y_{jl} \cos\theta'_l,\, -a^x_{jl} \cos\theta'_l,\, a^x_{jl} \sin\theta'_l \sin\phi'_l - a^y_{jl} \sin\theta'_l \cos\phi'_l\right) \\ &= \mathbf{n}_l - \alpha(\mathbf{a}_{jl} \times \mathbf{n}_l). \end{aligned} \tag{5.91}$$

Note that the equations above are expanded up to first order in $\alpha$, but they still have high accuracy because we are working on the limit of small spin orbit interaction $\alpha \ll 1$.

The Berry phase in this new reference frame and under the previous considerations takes

a rather simple form

$$\begin{aligned}\gamma_{jkl} = \frac{\Omega'_{jkl}}{2} &= \arctan\left[\frac{\mathbf{n}'_j \cdot (\mathbf{n}'_k \times \mathbf{n}'_l)}{n'_j n'_k n'_l + (\mathbf{n}'_j \cdot \mathbf{n}'_k) n'_l + (\mathbf{n}'_j \cdot \mathbf{n}'_l) n'_k + (\mathbf{n}'_k \cdot \mathbf{n}'_l) n'_k}\right] \\ &= \pi - 6\alpha + \mathcal{O}(\alpha^2).\end{aligned} \tag{5.92}$$

In this section we transformed the original (local) reference frame, where the SOC was gauged away to a new reference frame. In the new reference frame, a finite real-space Berry curvature exists, even when in the original frame this could not be possible because of the non-existence of the SOC (which implies that the Wilson loop operator is the identity). The importance of this is that even when the magnetic ordering is collinear or coplanar in the local reference frame, the ordering is non-coplanar in a different reference frame, which shows us that there is no need of a non-coplanar ordering in the local frame [40].

## 5.3 Continuum Limit

In the last two sections we worked on how the Berry phase and the Berry curvature change under different circumstances using the algebraic approach. A discussion of the same ideas can be done in a more formal and elegant way if we take the continuum limit.

If the Wilson loop bond field is related to the SOC and if "the magnetic texture vary slowly over a length scale which is longer than the lattice parameter", the continuum limit is appropriate. To fulfill the first condition, we need to induce long-wavelength deformations in the lattice using a strain. The second condition is fulfilled in materials whose magnetic ordering wave vector is very small.

In this section we are seeking to compute the Berry phase that the electronic wavefunction acquires when the electron is moving along a closed path $\mathcal{C}$, defined as

$$\mathcal{C} = \{x_\mu(\tau),\, x_\mu(0) = x_\mu(T)\}, \tag{5.93}$$

where $\tau \in [0,\, T]$. In this section, we are going to derive an expression of the Berry phase for the SU(2) invariant case. This result will be useful to get a general expression for the case with spin-orbit interaction.

### 5.3.1 SU(2) Invariant Case

For the SU(2) invariant case, we have seen that for a closed loop in the lattice

$$\mathcal{C} : j \to k \to l \to ... \to m \to j, \tag{5.94}$$

the Berry phase is

$$\gamma_{\mathcal{C}} = \arg[\langle \mathbf{n}_j | \mathbf{n}_m \rangle ... \langle \mathbf{n}_l | \mathbf{n}_k \rangle \langle \mathbf{n}_k | \mathbf{n}_j \rangle]. \tag{5.95}$$

Note that we got the expression for an arbitrary loop from a superposition of the elementary triangle loops. To do the continuum limit in equation (5.95) we need to divide the interval $T$ into $N$ intervals so that

$$\Delta\tau = \frac{T}{N}. \tag{5.96}$$

In the limit $N \to \infty$, the Berry phase can be rewritten as

$$\gamma_{\mathcal{C}} = \lim_{N\to\infty} \arg \left[ \prod_{j=0}^{N-1} \langle \mathbf{n}_{\mathbf{x}(\tau_j+\Delta\tau)} | \mathbf{n}_{\mathbf{x}(\tau_j)} \rangle \right]. \tag{5.97}$$

Doing a Taylor expansion on the ket vector $|\mathbf{n}_{\mathbf{x}(\tau_j+\Delta\tau)}\rangle$ for $\Delta\tau$ small, that is,

$$|\mathbf{n}_{\mathbf{x}(\tau_j+\Delta\tau)}\rangle = |\mathbf{n}_{\mathbf{x}(\tau_j)}\rangle + \Delta\tau \frac{\partial}{\partial_{\tau_j}} |\mathbf{n}_{\mathbf{x}(\tau_j)}\rangle + \mathcal{O}\left(\Delta\tau^2\right), \tag{5.98}$$

we arrive at

$$\gamma_{\mathcal{C}} = \lim_{N\to\infty} \arg \left[ \prod_{j=0}^{N-1} \langle \mathbf{n}_{\mathbf{x}(\tau_j)}| + \Delta\tau \left( \frac{\partial}{\partial_\tau} |\mathbf{n}_{\mathbf{x}(\tau_j)}\rangle \right)^\dagger + \mathcal{O}\left(\Delta\tau^2\right) \right] |\mathbf{n}_{\mathbf{x}(\tau_j)}\rangle. \tag{5.99}$$

Noticing further that

$$\left( \frac{\partial}{\partial_\tau} |\mathbf{n}_{\mathbf{x}(\tau_j)}\rangle \right)^\dagger |\mathbf{n}_{\mathbf{x}(\tau_j)}\rangle = \langle \frac{\partial}{\partial_\tau} \mathbf{n}_{\mathbf{x}(\tau_j)} | \mathbf{n}_{\mathbf{x}(\tau_j)} \rangle = - \langle \mathbf{n}_{\mathbf{x}(\tau_j)} | \partial_\tau | \mathbf{n}_{\mathbf{x}(\tau_j)} \rangle, \tag{5.100}$$

and substituting this result in the previous derivation, we obtain the following formula for the Berry phase

$$\gamma_{\mathcal{C}} = \lim_{N\to\infty} \arg \left[ \prod_{j=0}^{N-1} \left( 1 - \langle \mathbf{n}_{\mathbf{x}(\tau_j)} | \partial_\tau | \mathbf{n}_{\mathbf{x}(\tau_j)} \rangle \Delta\tau + \mathcal{O}\left(\Delta\tau^2\right) \right) \right]. \tag{5.101}$$

We can use the definition of exponential in the Taylor series to rewrite the Berry phase as

$$\begin{aligned}\gamma_{\mathcal{C}} &= \lim_{\Delta\tau\to 0} \arg\left\{\prod_{j=0}^{N-1} \exp\left[-\langle \mathbf{n}_{\mathbf{x}(\tau_j)}|\partial_\tau|\mathbf{n}_{\mathbf{x}(\tau_j)}\rangle\,\Delta\tau + \mathcal{O}\left(\Delta\tau^2\right)\right]\right\} \\ &= i\lim_{\Delta\tau\to 0}\left[\sum_{j=0}^{N-1}\langle \mathbf{n}_{\mathbf{x}(\tau_j)}|\partial_\tau|\mathbf{n}_{\mathbf{x}(\tau_j)}\rangle\,\Delta\tau + \mathcal{O}\left(N\Delta\tau^2\right)\right],\end{aligned} \tag{5.102}$$

and using the definition of the Riemann integral for a function $f \in [a,\, b]$

$$\int_a^b f(x)dx = \lim_{\Delta\to 0}\sum_{i=1}^{n} f(\epsilon_i)\Delta x_i, \tag{5.103}$$

we can rewrite the Berry phase expression as

$$\gamma_{\mathcal{C}} = i\int_0^T \langle \mathbf{n}_{\mathbf{x}(\tau)}|\partial_\tau|\mathbf{n}_{\mathbf{x}(\tau)}\rangle\, d\tau, \tag{5.104}$$

where the integral limits are given by the range of $x_\mu(\tau)$ which is $\tau \in [0,\, T]$. Recalling that the definition of the line integral of a vector field $\mathbf{F}$ along a loop $\mathcal{C}$ in the direction $\mathbf{r}$ is

$$\oint_{\mathcal{C}} \mathbf{F}(\mathbf{r})\cdot d\mathbf{r} = \int_a^b \mathbf{F}(\mathbf{r}(t))\cdot \mathbf{r}'dt, \tag{5.105}$$

we have that

$$\gamma_{\mathcal{C}} = i\oint_{\mathcal{C}} \langle \mathbf{n}|\partial_\mu|\mathbf{n}\rangle\, dx_\mu = \frac{\Omega_C}{2}, \tag{5.106}$$

where $\Omega_C$ is the solid angle created by the vector $\mathbf{n}$ around the loop $\mathcal{C}$.

### 5.3.2 General Case with Spin-orbit Interaction

For the general case with the spin orbit interaction, we need to introduce the operators that represents the rotation matrices in the expression of the Berry phase given in the equation (5.95)

$$\gamma_{\mathcal{C}} = \arg\left[\langle \mathbf{n}_j|U_{jm}|\mathbf{n}_m\rangle \ldots \langle \mathbf{n}_l|U_{lk}|\mathbf{n}_k\rangle\,\langle \mathbf{n}_k|U_{kj}|\mathbf{n}_j\rangle\right]. \tag{5.107}$$

In the continuum limit, the bond matrices $U_{kj}$ represent an infinitesimal SU(2) rotation that connects the point $\mathbf{x}$ to the point $\mathbf{x} + d\mathbf{x}$ by

$$U_{\mathbf{x}+d\mathbf{x},\,\mathbf{x}} = \exp\left[\frac{1}{2}\sigma^a A^a_\mu dx_\mu\right]. \tag{5.108}$$

In the continuum limit

$$\begin{aligned} j &\to \mathbf{x}(\tau), \\ k &\to \mathbf{x}(t) + \dot{\mathbf{x}}(\tau)d\tau, \\ U_{kj} &\to \mathrm{e}^{iA(\tau)d\tau}. \end{aligned} \tag{5.109}$$

Notice that we can expand

$$\mathrm{e}^{iA(\tau)d\tau} = \mathbb{I} + iA(\tau)d\tau + \mathcal{O}(d\tau^2), \tag{5.110}$$

where

$$A(\tau) = \frac{1}{2}\sigma^a A^a_\mu \dot{x}_\mu(\tau). \tag{5.111}$$

We computing

$$\langle \mathbf{n}_{\mathbf{x}(\tau+d\tau)} | \mathrm{e}^{iA(\tau)d\tau} | \mathbf{n}_{\mathbf{x}(\tau)} \rangle = \langle \mathbf{n}_{\mathbf{x}(\tau+d\tau)} | \mathbf{I} + iA(\tau)d\tau + \mathcal{O}(d\tau^2) | \mathbf{n}_{\mathbf{x}(\tau)} \rangle \,, \tag{5.112}$$

note that

$$\langle \mathbf{n}_{\mathbf{x}(\tau+d\tau)} | \mathrm{e}^{iA(\tau)d\tau} | \mathbf{n}_{\mathbf{x}(\tau)} \rangle = \left[ \langle \mathbf{n}_{\mathbf{x}(\tau)} | - d\tau \, \langle \mathbf{n}_{\mathbf{x}(\tau)} \partial_\tau | \right] \mathrm{e}^{iA(\tau)d\tau} \, | \mathbf{n}_{\mathbf{x}(\tau)} \rangle \,. \tag{5.113}$$

and following a procedure analogous to the one done in the previous section, we arrive to the following conclusion

$$\langle \mathbf{n}_{\mathbf{x}(\tau+d\tau)} | \mathrm{e}^{iA(\tau)d\tau} | \mathbf{n}_{\mathbf{x}(\tau)} \rangle = 1 + \left[ i \, \langle \mathbf{n}_{\mathbf{x}(\tau)} | A(t) | \mathbf{n}_{\mathbf{x}(\tau)} \rangle + \langle \mathbf{n}_{\mathbf{x}(\tau)} | \partial_\tau | \mathbf{n}_{\mathbf{x}(\tau)} \rangle \right] d\tau + \mathcal{O}(d\tau^2). \tag{5.114}$$

Taking the product operator, extracting the argument of it, using the Riemann integral definition and rewriting the result, we can get that the Berry phase in a closed path is

$$\gamma_{\mathcal{C}} = i \oint_{\mathcal{C}} \langle \mathbf{n} | \mathcal{D}_\mu | \mathbf{n} \rangle \, dx_\mu \equiv \oint_{\mathcal{C}} \mathcal{A}_\mu x^\mu, \tag{5.115}$$

where

$$\mathcal{D}_\mu \equiv \partial_\mu - \frac{i\sigma^a}{2} A^a_\mu, \tag{5.116}$$

in which

$$\mathcal{A}_\mu = i \, \langle \mathbf{n} | \partial_\mu | \mathbf{n} \rangle + \frac{1}{2} n^a A^a_\mu \tag{5.117}$$

is the covariant Berry connection and we have defined

$$n^a \equiv \langle \mathbf{n} | \sigma^a | \mathbf{n} \rangle \,. \tag{5.118}$$

We can use now Stokes' theorem so that

$$\begin{aligned}\oint_{\mathcal{C}} \mathcal{A}_\mu dx^\mu &= \int_{S_\mathcal{C}} [\partial_\mu A_\nu - \partial_\nu \mathcal{A}_\mu] d^2\sigma^{\mu\nu} \\ &= \int_{S_\mathcal{C}} \left\{ \partial_\mu \left[ i \langle \mathbf{n}|\partial_\nu|\mathbf{n}\rangle + \frac{1}{2} n^a A^a_\nu \right] - \partial_\nu \left[ i \langle \mathbf{n}|\partial_\mu|\mathbf{n}\rangle + \frac{1}{2} n^a A^a_\mu \right] \right\} d^2\sigma^{\mu\nu} \\ &= \frac{1}{2} \int_{S_\mathcal{C}} [\partial_\mu (n^a A^a_\nu) - \partial_\nu (n^a A^a_\mu)] d^2\sigma^{\mu\nu} + i \int_{S_\mathcal{C}} [\partial_\mu \langle \mathbf{n}|\partial_\nu|\mathbf{n}\rangle - \partial_\nu \langle \mathbf{n}|\partial_\mu|\mathbf{n}\rangle] d^2\sigma^{\mu\nu}.\end{aligned} \tag{5.119}$$

Note that

$$i[\partial_\mu \langle \mathbf{n}|\partial_\nu|\mathbf{n}\rangle - \partial_\nu \langle \mathbf{n}|\partial_\mu|\mathbf{n}\rangle] = \frac{1}{2} \mathbf{n} \cdot (\partial_\mu \mathbf{n} \times \partial_\nu \mathbf{n}), \tag{5.120}$$

and as a consequence of this

$$\oint_{\mathcal{C}} \mathcal{A}_\mu dx^\mu = \frac{1}{2} \int_{S_\mathcal{C}} [\partial_\mu (n^a A^a_\nu) - \partial_\nu (n^a A^a_\mu)] d^2\sigma^{\mu\nu} + \frac{1}{2} \int_{S_\mathcal{C}} [\mathbf{n} \cdot (\partial_\mu \mathbf{n} \times \partial_\nu \mathbf{n})] d^2\sigma^{\mu\nu}. \tag{5.121}$$

Note that in equation (5.121), the second term vanishes for a magnetic moment collinear or coplanar configuration, while the first contribution could be finite, which implies that even for this configuration, the SOC induces an effective magnetic field. This effective magnetic field is given by

$$B_\eta = \frac{1}{2} \epsilon_{\eta\mu\nu} \partial_\mu (n^a A^a_\nu). \tag{5.122}$$

We are seeking to compute the equation (5.121) in its covariant form. If the first term of this equation is manipulated, it can be seen that

$$\begin{aligned} & i \int_{S_\mathcal{C}} [\partial_\mu \langle \mathbf{n}|\partial_\nu|\mathbf{n}\rangle - \partial_\nu \langle \mathbf{n}|\partial_\mu|\mathbf{n}\rangle]] d^2\sigma^{\mu\nu} \\ &= \int_{s_\mathcal{C}} \left[ n^a \partial_\mu A^a_\nu + (\partial_\mu n^a) A^a_\nu - n^a \partial_\nu A^a_\mu - (\partial_\nu n^a) A^a_\mu \right] d^2\sigma^{\mu\nu}. \end{aligned} \tag{5.123}$$

We know that the non-Abelian field strength is

$$F^a_{\mu\nu} \equiv \partial_\mu A^a_\nu - \partial_\nu A^a_\mu - \epsilon^{abc} A^b_\mu A^c_\nu, \tag{5.124}$$

and then we can write

$$\begin{aligned} & i \int_{S_\mathcal{C}} [\partial_\mu \langle \mathbf{n}|\partial_\nu|\mathbf{n}\rangle - \partial_\nu \langle \mathbf{n}|\partial_\mu|\mathbf{n}\rangle]] d^2\sigma^{\mu\nu} \\ &= \int_{s_\mathcal{C}} \left[ n^a \left( \partial_\mu A^a_\nu - \partial_\nu A^a_\mu - \epsilon^{abc} A^b_\mu A^c_\nu \right) + n^a \epsilon^{abc} A^b_\mu A^c_\nu + A^a_\nu \partial_\mu n^a - A^a_\mu \partial_\nu n^a \right] d^2\sigma^{\mu\nu} \\ &= \int_{s_\mathcal{C}} \left[ n^a F^a_{\mu\nu} + n^a \epsilon^{abc} A^b_\mu A^c_\nu + A^a_\nu \partial_\mu n^a - A^a_\mu \partial_\nu n^a \right] d^2\sigma^{\mu\nu}. \end{aligned} \tag{5.125}$$

Let us now introduce the covariant derivative $D_\mu$ defined as

$$D_\mu = \partial_\mu - L^a A^a_\mu. \tag{5.126}$$

Note that if equation (5.116) is compared to equation (5.126) we can see that $\frac{i\sigma^a}{2}$ has been substituted with the SO(3) generator $L^a$.

The covariant form of the solid angle density is

$$\begin{aligned}
\mathbf{n}\cdot(D_\mu\mathbf{n}\times D_\nu\mathbf{n}) &= \mathbf{n}\cdot[(\partial_\mu - L^a A^\nu_\mu)\mathbf{n}\times(\partial_\nu - L^a A^a_\nu)\mathbf{n}] \\
&= \mathbf{n}\cdot[(\partial_\mu\mathbf{n} - L^a A^\nu_\mu\mathbf{n})\times(\partial_\nu\mathbf{n} - L^a A^a_\nu\mathbf{n}) \\
&= \epsilon^{abc}n^a\left(\delta^{bn}\partial_\mu n^n - \epsilon^{bmn}A^m_\mu n^n\right)\left(\delta^{cl}\partial_\nu n^l - \epsilon^{ckl}A^k_\nu n^l\right) \\
&= \epsilon^{abc}n^a\delta^{bn}\partial_\mu n^n\delta^{cl}\partial_\nu n^l - \epsilon^{abc}n^a\delta^{bn}\partial_\mu n^n\epsilon^{ckl}A^k_\nu n^l - \epsilon^{abc}n^a\epsilon^{bmn}A^k_\nu n^n\delta^{cl}\partial_\nu n^l \\
&+ \epsilon^{abc}n^a\epsilon^{bmn}A^m_\mu n^n\epsilon^{ckl}A^k_\nu n^l,
\end{aligned} \tag{5.127}$$

where

$$\epsilon^{abc}n^a\delta^{bn}\partial_\mu n^n\delta^{cl}\partial_\nu n^l = \epsilon^{abc}n^a\partial_\mu n^b\partial_\nu n^c, \tag{5.128}$$

$$-\epsilon^{abc}n^a\delta^{bn}\partial_\mu n^n\epsilon^{ckl}A^k_\nu n^l = -n^a\partial_\mu n^b A^a_\nu n^b + n^a\partial_\mu n^b A^b_\nu n^a = \partial_\mu n^b A^b_\nu, \tag{5.129}$$

$$-\epsilon^{abc}n^a\epsilon^{bmn}A^k_\nu n^n\delta^{cl}\partial_\nu n^l = -n^a A^c_\mu n^a\partial_\nu n^c + n^a A^a_\mu n^c\partial_\nu n^c = -\partial_\nu n^c A^c_\mu, \tag{5.130}$$

and

$$\epsilon^{abc}n^a\epsilon^{bmn}A^m_\mu n^n\epsilon^{ckl}A^k_\nu n^l = n^a A^c_\mu n^a\epsilon^{ckl}A^k_\nu n^l - n^a A^a_\mu n^c\epsilon^{ckl}A^k_\nu n^l. \tag{5.131}$$

Note that $(\partial_\mu n^b)n^b$ and $n^c(\partial_\nu n^c)$ are equal to zero because both represent the dot product between a unit vector and its vector derivative, which is tangent to the vector itself. Also

$$\begin{aligned}
\epsilon^{ckl}n^c A^k_\nu n^l &= \epsilon^{123}n^1A^2_\nu n^3 + \epsilon^{132}n^1A^3_\nu n^2 + \epsilon^{213}n^2A^1_\nu n^3 + \epsilon^{231}n^2A^3_\nu n^1 + \epsilon^{312}n^3A^1_\nu n^2 + \epsilon^{321}n^3A^2_\nu n^1 \\
&= n^1A^2_\nu n^3 - n^3A^2_\nu n^1 + n^3A^1_\nu n^2 - n^2A^1_\nu n^3 + n^2A^3_\nu n^1 - n^1A^3_\nu n^2 = 0,
\end{aligned} \tag{5.132}$$

and as a result of this, the second term in equation (5.131) vanishes, and the covariant form of the solid angle density is

$$\begin{aligned}
\mathbf{n}\cdot(D_\mu\mathbf{n}\times D_\nu\mathbf{n}) &= \mathbf{n}\cdot[(\partial_\mu - L^a A^\nu_\mu)\mathbf{n}\times(\partial_\nu - L^a A^a_\nu)\mathbf{n}] \\
&= \epsilon^{abc}n^a\partial_\mu n^b\partial_\nu n^c - \partial_\nu n^c A^a_\mu + \partial_\mu n^b A^b_\nu + \epsilon^{clk}A^c_\mu A^k_\nu n^l.
\end{aligned} \tag{5.133}$$

Recall also that

$$\mathbf{n}\cdot(\partial_\mu\mathbf{n}\times\partial_\nu\mathbf{n}) = \epsilon^{abc}n^a\partial_\mu n^b\partial_\nu n^c, \tag{5.134}$$

so, gathering results, the Berry phase becomes

$$\begin{aligned}\gamma_{\mathcal{C}} &= \frac{1}{2}\int_{S_{\mathcal{C}}} \left[n^a F^a_{\mu\nu} + n^a \epsilon^{abc} A^b_\mu A^c_\nu + A^a_\nu \partial_\mu n^a - A^a_\mu \partial_\nu n^a + \mathbf{n}\cdot(\partial_\mu \mathbf{n}\times\partial_\nu \mathbf{n})\right] d^2\sigma^{\mu\nu} \\ &= \frac{1}{2}\int_{S_{\mathcal{C}}} \left[n^a F^a_{\mu\nu} + n^a \epsilon^{abc} A^b_\mu A^c_\nu + A^a_\nu \partial_\mu n^a - A^a_\mu \partial_\nu n^a + \epsilon^{abc} n^a \partial_\mu n^b \partial_\nu n^c\right] d^2\sigma^{\mu\nu} \\ &= \frac{1}{2}\int_{S_{\mathcal{C}}} \left[n^a F^a_{\mu\nu} + \mathbf{n}\cdot(D_\mu \mathbf{n}\times D_\nu \mathbf{n})\right] d^2\sigma^{\mu\nu}.\end{aligned} \tag{5.135}$$

In this last equation, it can be seen that the strength of the effective gauge field generated by the localized magnetic moments is the sum of the projection of the SU(2) field strength along the direction $\mathbf{n}$ and the covariant scalar spin chirality $\mathcal{S}$ [54, 55], which is defined as

$$\mathcal{S} \equiv \mathbf{S}_i \cdot (\mathbf{S}_j \times \mathbf{S}_k), \tag{5.136}$$

where $\mathbf{S}_i$, $\mathbf{S}_j$ and $\mathbf{S}_k$ are the three local spins. The scalar spin chirality only appears in non-coplanar spin configurations and, if an electron is hopping between these sites, it acquires a Berry phase that induces an AHE[1] [56].

The other big contribution of equation (5.135) is that it can be generalized immediately to a case of time-dependent magnetic configurations. This can be done if the Greek indices $\mu$ and $\nu$ take values from 0 to $d$, where 0 represents the time coordinate and $d$ is the spatial dimension of the system under study. The zeroth component of the SU(2) vector potential, that corresponds to the time coordinate, is given by

$$A^a_0 = \frac{-g\mu_B}{2} H^a, \tag{5.137}$$

where $g$ is the gyro-magnetic factor. Note that this contribution arises from the Zeeman coupling (anomalous Zeeman effect) between the external magnetic field $\mathbf{H}$ and the spin of the conduction electrons. The action is

$$S[\Psi] = \int dt d\mathbf{x} \left(\Psi^\dagger i\partial_t \Psi - \mathcal{H}\right), \tag{5.138}$$

and it is invariant under local-space transformations of the original spin reference frame. Indeed, consider the following local space-time transformation

$$\mathcal{U} = \exp\left[i\theta^a(\mathbf{x},\, t)\sigma^a/2\right]. \tag{5.139}$$

under which the wavefunction $\Psi$ in the continuum limit transform as $\Psi \to \mathcal{U}\Psi$, and

$$A^a_\mu \sigma^a \to \mathcal{U} A^a_\mu \sigma^a \mathcal{U}^{-1} - 2i(\partial_\mu \mathcal{U})\mathcal{U}^{-1}. \tag{5.140}$$

[1] When the AHE is originated by a non-zero scalar spin chirality, it is called *Topological Hall effect* (THE) [54].

One can show that, indeed, this transformation leaves the action invariant.

In the next chapter we will apply these concepts to a two-dimensional system with a kagome crystal structure.

# Chapter 6

# The Berry Curvature in Momentum Space

In the following, we will use an example to explore the Berry curvature notion that we introduced in the previous sections. For this example it is necessary to present the kagome lattice.

## 6.1 The Kagome Lattice

The kagome lattice receives its name from the Japanese words *kago*, that means basket, and *me*, whose meaning is woven pattern (Figure 6.1). In a bamboo basket that has been woven in a kagome pattern, it can be seen that the lattice is composed by triangles that overlap. Each lattice site has four nearest neighbors. The name of this special lattice structure was given by the first researchers that studied the concept of frustration [57].

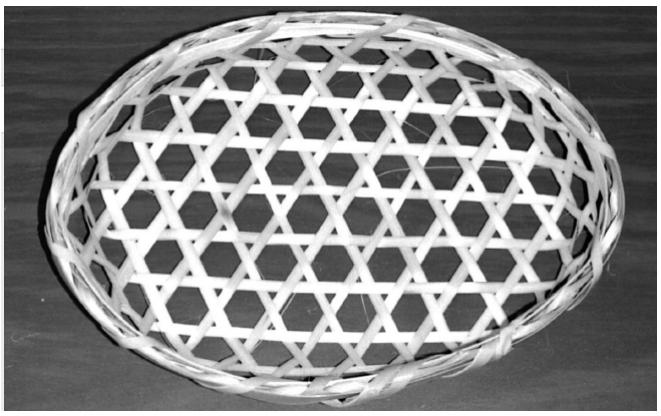

**Figure 6.1:** A bamboo basket that has been woven in a kagome pattern. It can be seen that the triangles overlap. Image from [57].

In Physics, a kagome lattice (Figure 6.2), according to Wang [58], is described as an "intersecting web of *corner-sharing triangles*". The interest in studying these lattices arises from their geometric frustration.

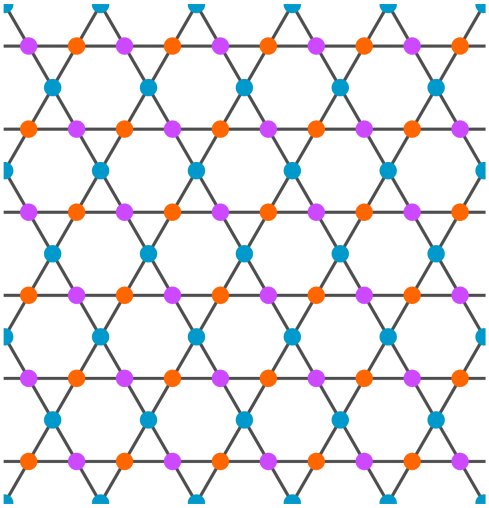

**Figure 6.2:** The kagome lattice.

### 6.1.1 Geometric Frustration

The geometric frustration is a phenomenon whereby a system has highly degenerated ground state, which is the result of the geometry of the system itself [59].

The geometric frustration takes an important role in the antiferromagnetic Heisenberg model because two of three spins are arranged antiparallel to each other, but the third spin is under frustration. This means, no matter in which configuration the third spin is, it will agree with one of the neighboring spins but disagree with the other (Figure 6.3) [60]. Due to the spin frustration, it is not possible to minimize the energies of all bonds, even if the spins are classical, and when the basic plaquette is a triangle [1].

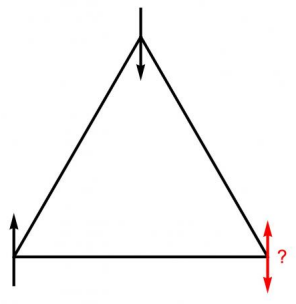


**Figure 6.3:** Geometric frustration in a triangle plaquette in the antiferromagnetic Heisenberg model. Image from [60].

If we were to allow the spins to be classical and continuous variables, the spins would order themselves in the configuration shown in Figure 6.4. Note that in this spin configuration, the total energy of the triangle is minimized, whilst the individual bonds energies are not minimized [1].

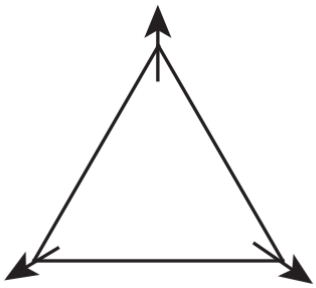

**Figure 6.4:** Triangle plaquette with nearest-neighbor antiferromagnetic couplings. In this spin configuration the total triangle energy is minimized, while the individual bond energy is not minimized. Image from [1].

Because of the geometry frustration, the kagome lattice in a nearest-neighbor antiferromagnetic spin configuration presents a ground state similar to a spin liquid, whose spin distribution presents disorder even at zero temperature. Quantum spin liquids present other interesting properties such as having fractional excitations, forming quasi-particles that have, according to Han and collaborators [61], an "effective spin or charge that is smaller than that of their constituents"and sharing many of their properties with those of high-temperature superconductors [1, 59, 60].

The geometric frustration of the kagome lattice also affects its band structure [59, 60, 62].

### 6.1.2 The Band Structure of the Kagome Lattice in the Tight-binding Method

#### Crystal Structure of the Kagome Lattice

In solid state physics, an ideal crystal is conformed by an infinite and periodical repetition of an atom (or group of atoms). The position of this atom (or atoms) is usually referred to as the atomic basis, which is fixed to the lattice, being the latter a group of mathematical points where the basis is repeated.

In the kagome lattice, the atomic basis is conformed by three atoms, that will be labeled as 1, 2 and 3 (Figure 6.5c). These atoms are infinitely repeated in the lattice (Figure 6.5a). The translation between the lattice points in the kagome lattice is achieved by the following primitive lattice vectors:

$$\mathbf{u}_1 = \hat{\mathbf{x}}, \tag{6.1}$$

and

$$\mathbf{u}_2 = \frac{1}{2}\hat{\mathbf{x}} + \frac{\sqrt{3}}{2}\hat{\mathbf{y}}. \tag{6.2}$$

The lattice vectors also allow us to determine what kind of Bravais lattice we are dealing with. In this case, due to geometry, the Bravais lattice corresponds to a hexagonal one (Figure 6.5b).

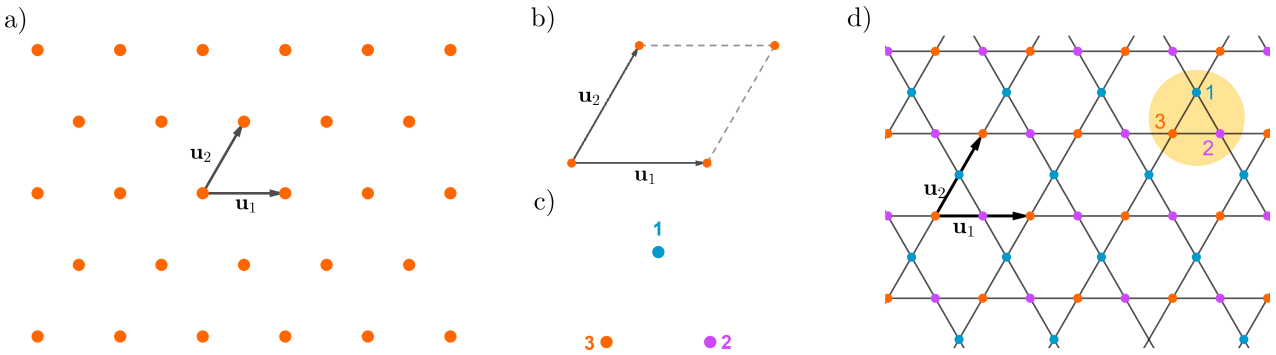


**Figure 6.5:** Crystallography structure of the kagome lattice in real space: a) the points of the lattice, b) the primitive cell, c) the basis and d) the kagome lattice conformed by the three atomic basis (underlined in a yellow circle) repeated at each lattice point (orange points). Here the primitive vectors are shown as black arrows.

The crystallography structure of a lattice allows us to obtain the reciprocal space lattice.

### Reciprocal Space of the Kagome Lattice

The reciprocal space, also called $k$-space, is the Fourier transformation of the real space. This space is important because of the information we can obtain from it as, for instance, the energy band structure. The reciprocal vectors for the kagome lattice are

$$\mathbf{b}_1 = 2\pi\hat{\mathbf{x}} - \frac{2\pi}{\sqrt{3}}\hat{\mathbf{y}}, \tag{6.3}$$

$$\mathbf{b}_2 = \frac{4\pi}{\sqrt{3}}\hat{\mathbf{y}}, \tag{6.4}$$

and

$$\mathbf{b}_3 = 2\pi\hat{\mathbf{z}}, \tag{6.5}$$

and they fulfil the condition

$$\mathbf{u}_i \cdot \mathbf{b}_j = 2\pi\delta_{ij}. \tag{6.6}$$

With these vectors, we can find the reciprocal lattice (Figure 6.6a) and, using the Wigner-Seitz method, the 1BZ is shown in Figure 6.6b. In Figure 6.6c, the irreducible Brillouin zone is drawn (pink triangle) and the high symmetry points are also marked. These points are

$$\Gamma = 0\mathbf{b}_1 + 0\mathbf{b}_2, \tag{6.7}$$

$$\mathrm{M} = 0\mathbf{b}_1 + \frac{1}{2}\mathbf{b}_2, \tag{6.8}$$

and

$$\mathrm{K} = \frac{1}{3}\mathbf{b}_1 + \frac{2}{3}\mathbf{b}_2. \tag{6.9}$$

The labels Λ, T and Σ are used for those points at the lines that define the boundary of the irreducible Brillouin zone.

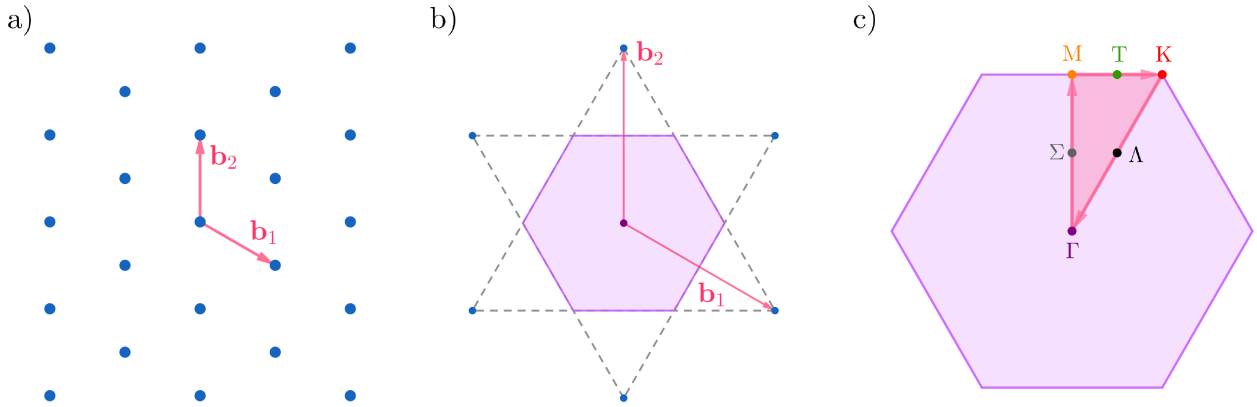


**Figure 6.6:** Reciprocal space for a kagome lattice: a) the reciprocal lattice, b) the 1BZ (purple) obtained with the Wigner-Seitz method and c) the 1BZ (purple), the irreducible Brillouin zone (pink) and the high symmetry points.

### The Kagome Lattice Band Structure

To understand the band structure that usually appears on systems interacting on a kagome lattice, we start with a simple model: a bipartite lattice (specifically, a honeycomb lattice) whose sites will be labeled as A and B.

Let us assume that we have a honeycomb lattice in which an atom $A$ connects with its three neighbouring atoms of type $B$. Then, a tight-binding Hamiltonian capturing the free motion of particles in this system is

$$H = -t \sum_{n} \sum_{<j,n>} \left( \mathbf{a}_n^\dagger \mathbf{b}_j + \mathbf{b}_j^\dagger \mathbf{a}_n \right). \tag{6.10}$$

To express the Hamiltonian in $k$-space, we transform the above creation and annihilation operators to said space. That is

$$\mathbf{a}_n = \frac{1}{\sqrt{N}} \sum_{\mathbf{k}} \mathrm{e}^{i\mathbf{k}\cdot\mathbf{r}_{\mathrm{A},n}} \mathbf{a}_{\mathbf{k}}, \tag{6.11}$$

and

$$\mathbf{b}_j = \frac{1}{\sqrt{N}} \sum_{\mathbf{q}} \mathrm{e}^{i\mathbf{q}\cdot\mathbf{r}_{\mathrm{B},j}} \mathbf{b}_{\mathbf{q}}, \tag{6.12}$$

so the Hamiltonian is rewritten as

$$H = -\frac{t}{N}\sum_{n}\sum_{j,n}\sum_{\mathbf{k},\mathbf{q}}\left(\mathrm{e}^{-i\mathbf{k}\cdot\mathbf{r}_{\mathrm{A},n}}\mathrm{e}^{i\mathbf{q}\cdot\mathbf{r}_{\mathrm{B},j}}\mathbf{a}_{\mathbf{k}}^{\dagger}\mathbf{b}_{\mathbf{q}} + H.C.\right) \tag{6.13}$$

Using the identity $\sum_n \mathrm{e}^{i(\mathbf{q}-\mathbf{k})\cdot\mathbf{r}_{\mathrm{A},n}} = N\delta(\mathbf{q}-\mathbf{k})$, the Hamiltonian becomes

$$= \sum_{\mathbf{k}}\begin{pmatrix}\mathbf{a_k}^{\dagger} & \mathbf{b_k}^{\dagger}\end{pmatrix}\underbrace{\begin{pmatrix}0 & -t\sum_j \mathrm{e}^{i\mathbf{k}\cdot\mathbf{r}_{NN}^{j}} \\ -t\sum_j \mathrm{e}^{-i\mathbf{k}\cdot\mathbf{r}_{NN}^{j}} & 0\end{pmatrix}}_{\mathcal{H}_{\mathbf{k}}}\begin{pmatrix}\mathbf{a_k} \\ \mathbf{b_k}\end{pmatrix}, \tag{6.14}$$

where $\mathcal{H}_{\mathbf{k}}$ is the Hamiltonian matrix representation for the honeycomb lattice, $\{\mathbf{r}_{NN}^{j}\}$ is the set of vectors that connect the site A with its neighbors B, so that

$$\mathbf{r}_{\mathrm{B},j} = \mathbf{r}_{\mathrm{A},n} + \mathbf{r}_{NN}^{j}. \tag{6.15}$$

The last analysis can be extended to the kagome lattice, considering that an atom A has two nearest neighbor B and two nearest neighbor C. The Hamiltonian matrix representation for the kagome lattice is

$$\mathcal{H}_{\mathbf{k}} = -2t\begin{pmatrix}0 & \cos\left(\mathbf{k}\cdot\mathbf{r}_{\mathrm{AB}}\right) & \cos\left(\mathbf{k}\cdot\mathbf{r}_{\mathrm{AC}}\right) \\ \cos\left(\mathbf{k}\cdot\mathbf{r}_{\mathrm{AB}}\right) & 0 & \cos\left(\mathbf{k}\cdot\mathbf{r}_{\mathrm{BC}}\right) \\ \cos\left(\mathbf{k}\cdot\mathbf{r}_{\mathrm{AC}}\right) & \cos\left(\mathbf{k}\cdot\mathbf{r}_{\mathrm{BC}}\right) & 0\end{pmatrix}, \tag{6.16}$$

with

$$\mathbf{r}_{\mathrm{AB}} = \frac{1}{2}\hat{\mathbf{x}}, \tag{6.17}$$

$$\mathbf{r}_{\mathrm{AC}} = \frac{1}{4}\hat{\mathbf{x}} + \frac{\sqrt{3}}{4}\hat{\mathbf{y}}, \tag{6.18}$$

and

$$\mathbf{r}_{\mathrm{BC}} = -\frac{1}{4}\hat{\mathbf{x}} + \frac{\sqrt{3}}{4}\hat{\mathbf{y}}. \tag{6.19}$$

With this information we can obtain the energy band structure of a simple system of particles on a kagome lattice in the tight-binding approximation (Figure 6.7).

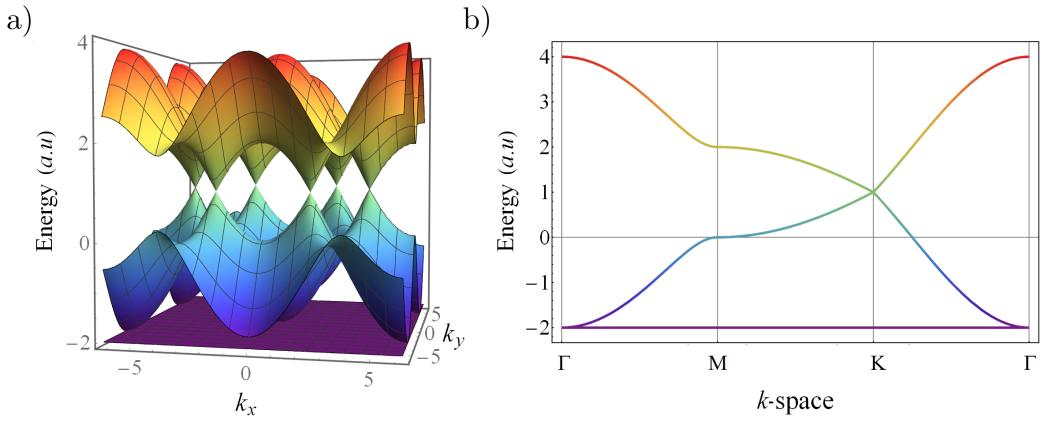


**Figure 6.7:** The energy band structure of the kagome lattice a) in 3D and b) along the path $\Gamma - M - K - \Gamma$ in the irreducible Brillouin zone.

As it can be seen in Figure 6.7a, the band structure of the kagome lattice in the tight-binding approximation has three bands. The third[1] band (orange-yellow) reaches the highest energy and touches the second band (cyan-blue) at six points, where the six Dirac cones are formed. In the tight-binding approximation, the first band is a flat band, in which the velocity of the electrons is zero and due to the strong electron correlation, interesting effects related to the topology can be observed: fractional Hall effect, superconductivity at high temperatures, among others [59, 60, 62].

In Figure 6.7b, the band diagram along the irreducible Brillouin zone ($\Gamma - M - K - \Gamma$) shows that the Dirac point is at the K point. Also the maximum separation between the first and the second band is at the $\Gamma$ point, where the second and third bands touch each other, which could imply that the electronic transition between these bands at the center of the 1BZ can be achieved easily.

The Figure 6.7 is going to be useful in the next section, where we are going to use the double exchange mechanism to obtained the energy band structure of the kagome lattice when the SOC is present.

## 6.2 The Berry Phase in a Kagome Lattice

We are taking the Hamiltonian of equation (4.16) where $H_t$ is a tight-binding Hamiltonian that considers SOC, $t$ represents the hopping between the nearest neighbor and $H_J$ carries the information about the exchange coupling. Now, we are adding the Hamiltonian $H_H$, which

[1] In this section, the bands are numbered from 1 to $n$, where n is the total number of bands. The band with the lowest energy is called the first band, while the highest energy band is the $n$-th band. The bands in between are numbered as their energy increase.

gives the spin ordering that is shown in Figure 6.8.

$$H_H = \sum_{<jk>} S_j^{\mu} \mathcal{J}_{jk}^{\mu\nu} S_k^{\nu} \tag{6.20}$$

This Hamiltonian stabilizes the magnetic ordering $\mathbf{S}_j = S\mathbf{n}_j$, so it is necessary to know the normalized vectors. Taking into consideration the single triangular plaquette (Figure 6.8), these vectors are

$$\mathbf{n}_1 = \hat{\mathbf{y}}, \tag{6.21}$$

$$\mathbf{n}_2 = \frac{\cos(30°)\hat{\mathbf{x}} - \sin(30°)\hat{\mathbf{y}}}{|\cos(30°)\hat{\mathbf{x}} - \sin(30°)\hat{\mathbf{y}}|} = \frac{\frac{\sqrt{3}}{2}\hat{\mathbf{x}} - \frac{1}{2}\hat{\mathbf{y}}}{\sqrt{\frac{3}{4} + \frac{1}{4}}} = \frac{\sqrt{3}\hat{\mathbf{x}}}{2} - \frac{\hat{\mathbf{y}}}{2}, \tag{6.22}$$

and

$$\mathbf{n}_3 = \frac{-\cos(30°)\hat{\mathbf{x}} - \sin(30°)\hat{\mathbf{y}}}{|-\cos(30°)\hat{\mathbf{x}} - \sin(30°)\hat{\mathbf{y}}|} = \frac{\frac{-\sqrt{3}}{2}\hat{\mathbf{x}} - \frac{1}{2}\hat{\mathbf{y}}}{\sqrt{\frac{3}{4} + \frac{1}{4}}} = \frac{-\sqrt{3}\hat{\mathbf{x}}}{2} - \frac{\hat{\mathbf{y}}}{2}. \tag{6.23}$$

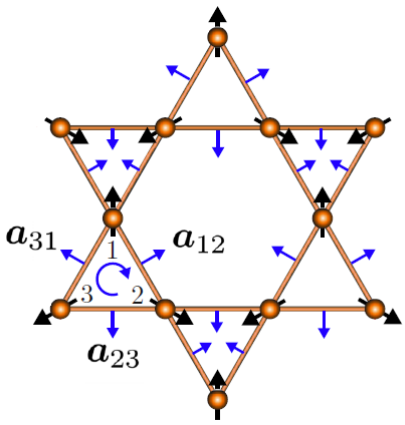


**Figure 6.8:** Kagome lattice with uniform 120° magnetic ordering. The spins are shown in black arrows ($\mathbf{n}_1$, $\mathbf{n}_2$ and $\mathbf{n}_3$) and the blue arrows represent the SOC in plane components. Image from [40].

The in-plane components of the $a$-vectors that appear in the expression of the SOC, are given by

$$\mathbf{a}_{ij}^{\parallel} = \epsilon_{ijk}\mathbf{n}_k, \tag{6.24}$$

so that these vectors point in the opposite direction to the unit vectors as it is shown in the following equations

$$\mathbf{a}_{23}^{\parallel} = -\hat{\mathbf{y}}, \tag{6.25}$$

$$\mathbf{a}_{31}^{\parallel} = -\frac{\sqrt{3}\hat{\mathbf{x}}}{2} + \frac{\hat{\mathbf{y}}}{2}, \tag{6.26}$$

and

$$\mathbf{a}_{12}^{\parallel} = \frac{\sqrt{3}\hat{\mathbf{x}}}{2} + \frac{\hat{\mathbf{y}}}{2}. \tag{6.27}$$

Using this, we find that the SOC vectors are

$$\mathbf{a}_{23} = \cos\theta \mathbf{a}_{23}^{\parallel} + \sin\theta\hat{\mathbf{z}}, \tag{6.28}$$

$$\mathbf{a}_{31} = \cos\theta \mathbf{a}_{31}^{\parallel} + \sin\theta\hat{\mathbf{z}}, \tag{6.29}$$

and

$$\mathbf{a}_{12} = \cos\theta \mathbf{a}_{12}^{\parallel} + \sin\theta\hat{\mathbf{z}}. \tag{6.30}$$

### 6.2.1 Real-space Berry Phase in the Double Exchange Limit for Collinear Configurations

In the double exchange limit, where $\frac{J}{t} \to \infty$, the spin of the itinerant electrons must be parallel to the fixed underlying local spins, because the tight-binding part is the one that considers the change in the spin direction of the itinerant electrons. If $\theta = \frac{\pi}{2}$, all the SOC vectors are

$$\mathbf{a}_{ij} = \sin\frac{\pi}{2}\hat{\mathbf{z}} = \hat{\mathbf{z}}, \tag{6.31}$$

so that the three vectors are collinear and point into the $\hat{\mathbf{z}}$ direction. An electron that moves along the triangle plaquette, acquires a Berry phase $\gamma_{123} = \frac{\Omega_{123}}{2} = \pi$, because it is similar to the case where the SOC is absent. The Berry phase is a constant, so it is an invariant quantity under time reversal symmetry, and there is no real magnetic field being generated. In this case the band structure of the tight-binding Hamiltonian shows two Dirac points (see references [63, 64]) at the K point in the Brillouin zone.

### 6.2.2 Real-space Berry Phase in the Double Exchange Limit for Coplanar Configurations

If the angle $\theta = 0$, the SOC vectors are the in-plane contributions

$$\mathbf{a}_{23} = \mathbf{a}_{23}^{\parallel}, \tag{6.32}$$

$$\mathbf{a}_{31} = \mathbf{a}_{31}^{\parallel} \tag{6.33}$$

and

$$\mathbf{a}_{12} = \mathbf{a}_{12}^{\parallel}, \tag{6.34}$$

and the electron that moves along this plaquette has a Berry phase given by $\gamma_{123} = \pi - 6\alpha$ (agreeing with the algebraic approach) where we are only considering up to first order in $\alpha$. In this case a magnetic flux appears. This magnetic flux separates the Dirac points and the bands acquire a Chern number, so they are topological non-trivial.

### 6.2.3 Momentum-space Berry Phase

We want to analyze the problem away from the double-exchange limit. Now, we need to consider the reciprocal space of the Hamiltonian. The $k$-matrix representation of the tight-binding Hamiltonian is

$$\mathcal{H}_k^{12} = t\mathrm{e}^{\frac{i\alpha}{2}\boldsymbol{\sigma}\cdot\mathbf{a}_{12}}\left(1+\mathrm{e}^{-i\mathbf{k}\cdot(\mathbf{u}_2-\mathbf{u}_1)}\right), \tag{6.35}$$

$$\mathcal{H}_k^{23} = t\mathrm{e}^{\frac{i\alpha}{2}\boldsymbol{\sigma}\cdot\mathbf{a}_{23}}\left(1+\mathrm{e}^{-i\mathbf{k}\cdot\mathbf{u}_1}\right), \tag{6.36}$$

$$\mathcal{H}_k^{31} = t\mathrm{e}^{\frac{i\alpha}{2}\boldsymbol{\sigma}\cdot\mathbf{a}_{31}}\left(1+\mathrm{e}^{i\mathbf{k}\cdot\mathbf{u}_2}\right). \tag{6.37}$$

On the other hand, the $k$-matrix representation of the antiferromagnetic Hamiltonian is

$$\mathcal{H}_k^{11} = -\frac{JS}{2}\mathbf{n}_1\cdot\boldsymbol{\sigma}, \tag{6.38}$$

$$\mathcal{H}_k^{22} = -\frac{JS}{2}\mathbf{n}_2\cdot\boldsymbol{\sigma}, \tag{6.39}$$

$$\mathcal{H}_k^{33} = -\frac{JS}{2}\mathbf{n}_3\cdot\boldsymbol{\sigma}, \tag{6.40}$$

so that the matrix representation of the Hamiltonian in $k$-space is

$$\mathcal{H}_k = \begin{bmatrix} \mathcal{H}_k^{11} & \mathcal{H}_k^{12} & (\mathcal{H}_k^{13})^\dagger \\ (\mathcal{H}_k^{12})^\dagger & \mathcal{H}_k^{22} & \mathcal{H}_k^{23} \\ \mathcal{H}_k^{31} & (\mathcal{H}_k^{23})^\dagger & \mathcal{H}_k^{33} \end{bmatrix}, \tag{6.41}$$

which can be used to obtain the energy bands. We have computed the energy band structure for $t = 1$, $-JS/2 = 0.5t$ and $\theta = 0$. The latter was chosen with the purpose of studying the case of the coplanar configuration. The band structure was computed for the case in the absence of SOC and for the case when the SOC is present. It can be observed, in both cases, that instead of having three bands (Figure 6.7) we have six bands due to the spin degree of freedom. In the case where the SOC vanished, two bands touch each other, but they do not form a Dirac cone, because the energy dispersion is no longer linear. When the SOC is present, the bands that were touching each other shows a gap.

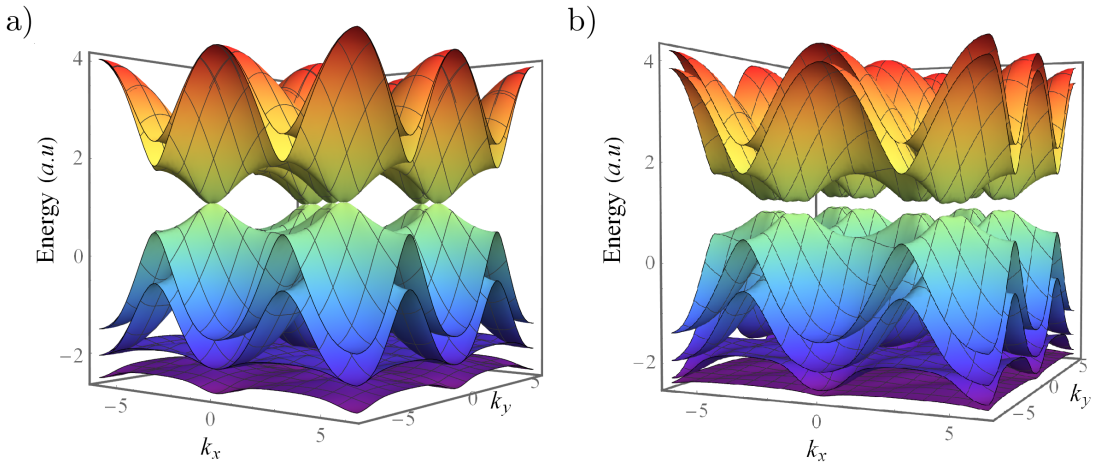


**Figure 6.9:** Energy band structure for kagome lattice with $-JS/2 = 0.5t$, $\theta = 0$ when a) there is no SOC and b) when the SOC appears ($\alpha = 0.2\pi$).

Then, we proceeded in showing cuts of the energy bands. The resulting energy band structures of the Kagome lattice is shown in Figure 6.10. The Figure 6.10a corresponds to the band structure in the absence of SOC, while the Figure 6.10b is the one in the presence of the SOC[2]. Note that the first and the second bands (the latter appearing from the former due to the extra spin degree of freedom) are almost flat due to the inherent geometric frustration of antiferromagnetic model on a triangular configuration.

In the case without SOC (Figure 6.10a), the first and the second band do touch, but they do not form Dirac points. The third band touches the second band at the $\Gamma = (0, 0)$ point. The fourth and the fifth bands touch each other, but they do not generate Dirac points because the energy dispersion is not linear. Finally, the fifth and the sixth bands share the same value in energy at the $\Gamma$ point. On the other hand, in the presence of SOC (Figure 6.10b) the bands do not touch each other at any point, that is, the SOC generates an overall gap between the bands.

Finally, we obtained the band structure along a path in the irreducible Brillouin zone for different $\alpha$ values. The Figure 6.11a is for $\alpha = 0$, this is the case were the SOC is absent. Figures 6.11b, 6.11c, and 6.11d are for $\alpha = 0.2\pi$, $\alpha = 0.4\pi$, and $\alpha = 0.8\pi$. None of the computed band structures show a Dirac point in the high symmetry point K. As we can see, the gap between consecutive bands overall increases and they become flatter as the value for the angle $\alpha$ gets closer to $\pi$. The latter is consequence of the SOC.

[2]In this chapter we are going to name the bands from first to sixth, starting with the lowest band and ending with the highest one.

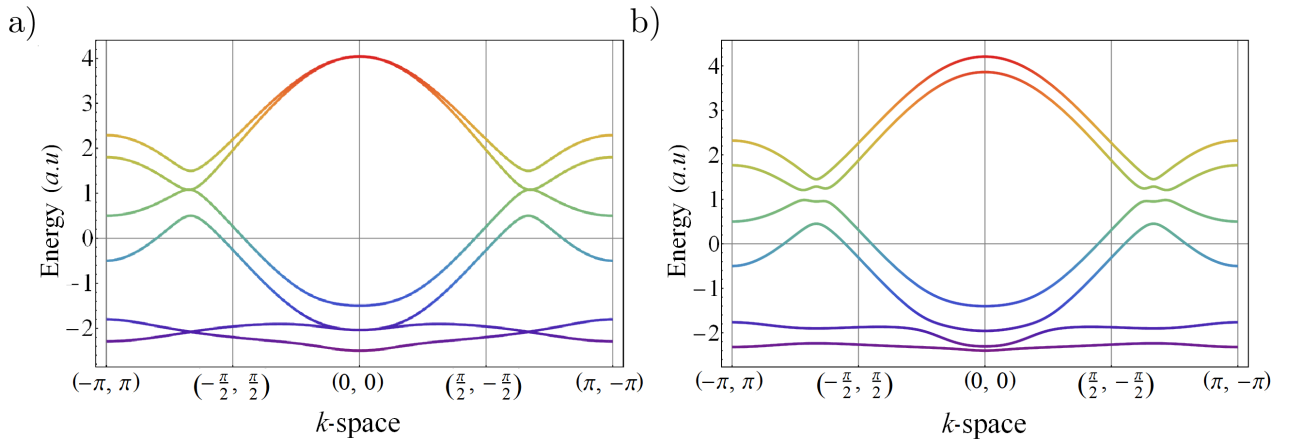


**Figure 6.10:** Energy band structure for $-JS/2 = 0.5t$, $\theta = 0$ in the a) absence and b) in the presence of SOC ($\alpha = 0.2\pi$). The mapping for these band structures goes from $(-\pi, \pi)$ to $(\pi, -\pi)$.

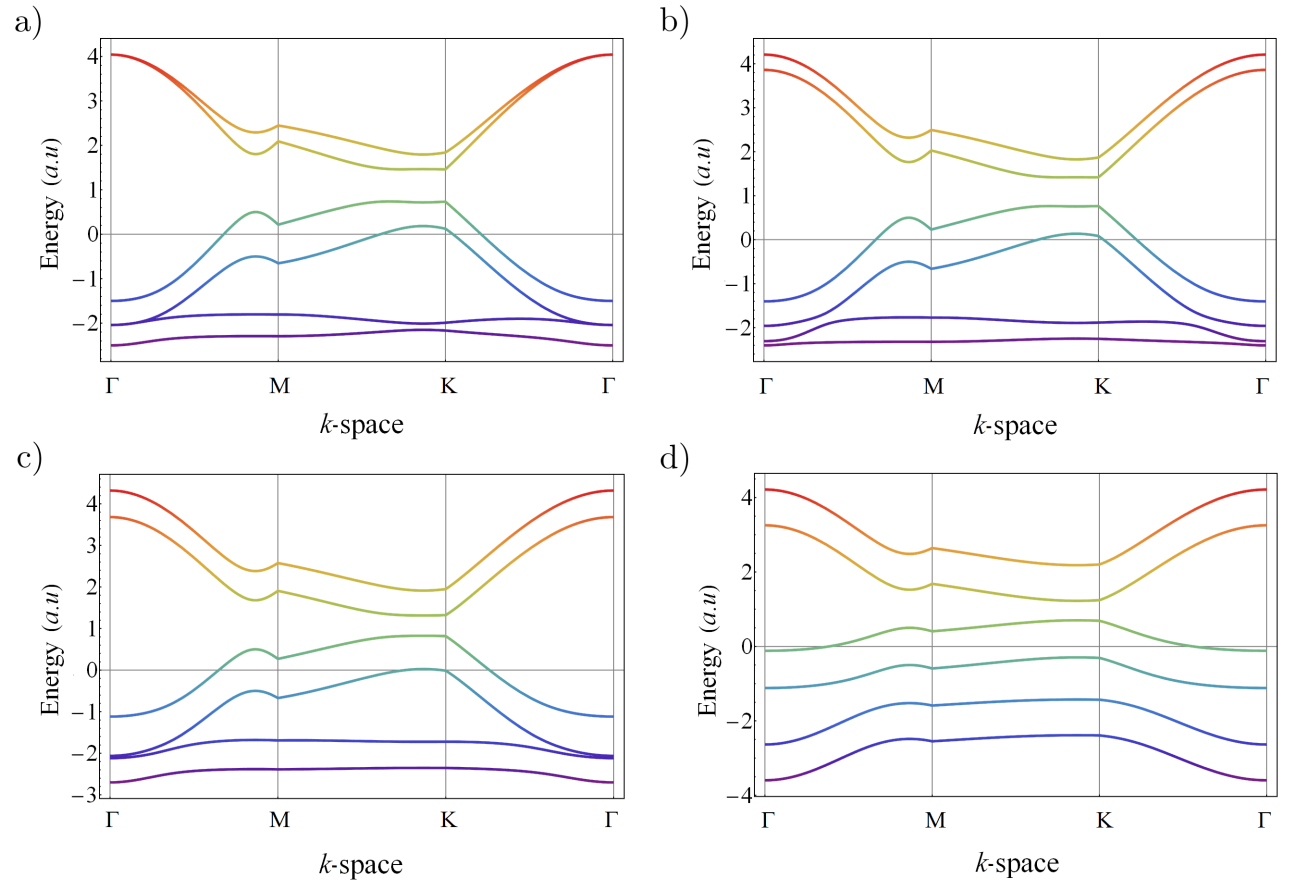


**Figure 6.11:** Energy band structure for $-JS/2 = 0.5t$, $\theta = 0$, a) without SOC, b) with SOC $\alpha = 0.2\pi$, c) with SOC $\alpha = 0.4\pi$, and d) with SOC $\alpha = 0.8\pi$

# Conclusions

In this work, a theoretical study of the Berry curvature and the Berry phase was done. We started by presenting the basic topology concepts and then we derived the expression for the Berry connection, curvature and phase. Then we introduced the AHE, whose origin can be attributed to the Berry Phase.

In this thesis, we reproduced meticulously the derivations done by [40] of the Berry connection and of the Berry phase for an electron moving around a triangular plaquette, while it interacts with the local magnetic moments. The analysis was done for three different approaches: geometric, algebraic and in the continuum limit.

In the geometric approach, a spin state in the Bloch sphere is moved following a geodesic path from its original direction to the direction of another spin state. This translation is done using rotation matrices. In the SU(2) invariant case, it was obtained that the Berry phase is half of the solid angle subtended by three vectors, whose Berry connections were added to obtain that phase. When the SOC is present the Berry phase is half the solid angle of the nonagon created by nine different vectors, and then, nine Berry connections were added. This approach showed us that, when the SOC is present, an effective magnetic field appears even if the spin configuration is collinear or coplanar.

In the algebraic approach we arrived to the conclusion that in systems with SOC the electron that moves in a triangle plaquette picks up a non-trivial Berry phase that acts as a fictitious magnetic flux. This Berry phase has an extra component that is proportional to the Wilson loop.

In the continuum limit, the Berry phase was also analyzed, noticing that this limit could be achieved with the superposition of multiple loops. In the case with SOC, we arrived to the conclusion that the Berry phase can be written covariantly. This form contains the Abelian field strength and the covariant form of the solid angle density. We also found that collinear configurations can also produce an effective magnetic field when the SOC is present.

Finally, we studied the case of the kagome lattice with a coplanar ordering. We analyzed

the band structures for three different situations: for the tight-binding model, and for the model proposed by [40] in the absence and in the presence of SOC. From this analysis, we conclude that the SOC has an important role of modulating the band structures.

For future work, we suggest to apply this analysis to materials containing this type of interaction and compare the type of analysis done here with those obtained by other means, as for instance, density functional theory or experimental measurements. .

# Appendix A

# The Adiabatic Evolution in Quantum Mechanics

We say that a system evolves adiabatically when its evolution is "infinitely slow" [65]. In non-relativistic quantum mechanics, the adiabatic theorem tells us how the solutions of the Schrödinger equation behave when the Hamiltonian is slowly varied in time [65].

In this appendix we are going to follow the procedure done by Dariusz Chruściński and Andrzej Jamiołkowski [65]. Consider a time-dependent Hamiltonian $H(t)$, whose spectrum is non-degenerate and discrete. Its eigenfunctions and eigenvalues are time-dependent

$$H(t)\left|m(t)\right\rangle = \mathcal{E}_m(t)\left|m(t)\right\rangle, \tag{A.1}$$

and the eigenvectors fulfill that $\langle m(t)|l(t)\rangle = \delta_{ml}$. At a given time $t$, a quantum state $|\psi(t)\rangle$ of the system can be written as

$$\left|\psi(t)\right\rangle = \sum_m c_m(t)\mathrm{e}^{i\theta_m(t)}\left|m(t)\right\rangle, \tag{A.2}$$

where

$$\mathrm{e}^{i\theta_m(t)} = \exp\left[-\frac{i}{\hbar}\int_0^t \mathcal{E}_m(\tau)d\tau\right] \tag{A.3}$$

is the so-called dynamical phase. We are interested in finding an expression for $c_m(t)$, solution of the Schrödinger equation

$$i\hbar\frac{d}{dt}\left|\psi(t)\right\rangle = H(t)\left|\psi(t)\right\rangle \tag{A.4}$$

Using equations (A.1) and (A.2), we get that

$$i\hbar\frac{d}{dt}\left[\sum_m c_m(t)\mathrm{e}^{i\theta_m(t)}\left|m(t)\right\rangle\right] = H(t)\sum_m c_m(t)\mathrm{e}^{i\theta_m(t)}\left|m(t)\right\rangle \tag{A.5}$$

$$\sum_m\left[\dot{c}_m(t)\mathrm{e}^{i\theta_m(t)}\left|m(t)\right\rangle + ic_m(t)\dot{\theta}_m(t)\mathrm{e}^{i\theta_m(t)} + c_m\mathrm{e}^{i\theta_m(t)}\left|\dot{m}(t)\right\rangle\right] = \frac{1}{i\hbar}\sum_m \mathcal{E}_m(t)c_m(t)\mathrm{e}^{i\theta_m(t)}\left|m(t)\right\rangle \tag{A.6}$$

and then

$$\begin{aligned}\sum_m \dot{c}_m(t)\mathrm{e}^{i\theta_m(t)}\left|m(t)\right\rangle &= \frac{-i}{\hbar}\sum_m \mathcal{E}_m(t)c_m(t)\mathrm{e}^{i\theta_m(t)}\left|m(t)\right\rangle + \frac{i}{\hbar}\sum_m \mathcal{E}_m c_m(t)\mathrm{e}^{i\theta_m(t)}\left|m(t)\right\rangle \\ &\quad - \sum_m c_m(t)\mathrm{e}^{i\theta_m(t)}\left|\dot{m}(t)\right\rangle \\ &= -\sum_m c_m(t)\mathrm{e}^{i\theta_m(t)}\left|\dot{m}(t)\right\rangle .\end{aligned} \tag{A.7}$$

Next we do the expectation value using the bra state $\langle l(t)|$ in the last equation

$$\sum_m \langle l(t)|\dot{c}_m(t)\mathrm{e}^{i\theta_m(t)}|m(t)\rangle = -\sum_m \langle l(t)|c_m(t)\mathrm{e}^{i\theta_m(t)}|\dot{m}(t)\rangle \tag{A.8}$$

$$\dot{c}_l(t)\mathrm{e}^{i\theta_l(t)} = -\sum_m \langle l(t)|c_m\mathrm{e}^{i\theta_m(t)}|\dot{m}(t)\rangle \tag{A.9}$$

$$\dot{c}_l(t) = -\sum_m c_m(t)\mathrm{e}^{i(\theta_m-\theta_l)}\left\langle l(t)\right|\frac{d}{dt}\left|m(t)\right\rangle . \tag{A.10}$$

Finally, we found that

$$\dot{c}_l(t) = -c_l(t)\left\langle l(t)\right|\frac{d}{dt}\left|l(t)\right\rangle - \sum_{m(\neq l)}\exp\left[-\frac{i}{\hbar}\int_0^t\left(\mathcal{E}_l(\tau)-\mathcal{E}_m(\tau)\right)d\tau\right]\left\langle m(t)\right|\frac{d}{dt}\left|l(t)\right\rangle . \tag{A.11}$$

Now, we are interested in finding the adiabatic condition. In order to do this, we compute the time-derivative of equation (A.1)

$$\dot{H}(t)\left|l(t)\right\rangle + H(t)\left|\dot{l}(t)\right\rangle = \dot{\mathcal{E}}_l(t)\left|l(t)\right\rangle + \mathcal{E}_l(t)\left|\dot{l}(t)\right\rangle , \tag{A.12}$$

then we do the expectation value using $\langle m(t)|$, so that

$$\begin{aligned}\left\langle m(t)\right|\dot{H}(t)\left|l(t)\right\rangle + \left\langle m(t)\right|H(t)\left|\dot{l}(t)\right\rangle &= \left\langle m(t)\right|\dot{\mathcal{E}}_l(t)\left|l(t)\right\rangle + \left\langle m(t)\right|\mathcal{E}_l(t)\left|\dot{l}(t)\right\rangle \\ &= \mathcal{E}_l(t)\left\langle m(t)\right|\left.\dot{l}(t)\right\rangle .\end{aligned} \tag{A.13}$$

$$\langle m(t)|\dot{H}(t)|l(t)\rangle + \mathcal{E}_m(t)\left\langle m(t)\right|\left.\dot{l}(t)\right\rangle = \mathcal{E}_l(t)\left\langle m(t)\right|\left.l(t)\right\rangle \tag{A.14}$$

and rearranging we find that:

$$\langle m(t)|\dot{l}(t)\rangle = \frac{\langle m(t)|\dot{H}(t)|l(t)\rangle}{\mathcal{E}_l(t) - \mathcal{E}_m(t)}, \tag{A.15}$$

for $m \neq l$. We can say that the Hamiltonian evolution is adiabatic if

$$|\langle m(t)|\dot{H}|l(t)\rangle| \ll \frac{|\mathcal{E}_l - \mathcal{E}_m|}{\Delta T_{lm}}, \tag{A.16}$$

where the characteristic transition time between the states $|l(t)\rangle$ and $|m(t)\rangle$ is given by $\Delta T_{lm}$. In the adiabatic limit $\Delta T_{lm} \to \infty$, and so in equation (A.16), the term $|\langle m(t)|\dot{H}|l(t)\rangle| \to 0$. This condition implies that in the equation (A.15), the term $\langle m(t)|\dot{l}(t)\rangle = 0$ for $m \neq l$. Then, the second term in the equation (A.11) vanishes and the derivative of the coefficient $c_l(t)$ is only

$$\dot{c}_l(t) = -c_l(t)\,\langle l(t)|\frac{d}{dt}|l(t)\rangle\,. \tag{A.17}$$

From this last equation, we can conclude that the coefficient $c_l(t)$ has the form $\mathrm{e}^{i\gamma_l(t)}$, where $\gamma_l(t) = i\,\langle l(t)|\dot{l}(t)\rangle$. Finally, equation (A.2) becomes

$$|\psi(t)\rangle = \sum_m \mathrm{e}^{i\gamma_m(t)} \exp\left[-\frac{i}{\hbar}\int_0^t \mathcal{E}_m(\tau)d\tau\right]|m(t)\rangle\,. \tag{A.18}$$

For many years the phase $\mathrm{e}^{i\gamma_m(t)}$ was absorbed in the eigenvector, but in the last few years it was found that this phase cannot be ignored because sometimes (as in the Berry phase) it has physical implications [65].

# Appendix B

# The Anomalous Velocity in the AHE

We mentioned, that in the AHE the electron's group velocity acquires a new contribution: the anomalous velocity. In this appendix we are going to show the derivation of this contribution following the procedure shown by Girvin [1].

Let us consider the following Schrödinger equation:

$$H\left|\psi(\mathbf{r})\right\rangle = \left\{\frac{1}{2m}\left[\mathbf{p}+\frac{e}{c}\mathbf{A}(\mathbf{r})\right]^2 + V(\mathbf{r})\right\}\left|\psi(\mathbf{r})\right\rangle = \mathcal{E}\left|\psi(\mathbf{r})\right\rangle, \tag{B.1}$$

where $V(\mathbf{r})$ is the periodic potential with the lattice periodicity, and $|\psi(\mathbf{r})\rangle$ is the eigenfunction. If we think on a Bloch wavefunction $|\psi_{n\mathbf{k}}(\mathbf{r})\rangle$, with wave vector $\mathbf{k}$ and $n$ labeling the bands, it fulfils, according to Bloch's theorem, that the eigenfunctions of a crystal "in the independent electron model are plane-waves modulated by a periodic function" [1], so that

$$\left|\psi_{n\mathbf{k}}(\mathbf{r})\right\rangle = \mathrm{e}^{i\mathbf{k}\cdot\mathbf{r}}\left|u_{n\mathbf{k}}(\mathbf{r})\right\rangle, \tag{B.2}$$

where $|u_{n\mathbf{k}}(\mathbf{r})\rangle$ has the periodicity of the Bravais lattice [1]. Using equation (B.2), and considering that $\mathbf{p} = -i\hbar\boldsymbol{\nabla}$, then [66, 67]

$$\mathbf{p}\left|\psi_{n\mathbf{k}}(\mathbf{r})\right\rangle = -i\hbar\boldsymbol{\nabla}\left[\mathrm{e}^{i\mathbf{k}\cdot\mathbf{r}}\left|u_{n\mathbf{k}}(\mathbf{r})\right\rangle\right] = \hbar\mathbf{k}\mathrm{e}^{i\mathbf{k}\cdot\mathbf{r}}\left|u_{n\mathbf{k}}(\mathbf{r})\right\rangle + \mathrm{e}^{i\mathbf{k}\cdot\mathbf{r}}\mathbf{p}\left|u_{n\mathbf{k}}(\mathbf{r})\right\rangle = \mathrm{e}^{i\mathbf{k}\cdot\mathbf{r}}(\mathbf{p}+\hbar\mathbf{k})\left|u_{n\mathbf{k}}(\mathbf{r})\right\rangle. \tag{B.3}$$

Then, for a eigenvalue of the wave vector $\mathbf{k}$, we have an effective Hamiltonian $h_{\mathbf{k}}$ given by

$$h_{\mathbf{k}} = \frac{1}{2m}\left[\mathbf{p}+\hbar\mathbf{k}+\frac{e}{c}\mathbf{A}(\mathbf{r})\right]^2 + V(\mathbf{r}), \tag{B.4}$$

and, in turn, $|u_{n\mathbf{k}}(\mathbf{r})\rangle$ must obey the following eigenvalue equation [1]:

$$h_{\mathbf{k}}\left|u_{n\mathbf{k}}(\mathbf{r})\right\rangle = \mathcal{E}_n(\mathbf{k})\left|u_{n\mathbf{k}}(\mathbf{r})\right\rangle. \tag{B.5}$$

The expectation value of the velocity of an electron is

$$\begin{aligned}\langle\psi_{n\mathbf{k}}(\mathbf{r})|\mathbf{v}|\psi_{n\mathbf{k}}(\mathbf{r})\rangle &= \langle\psi_{n\mathbf{k}}(\mathbf{r})|\frac{\mathbf{p}}{m}|\psi_{n\mathbf{k}}(\mathbf{r})\rangle \\ &= \langle u_{n\mathbf{k}}(\mathbf{r})|\frac{(\mathbf{p}+\hbar\mathbf{k})}{m}|u_{n\mathbf{k}}(\mathbf{r})\rangle \\ &= \langle u_{n\mathbf{k}}(\mathbf{r})|\frac{1}{\hbar}\frac{\partial h_{\mathbf{k}}}{\partial\mathbf{k}}|u_{n\mathbf{k}}(\mathbf{r})\rangle \\ &= \frac{1}{\hbar}\frac{\partial\mathcal{E}_n(\mathbf{k})}{\partial\mathbf{k}},\end{aligned} \tag{B.6}$$

where in the last step we have used the Hellmann-Feynman theorem[1]. Now, we consider a perturbation given by the Hamiltonian

$$H' = e\mathbf{E}\cdot\mathbf{r}. \tag{B.8}$$

Then using perturbation theory up to first order, the perturbative wavefunction is

$$|\psi^1_{n\mathbf{k}}\rangle = \sum_{n,\,n',\,\mathbf{k},\,\mathbf{k}'}{}' \frac{|\psi_{n'\mathbf{k}'}\rangle\langle\psi_{n'\mathbf{k}'}|\,e\mathbf{E}\cdot\mathbf{r}\,|\psi_{n\mathbf{k}}\rangle}{\mathcal{E}_n(\mathbf{k})-\mathcal{E}_{n'}(\mathbf{k}')} = \sum_{n,\,n',\,\mathbf{k},\,\mathbf{k}'}{}' e\mathbf{E}\cdot\frac{|\psi_{n'\mathbf{k}'}\rangle\langle\psi_{n'\mathbf{k}'}|\,\mathbf{r}\,|\psi_{n\mathbf{k}}\rangle}{\mathcal{E}_n(\mathbf{k})-\mathcal{E}_{n'}(\mathbf{k}')}. \tag{B.9}$$

We want to relate the position $\mathbf{r}$ with the velocity $\mathbf{v}$, so we use the commutator between $\mathbf{r}$ and $H$, in order to relate it with the Heisenberg equation of motion, so

$$\langle\psi_{n'\mathbf{k}'}|[\mathbf{r},\,H]|\psi_{n\mathbf{k}}\rangle = \langle\psi_{n'\mathbf{k}'}|\mathbf{r}H - H\mathbf{r}|\psi_{n\mathbf{k}}\rangle = \langle\psi_{n'\mathbf{k}'}|\mathbf{r}|\psi_{n\mathbf{k}}\rangle\,[\mathcal{E}_n(\mathbf{k})-\mathcal{E}_{n'}(\mathbf{k}')], \tag{B.10}$$

so, using equations (B.9) and (B.10) the perturbation eigenvector can be rewritten as

$$|\psi^1_{n\mathbf{k}}\rangle = \sum_{n,\,n',\,\mathbf{k},\,\mathbf{k}'}{}' e\mathbf{E}\cdot\frac{|\psi_{n'\mathbf{k}'}\rangle\langle\psi_{n'\mathbf{k}'}|[\mathbf{r},\,H]|\psi_{n\mathbf{k}}\rangle}{[\mathcal{E}_n(\mathbf{k})-\mathcal{E}_{n'}(\mathbf{k}')]^2}. \tag{B.11}$$

Using the motion Heisenberg equation we have that

$$[\mathbf{r},\,H] = -[H,\,\mathbf{r}] = \frac{-\hbar}{i}\dot{\mathbf{r}} = i\hbar\mathbf{v}, \tag{B.12}$$

[1]The Hellmann-Feynman theorem states that when a Hamiltonian $H_\lambda$ and the state of the wavefunction $|\psi_\lambda\rangle$ depend on the same parameter $\lambda$, so that $H_\lambda|\psi_\lambda\rangle = \mathcal{E}_\lambda|\psi_\lambda\rangle$, $\langle\psi_\lambda|\psi_\lambda\rangle = 1$, and $\frac{d}{d\lambda}\langle\psi_\lambda|\psi_\lambda\rangle = 0$, the first derivative of a Hamiltonian expectation value does not include any wavefunction derivative. The proof of this theorem is the following:

$$\begin{aligned}\frac{d\mathcal{E}_\lambda}{d\lambda} &= \frac{d}{d\lambda}\langle\psi_\lambda|H_\lambda|\psi_\lambda\rangle = \mathcal{E}_\lambda\langle\frac{d}{d\lambda}\psi_\lambda|\psi_\lambda\rangle + \langle\psi_\lambda|\frac{d}{d\lambda}H_\lambda|\psi_\lambda\rangle + \mathcal{E}_\lambda\langle\psi_\lambda|\frac{d}{d\lambda}\psi_\lambda\rangle \\ &= \mathcal{E}_\lambda\frac{d}{d\lambda}\langle\psi_\lambda|\psi_\lambda\rangle + \langle\psi_\lambda|\frac{d}{d\lambda}H_\lambda|\psi_\lambda\rangle = \langle\psi_\lambda|\frac{d}{d\lambda}H_\lambda|\psi_\lambda\rangle\,.\end{aligned} \tag{B.7}$$

so

$$|\psi^1_{n\mathbf{k}}\rangle = \sum_{n,\,n',\,\mathbf{k},\,\mathbf{k}'}{}' \, i\hbar e\mathbf{E}\cdot\frac{|\psi_{n'\mathbf{k}'}\rangle\langle\psi_{n'\mathbf{k}'}|\mathbf{v}|\psi_{n\mathbf{k}}\rangle}{[\mathcal{E}_n(\mathbf{k})-\mathcal{E}_{n'}(\mathbf{k}')]^2}. \tag{B.13}$$

Note that

$$\langle\psi_{n'\mathbf{k}'}|\mathbf{v}|\psi_{n\mathbf{k}}\rangle = \mathrm{e}^{-i(\mathbf{k}'-\mathbf{k})\cdot\mathbf{r}}\langle u_{n'\mathbf{k}'}|\mathbf{v}|u_{n\mathbf{k}}\rangle = \mathrm{e}^{-i(\mathbf{k}'-\mathbf{k})\cdot\mathbf{r}}\langle u_{n'\mathbf{k}'}|\frac{1}{\hbar}\frac{\partial h_{\mathbf{k}}}{\partial\mathbf{k}}|u_{n\mathbf{k}}\rangle\,\delta_{\mathbf{k},\,\mathbf{k}'} \tag{B.14}$$

where all the elements vanish unless $\mathbf{k}=\mathbf{k}'$, so

$$|u^1_{n\mathbf{k}}\rangle = ie\mathbf{E}\cdot\sum_{n\neq n'}\frac{|u_{n'\mathbf{k}}\rangle\langle u_{n'\mathbf{k}}|\frac{\partial h_{\mathbf{k}\mathbf{k}}}{\partial\mathbf{k}}|u_{n\mathbf{k}}\rangle}{[\mathcal{E}_n(\mathbf{k})-\mathcal{E}_{n'}(\mathbf{k})]^2}. \tag{B.15}$$

The eigenfunction $|u_{n\mathbf{k}}\rangle$ up to first order in perturbation theory is

$$|u^c_{n\mathbf{k}}\rangle = |u_{n\mathbf{k}}\rangle + |u^1_{n\mathbf{k}}\rangle\,, \tag{B.16}$$

so, the velocity expectation value is

$$\begin{aligned}\langle\mathbf{v}\rangle &= \langle u^c_{n\mathbf{k}}|\mathbf{v}|u^c_{n\mathbf{k}}\rangle = (\langle u_{n\mathbf{k}^1}| + \langle u_{n\mathbf{k}}|)\mathbf{v}(|u_{n\mathbf{k}}\rangle + |u^1_{n\mathbf{k}}\rangle)\\ &= \langle u^1_{n\mathbf{k}}|\mathbf{v}|u_{n\mathbf{k}}\rangle + \langle u^1_{n\mathbf{k}}|\mathbf{v}|u^1_{n\mathbf{k}}\rangle + \langle u_{n\mathbf{k}}|\mathbf{v}|u_{n\mathbf{k}}\rangle + \langle u_{n\mathbf{k}}|\mathbf{v}|u^1_{n\mathbf{k}}\rangle\,.\end{aligned} \tag{B.17}$$

Since we are only interested up to the first order in $\mathbf{E}$, we disregard the term $\langle u^1_{n\mathbf{k}}|\mathbf{v}|u^1_{n\mathbf{k}}\rangle$, and therefore

$$\begin{aligned}\langle\mathbf{v}\rangle &= \langle u_{n\mathbf{k}}|\mathbf{v}|u_{n\mathbf{k}}\rangle + \langle u^1_{n\mathbf{k}}|\mathbf{v}|u_{n\mathbf{k}}\rangle + \langle u_{n\mathbf{k}}|\mathbf{v}|u^1_{n\mathbf{k}}\rangle\\ &= \langle u_{n\mathbf{k}}|\frac{1}{\hbar}\frac{\partial h_{\mathbf{k}}}{\partial\mathbf{k}}|u_{n\mathbf{k}}\rangle + \underbrace{\langle u^1_{n\mathbf{k}}|\frac{1}{\hbar}\frac{\partial h_{\mathbf{k}}}{\partial\mathbf{k}}|u_{n\mathbf{k}}\rangle + \langle u_{n\mathbf{k}}|\frac{1}{\hbar}\frac{\partial h_{\mathbf{k}}}{\partial\mathbf{k}}|u^1_{n\mathbf{k}}\rangle}_{\mathbf{v}_a(n,\,\mathbf{k})}\\ &= \frac{1}{\hbar}\frac{\partial\mathcal{E}_n(\mathbf{k})}{\partial\mathbf{k}} + \mathbf{v}_a(n,\,\mathbf{k}),\end{aligned} \tag{B.18}$$

where $\mathbf{v}_a(n,\,\mathbf{k})$ is the anomalous velocity, which is a correction to the equation (B.5) [1]. Now, we are going to analyze the components of the anomalous velocity using equation (B.15). The first term is

$$\langle u^1_{n\mathbf{k}}|\frac{1}{\hbar}\frac{\partial h_{\mathbf{k}}}{\partial\mathbf{k}}|u_{n\mathbf{k}}\rangle = -\frac{ie}{\hbar}\sum_{n\neq n'}\frac{(\langle u_{n\mathbf{k}}|\frac{\partial h_{\mathbf{k}}}{\partial\mathbf{k}}|u_{n'\mathbf{k}}\rangle\langle u_{n'\mathbf{k}}|)\cdot\mathbf{E}\frac{\partial h_{\mathbf{k}}}{\partial\mathbf{k}}|u_{n\mathbf{k}}\rangle}{[\mathcal{E}_n(\mathbf{k})-\mathcal{E}_{n'}(\mathbf{k})]^2}, \tag{B.19}$$

$$\langle u_{n\mathbf{k}}|\frac{1}{\hbar}\frac{\partial h_{\mathbf{k}}}{\partial\mathbf{k}}|u^1_{n\mathbf{k}}\rangle = \frac{ie}{\hbar}\sum_{n\neq n'}\frac{\langle u_{n\mathbf{k}}|\frac{\partial h_{\mathbf{k}}}{\partial\mathbf{k}}\mathbf{E}\cdot(|u_{n'\mathbf{k}}\rangle\langle u_{n'\mathbf{k}}|\frac{\partial h_{\mathbf{k}}}{\partial\mathbf{k}}|u_{n\mathbf{k}}\rangle)}{[\mathcal{E}_n(\mathbf{k})-\mathcal{E}_{n'}(\mathbf{k})]^2}; \tag{B.20}$$

and so

$$\mathbf{v}_a(n,\,\mathbf{k}) = \frac{ie}{\hbar}\sum_{n\neq n'}\frac{\langle u_{n\mathbf{k}}|\frac{\partial h_{\mathbf{k}}}{\partial\mathbf{k}}|u_{n'\mathbf{k}}\rangle\left(\mathbf{E}\cdot\langle u_{n'\mathbf{k}}|\frac{\partial h_{\mathbf{k}}}{\partial\mathbf{k}}|u_{n\mathbf{k}}\rangle\right)}{[\mathcal{E}_n(\mathbf{k})-\mathcal{E}_{n'}(\mathbf{k})]^2} + C.C. \tag{B.21}$$

Using the vector triple product $\mathbf{a} \times (\mathbf{b} \times \mathbf{c}) = (\mathbf{a} \cdot \mathbf{c})\mathbf{b} - (\mathbf{a} \cdot \mathbf{b})\mathbf{c}$, where $\mathbf{a}$, $\mathbf{b}$ and $\mathbf{c}$ are vectors, we have that

$$\mathbf{v}_a(n,\, \mathbf{k}) = \frac{ie}{\hbar} \sum_{n \neq n'} \frac{\mathbf{E} \times \langle u_{n\mathbf{k}} | \frac{\partial h_{\mathbf{k}}}{\partial \mathbf{k}} | u_{n'\mathbf{k}} \rangle \times \langle u_{n'\mathbf{k}} | \frac{\partial h_{\mathbf{k}}}{\partial \mathbf{k}} | u_{n\mathbf{k}} \rangle}{[\mathcal{E}_n(\mathbf{k} - \mathcal{E}_{n'}(\mathbf{k}))]^2}, \tag{B.22}$$

where the Berry curvature given in equation (1.41) is present. It is important to mention that the $\mathbf{k}$-space is a 3D space, so

$$\mathbf{v}_a(n,\, \mathbf{k}) = \frac{e}{\hbar} \mathbf{E} \times \mathbf{b}^n(\mathbf{k}). \tag{B.23}$$

If the parameter $\mathbf{k}$ is on the $xy$ plane, the Berry curvature $\mathbf{b}^n(\mathbf{k})$ points in the $\hat{\mathbf{z}}$ direction [1]. Using that $-e\mathbf{E} = \hbar\dot{\mathbf{k}}$, the total electron's group velocity is

$$\langle \mathbf{v} \rangle = \frac{1}{\hbar} \frac{\partial \mathcal{E}_n(\mathbf{k})}{\partial \mathbf{k}} + \frac{e}{\hbar} \mathbf{E} \times \mathbf{b}^n(\mathbf{k}) = \frac{1}{\hbar} \frac{\partial \mathcal{E}_n(\mathbf{k})}{\partial \mathbf{k}} - \dot{\mathbf{k}} \times \mathbf{b}^n(\mathbf{k}), \tag{B.24}$$

and finally we arrive to the equation (3.15)

$$\hbar\dot{\mathbf{r}} = \frac{\partial \mathcal{E}_n(\mathbf{k})}{\partial \mathbf{k}} - \hbar\dot{\mathbf{k}} \times \mathbf{b}^n(\mathbf{k}), \tag{B.25}$$

were we can observe that the second term is the AHE contribution, and the Berry curvature is interpreted as a fictitious magnetic flux that is related to the energy eigenvectors [1].

# Bibliography


[1] S. M. Girvin and K. Yang, *Modern Condensed Matter Physics*. Cambridge University Press, 2019.

[2] R. C. for Emergent Matter Science, "Quantum matter theory research team."

[3] J. P. Liu, Z. Zhang, and G. Zhao, *Skyrmions: Topological Structures, Properties, and Applications*. CRC Press, 2016.

[4] L. De la Peña, *Introducción a la mecánica cuántica*. Fondo de Cultura Económica, 2014.

[5] A. Z. Capri, *Nonrelativistic Quantum Mechanics*. World Scientific Publishing, 3 ed., 2002.

[6] D. Kobe and E.-T. Wen, "Gauge invariance in quantum mechanics: Charged harmonic oscillator in an electromagnetic field," *Journal of Physics A: Mathematical and General*, vol. 15, no. 3, p. 787, 1982.

[7] M. V. Berry, "Quantal phase factors accompanying adiabatic changes," *Proceedings of the Royal Society of London. A. Mathematical and Physical Sciences*, vol. 392, no. 1802, pp. 45–57, 1984.

[8] M. T. Vaughn, *Introduction to Mathematical Physics*. John Wiley & Sons, 2008.

[9] M. Tarnowski, F. N. Ünal, N. Fläschner, B. S. Rem, A. Eckardt, K. Sengstock, and C. Weitenberg, "Measuring topology from dynamics by obtaining the chern number from a linking number," *Nature Communications*, vol. 10, no. 1, pp. 1–13, 2019.

[10] D. C. Mattis, *The Theory of Magnetism Made Simple: An Introduction to Physical Concepts and to Some Useful Mathematical Methods*. World Scientific Publishing Company, 2006.

[11] A. Beiser, *Concepts of Modern Physics*. McGraw-Hill, 2021.

[12] J. M. Coey, *Magnetism and Magnetic Materials*. Cambridge University Press, 2010.

[13] B. Friedrich and D. Herschbach, "Stern and Gerlach: How a Bad Cigar Helped Reorient Atomic Physics," *Physics Today*, vol. 56, no. 12, pp. 53–59, 2003.

[14] E. Santana Suárez, *Estudio de la conductividad Hall de espín en gases bidimensionales de electrones con interacción espín-órbita*. Bachelor's Degree Thesis, UNAM, 2019.

[15] P. Strange, *Relativistic Quantum Mechanics: with Applications in Condensed Matter and Atomic Physics*. Cambridge University Press, 1998.

[16] W. D. Callister Jr and D. G. Rethwisch, *Materials Science and Engineering: An Introduction*. John Wiley & Sons, 2020.

[17] F. W. Sears and M. W. Zemansky, *Física Universitaria, con Física Moderna, Volumen 2*. Pearson Educación, 2004.

[18] J. D. Patterson and B. C. Bailey, *Solid-State Physics: Introduction to the Theory*. Springer Science & Business Media, 2007.

[19] C. Kittel and P. McEuen, *Introduction to Solid State Physics*. John Wiley & Sons, 2018.

[20] K. von Klitzing, G. Dorda, and M. Pepper, "New method for high-accuracy determination of the fine-structure constant based on quantized hall resistance," *Physical Review Letters*, vol. 45, no. 6, p. 494, 1980.

[21] M. Paalanen, D. Tsui, and A. Gossard, "Quantized hall effect at low temperatures," *Physical Review B*, vol. 25, no. 8, p. 5566, 1982.

[22] A. Zangwill, *Modern Electrodynamics*. Cambridge University Press, 2013.

[23] R. B. Laughlin, "Quantized hall conductivity in two dimensions," *Physical Review B*, vol. 23, no. 10, p. 5632, 1981.

[24] J. Sinova, S. O. Valenzuela, J. Wunderlich, C. Back, and T. Jungwirth, "Spin hall effects," *Reviews of Modern Physics*, vol. 87, no. 4, p. 1213, 2015.

[25] M. I. D'Yakonov and V. Perel, "Possibility of orienting electron spins with current," *Soviet Journal of Experimental and Theoretical Physics Letters*, vol. 13, p. 467, 1971.

[26] M. I. Dyakonov and V. Perel, "Current-induced spin orientation of electrons in semiconductors," *Physics Letters A*, vol. 35, no. 6, pp. 459–460, 1971.

[27] J. Hirsch, "Spin hall effect," *Physical Review Letters*, vol. 83, no. 9, p. 1834, 1999.

[28] M. I. Dyakonov and A. Khaetskii, "Spin hall effect," in *Spin Physics in Semiconductors*, pp. 211–243, Springer, 2008.

[29] Y. K. Kato, R. C. Myers, A. C. Gossard, and D. D. Awschalom, "Observation of the spin hall effect in semiconductors," *Science*, vol. 306, no. 5703, pp. 1910–1913, 2004.

[30] Y. Shiomi, *Anomalous and Topological Hall Effects in Itinerant Magnets*. Springer Science & Business Media, 2013.

[31] A. W. Smith and R. Sears, "The hall effect in permalloy," *Physical Review*, vol. 34, no. 11, p. 1466, 1929.

[32] D. Culcer, "The anomalous hall effect," *ArXiv preprint arXiv:2204.02434*, 2022.

[33] R. Karplus and J. Luttinger, "Hall effect in ferromagnetics," *Physical Review*, vol. 95, no. 5, p. 1154, 1954.

[34] N. Nagaosa, J. Sinova, S. Onoda, A. H. MacDonald, and N. P. Ong, "Anomalous hall effect," *Reviews of Modern Physics*, vol. 82, no. 2, p. 1539, 2010.

[35] R. Kubo, "Statistical-mechanical theory of irreversible processes. i. general theory and simple applications to magnetic and conduction problems," *Journal of the Physical Society of Japan*, vol. 12, no. 6, pp. 570–586, 1957.

[36] R. Kubo, M. Yokota, and S. Nakajima, "Statistical-mechanical theory of irreversible processes. ii. response to thermal disturbance," *Journal of the Physical Society of Japan*, vol. 12, no. 11, pp. 1203–1211, 1957.

[37] J. Smit, "The spontaneous hall effect in ferromagnetics II," *Physica*, vol. 24, no. 1-5, pp. 39–51, 1958.

[38] L. Berger, "Application of the side-jump model to the hall effect and nernst effect in ferromagnets," *Physical Review B*, vol. 5, no. 5, p. 1862, 1972.

[39] D. J. Thouless, M. Kohmoto, M. P. Nightingale, and M. den Nijs, "Quantized hall conductance in a two-dimensional periodic potential," *Physical Review Letters*, vol. 49, no. 6, p. 405, 1982.

[40] S.-S. Zhang, H. Ishizuka, H. Zhang, G. B. Halász, and C. D. Batista, "Real-space berry curvature of itinerant electron systems with spin-orbit interaction," *Physical Review B*, vol. 101, no. 2, p. 024420, 2020.

[41] J. Ye, Y. B. Kim, A. Millis, B. Shraiman, P. Majumdar, and Z. Tešanović, "Berry phase theory of the anomalous hall effect: Application to colossal magnetoresistance manganites," *Physical Review Letters*, vol. 83, no. 18, p. 3737, 1999.

[42] T. Jungwirth, Q. Niu, and A. MacDonald, "Anomalous hall effect in ferromagnetic semiconductors," *Physical Review Letters*, vol. 88, no. 20, p. 207208, 2002.

[43] R. of the Universe, "Covalent bond, hydrogen molecule," *Online site: https://universe-review.ca/F12-molecule09.html*.

[44] E. Kaxiras and J. D. Joannopoulos, *Quantum Theory of Materials*. Cambridge University Press, 2019.

[45] N. W. Ashcroft and N. D. Mermin, *Solid State Physics*. Cengage Learning, 2022.

[46] M. Schiavello, *Photoelectrochemistry, Photocatalysis and Photoreactors Fundamentals and Developments*, vol. 146. Springer Science & Business Media pages=11, 2013.

[47] T. Moriya, *Spin Fluctuations in Itinerant Electron Magnetism*, vol. 56. Springer Science & Business Media, 2012.

[48] C. Zener, "Interaction between the d shells in the transition metals," *Physical Review*, vol. 81, no. 3, p. 440, 1951.

[49] P. W. Anderson and H. Hasegawa, "Considerations on double exchange," *Physical Review*, vol. 100, no. 2, p. 675, 1955.

[50] J. C. Cuevas and E. Scheer, *Molecular Electronics: an Introduction to Theory and Experiment*. World Scientific, 2010.

[51] V. I. Anisimov, "Electronic structure of strongly correlated materials," in *AIP Conference Proceedings*, vol. 1297, pp. 3–134, American Institute of Physics, 2010.

[52] V. G. Ivancevic and T. T. Ivancevic, *Applied Differential Geometry: a Modern Introduction*, ch. Applied Bundle Geometry, p. 527. World Scientific, 2007.

[53] C.-Y. Wong, *Introduction to high-energy heavy-ion collisions*, ch. Results from Lattice Gauge Theory, pp. 210–211. World scientific, 1994.

[54] Y. Shiomi, *Anomalous and Topological Hall Effects in Itinerant Magnets*. Springer Science & Business Media, 2013.

[55] N. Nagaosa, *Spin current*, ch. Multiferroics, p. 180. Oxford University Press, second ed., 2017.

[56] Y. Taguchi, Y. Oohara, H. Yoshizawa, N. Nagaosa, and Y. Tokura, "Spin chirality, berry phase, and anomalous hall effect in a frustrated ferromagnet," *Science*, vol. 291, no. 5513, pp. 2573–2576, 2001.

[57] M. Mekata, "Kagome: The story of the basketweave lattice," *Physics Today*, vol. 56, no. 2, p. 12, 2003.

[58] E. Hayward, "Kagome discoveries (interview with theoretical physicist ziqiang wang and researcher kun jiang)," *BC News, online site https://www.bc.edu/bc-web/bcnews/science-tech-and-health/physics/kagome-magnet.html*, 2018.

[59] S. Wexler, "E9: Optical kagome lattice," *Online site: http://ultracold.physics.berkeley.edu/research/e5*.

[60] C. Laboratory, "Optical kagome lattice," *Online site: https://www.manybody.phy.cam.ac.uk/Research/kagome*.

[61] T.-H. Han, J. S. Helton, S. Chu, D. G. Nocera, J. A. Rodriguez-Rivera, C. Broholm, and Y. S. Lee, "Fractionalized excitations in the spin-liquid state of a kagome-lattice antiferromagnet," *Nature*, vol. 492, no. 7429, pp. 406–410, 2012.

[62] Z. Sun, H. Zhou, C. Wang, S. Kumar, D. Geng, S. Yue, X. Han, Y. Haraguchi, K. Shimada, P. Cheng, *et al.*, "Observation of topological flat bands in the kagome semiconductor nb3cl8," *Nano Letters*, vol. 22, no. 11, pp. 4596–4602, 2022.

[63] M. El-Batanouny, *Advanced Quantum Condensed Matter Physics: One-Body, Many-Body, and Topological Perspectives*, ch. Dirac Materials and Dirac Fermions, pp. 332–336. Cambridge University Press, 2020.

[64] G.-G. Liu, P. Zhou, Y. Yang, H. Xue, X. Ren, X. Lin, H.-x. Sun, L. Bi, Y. Chong, and B. Zhang, "Observation of an unpaired photonic dirac point," *Nature Communications*, vol. 11, no. 1, p. 2, 2020.

[65] D. Chruściński and A. Jamiołkowski, *Geometric Phases in Classical and Quantum Mechanics*. Springer, 2004.

[66] Y. Chong, "Berry's phase and the anomalous velocity of bloch wavepackets," *Physical Review B*, vol. 81, no. 5, p. 052303, 2010.

[67] C. Kittel and C.-Y. Fong, *Quantum Theory of Solids*. Wiley, 1987.